



Preparing for the Standard Model Higgs Searches at the LHC with ATLAS

Aleandro Nisati

INFN – Roma

On behalf of the ATLAS Collaboration

“The Search for New States and Forces of Nature”

Galileo Galilei Institute

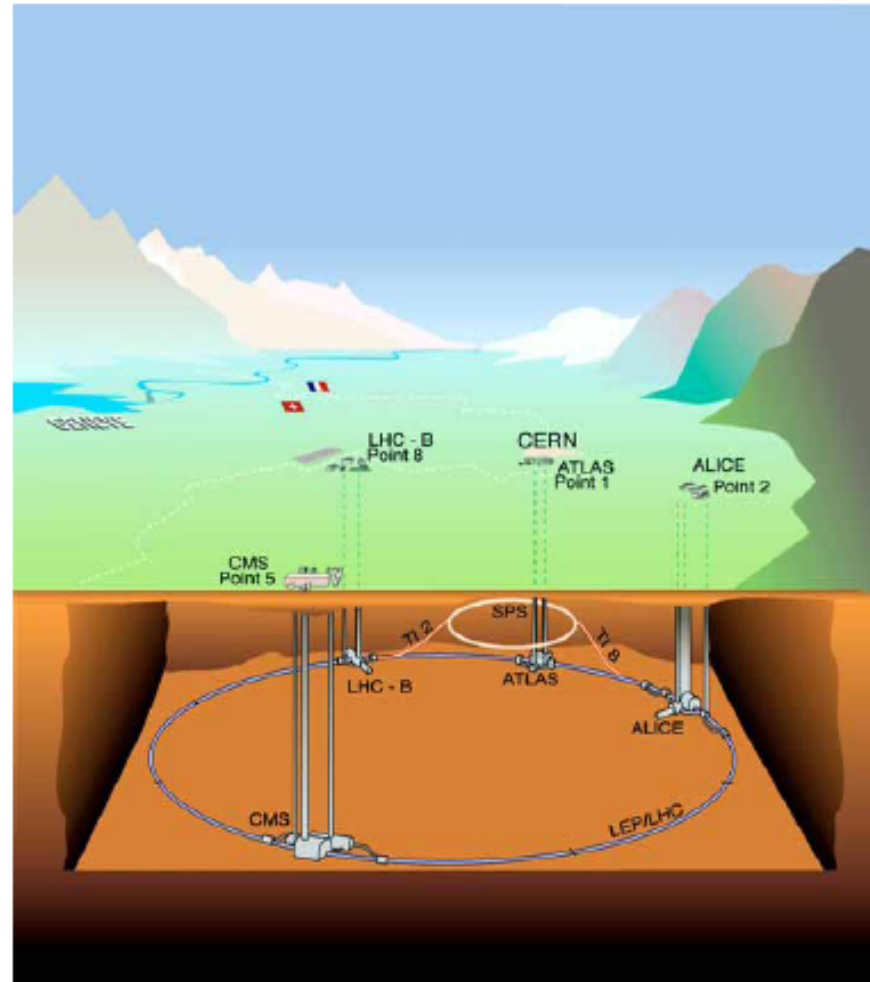
26 - 30 October 2009

Introduction

- The Large Hadron Collider – [see talk from R. Tenchini](#);
- The SM Higgs production at the LHC – [for Supersymmetric Higgs see talk from M. Carena](#);
- The search for the light Standard Model Higgs boson with the ATLAS detector
 - Some information on detector readiness
- Conclusions

The Large Hadron Collider

parameter	value
(design) CM energy	14 TeV
Luminosity	$10^{34} \text{ cm}^{-2} \text{ s}^{-1}$
Bunch crossing spacing	24.95 ns
Protons per bunch	1.15×10^{11}
Beam radius	16.7 μm
Main Dipoles	1232
Dipole field	8.33 T
Smaller magnets	7000
Stored energy	360 MJ/beam



The Large Hadron Collider

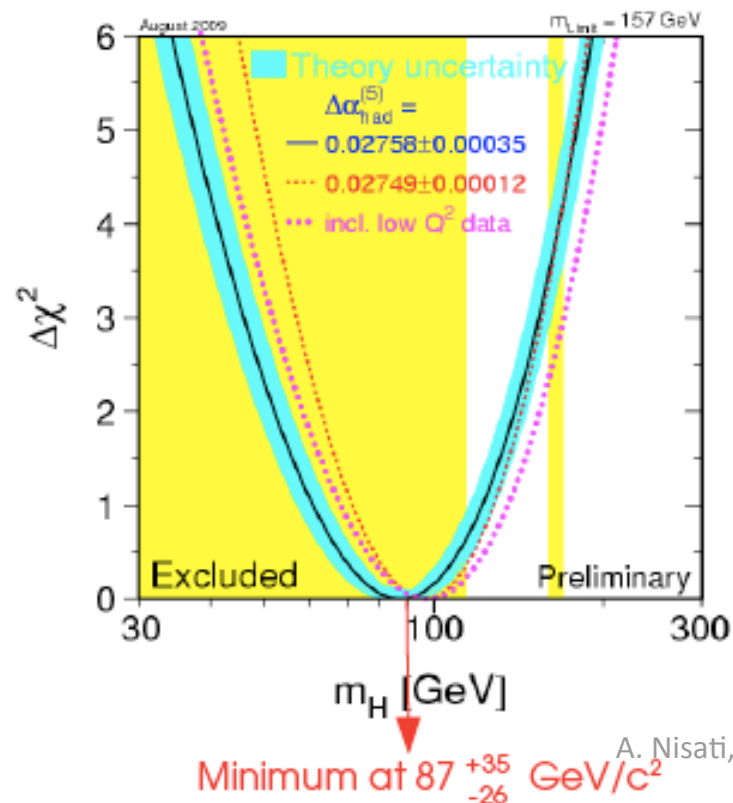
- LHC in 2009 / 2010; this could be a realistic scenario:
 - Energy: 7 to 10 TeV;
 - Instantaneous luminosity: from $L = 5 \times 10^{31} \text{ cm}^{-2} \text{ s}^{-1}$ to $L = \text{few} \times 10^{32} \text{ cm}^{-2} \text{ s}^{-1}$;
 - Bunch spacing: from 450 ns to 75, or 50 ns;
 - Integrated luminosity: about 200/pb;

Search for the SM light Higgs boson with ATLAS

- All results published here refer to:
 - $\sqrt{s}=14$ TeV
 - $L = 10^{33} \text{ cm}^{-2} \text{ s}^{-1}$
 - $\Delta t = 25$ ns
 - \rightarrow Average number of pp collisions x bunch: about 2.3
- I'll cover the main SM Higgs search channels showing the first and main steps to achieve the detector and data understanding to prepare the search analyses;
- Event pile-up taken into account in some cases;
- Detailed documentation in:
 - ATLAS: CERN-OPEN-2008-020 , <http://arxiv.org/abs/0901.0512>
 - CMS: CERN/LHCC 2006-021; J. Phys. G: Nucl. Part. Phys. 34 (2007) 995-1579.

Current information on SM Higgs

- LEP direct searches for a SM Higgs boson:
 - $m_H > 114.4 \text{ GeV}$ @ 95% C.L.
- Indirect searches constraints and global EWK fits seem to prefer a light Higgs boson:
 - $m_H > 157 \text{ GeV}$ @ 95% C.L.
 - <http://lepewwg.web.cern.ch/LEPEWWG>

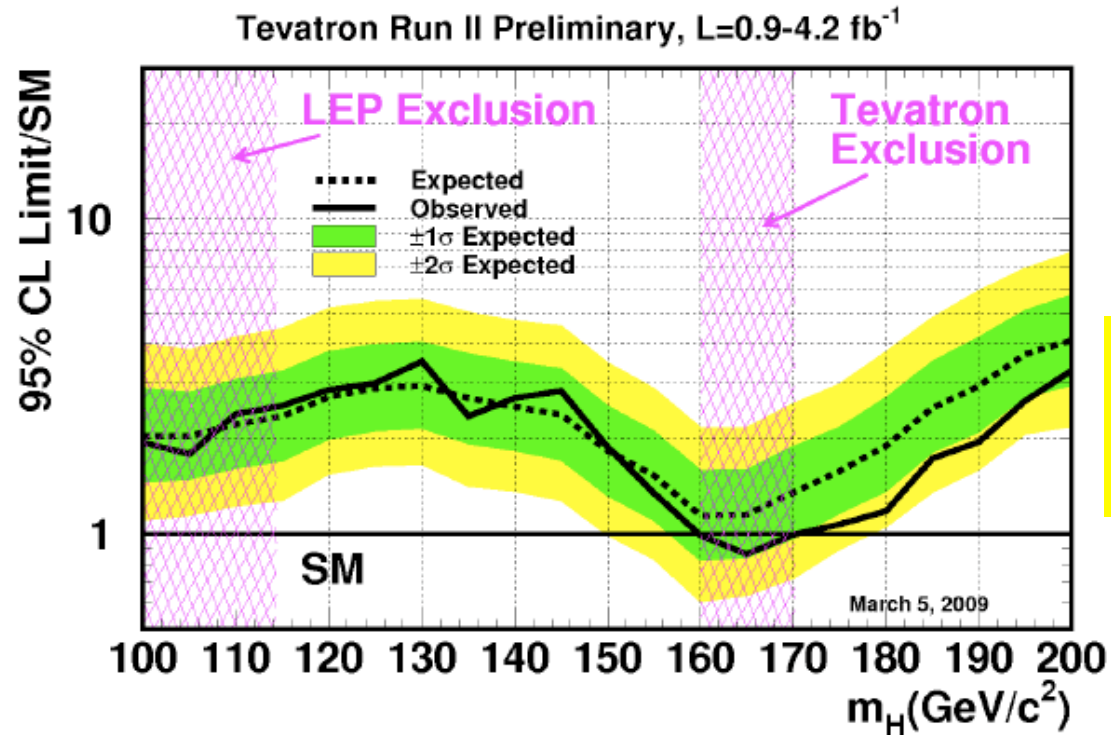


CDF and DØ at Tevatron are pursuing a direct search for a SM Higgs over a wide mass range:
 $100 < M_H < 200 \text{ GeV}$.

Current information on SM Higgs



Spring '09 Tevatron combination



0.9 - 4.2 fb^{-1}

Talk from M. Casarsa
WIN09, Perugia (I)
September 14-16

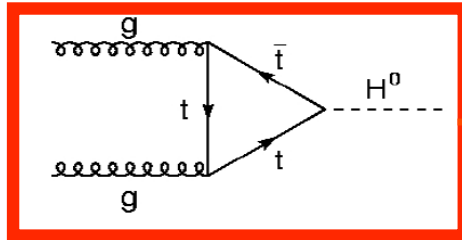
For $M_H = 115 \text{ GeV}/c^2$:

- ▶ expected limit = $2.4 \times \sigma_{\text{SM}}$
- ▶ observed limit = $2.6 \times \sigma_{\text{SM}}$

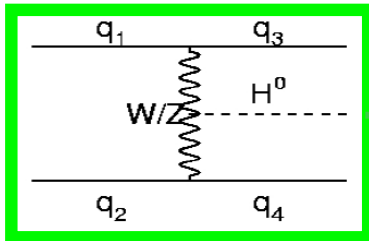
95% C.L. exclusion of
the mass range
 $160 < M_H < 170 \text{ GeV}/c^2$

SM Higgs production processes at LHC

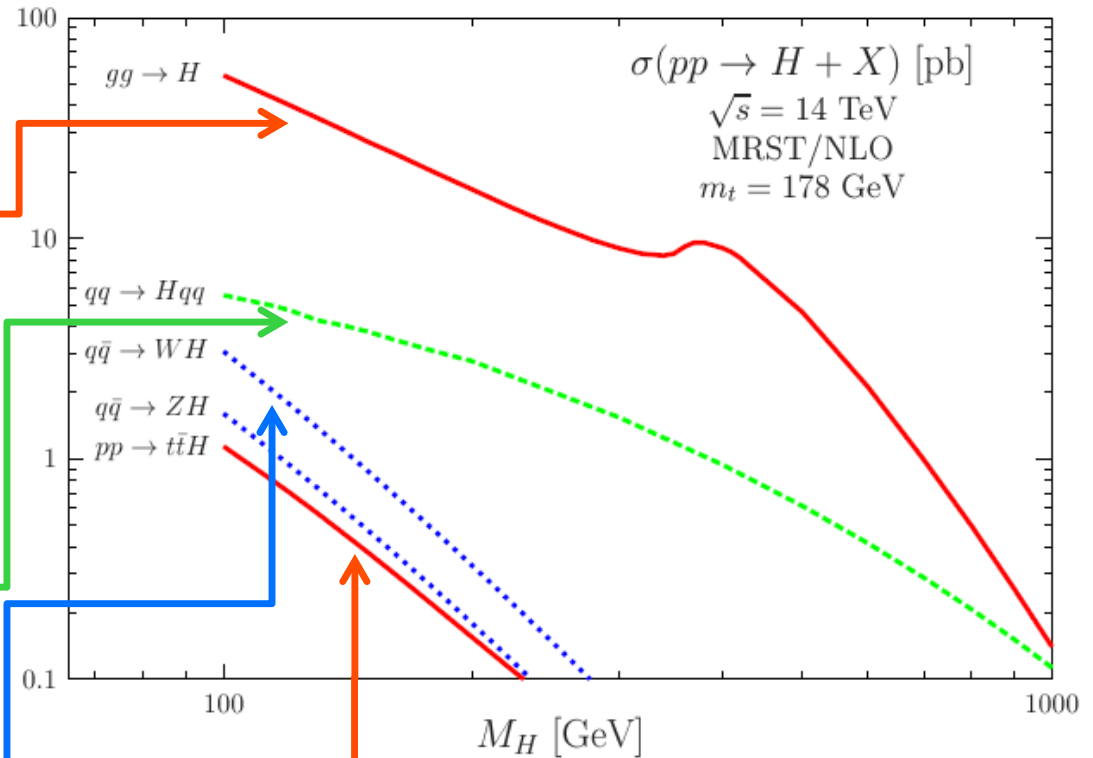
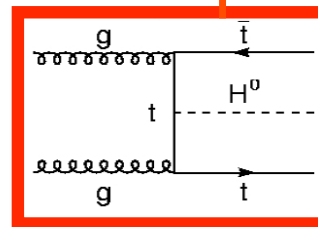
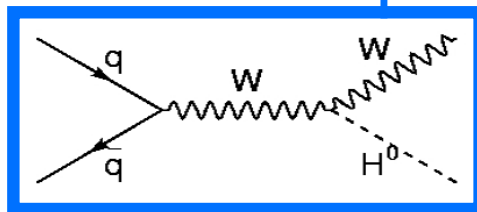
Gluon Fusion $H \rightarrow WW, ZZ, \gamma\gamma$



Vector Boson Fusion $H \rightarrow WW, \gamma\gamma, \tau\tau$



Associated Production

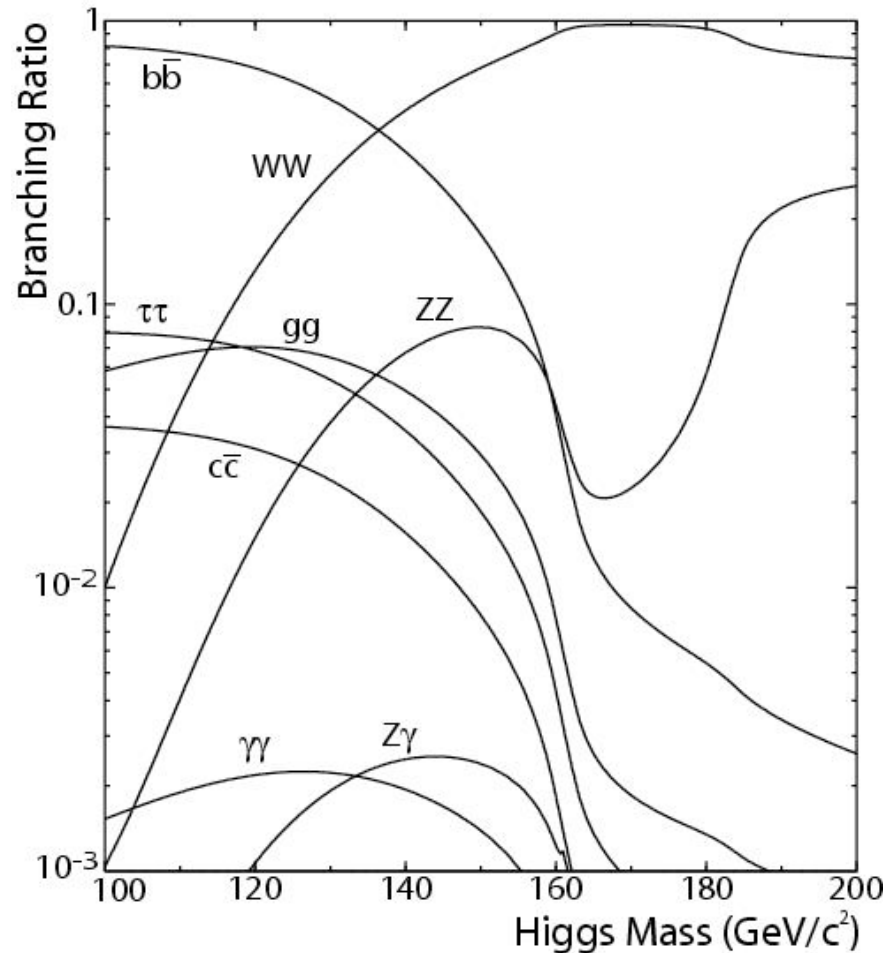


A.Djouadi, Phys. Rept.457:1-216.

$m_H = 120$ GeV

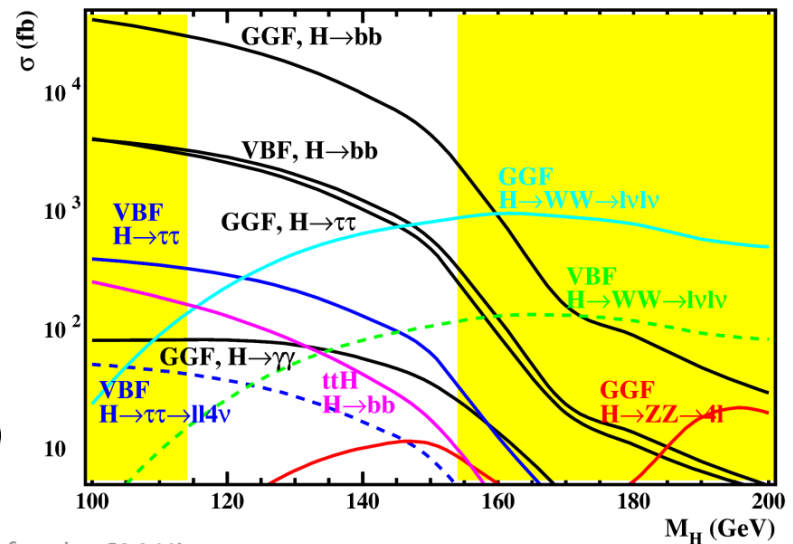
gg: ~ 38 pb;
VBF: ~ 4 pb;
ttH: ~ 0.7 pb;
W,ZH: $\sim 1.6 - 0.9$ pb;

Branching Fractions



$m_H = 120 \text{ GeV}$
 bb : $\sim 67\%$;
 WW^* : $\sim 13\%$;
 $\tau\tau$: $\sim 6.9\%$;
 $\gamma\gamma$: $\sim 0.2\%$;

Cross-section x B.R.



Branching Fractions

In the mass region below 150 GeV, we have many decay final states that can be used to search for the Higgs boson:

- **VBF $H \rightarrow \tau\tau$**
- **GGF $H \rightarrow \gamma\gamma$ (+ VBF and Associated Prod.)**
- **GGF and VBF $H \rightarrow WW^*$**
- **GGF $H \rightarrow ZZ^*$ (VBF useful at high mass)**

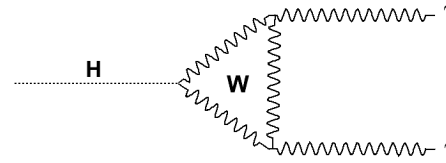
- **inclusive $H \rightarrow b\bar{b}$ and $H \rightarrow \tau\bar{\tau}$ are favorite by the very high branching fractions, but impossible to separate them from the huge QCD background;**
- **However $H \rightarrow b\bar{b}$ in Associated Mode appears possible:**
 - ttH: it is extremely challenging, a very good control of ttbb, and ttj production processes is required;
 - VH (V=W,Z) with H heavily boosted: See: *Phys. Rev. Lett.* 100, 242001 (2008) J. Butterworth, A. Davison, G. Salam, M. Rubin;
 - VH + γ (V=W,Z) appears very promising! **See next talk:** E.Gabrielli, F. Maltoni, B. Mele, M. Moretti, F. Piccinini, R. Pittau, **Nucl. Phys. B 781 (2007), 64; hep-ph/0702119;**

H \rightarrow $\gamma\gamma$

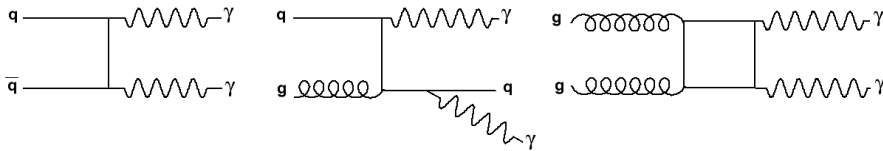
- small BR (about 0.002)
- decay due to W and t loops
- clean 2- γ signature

Higgs to 2 γ decay

$\sigma = 0.08 \text{ pb}$



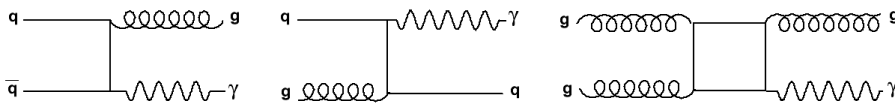
Irreducible background: $pp \rightarrow \gamma\gamma + X$



Born $O(\alpha^2)$ Bremsstrahlung $O(\alpha_s \alpha^2)$ Box diagram $O(\alpha_s^2 \alpha^2)$

Theoretical uncertainty: $\sim 25\%$ (NLO: 20%)

Reducible background: $pp \rightarrow \gamma j, jj + X$

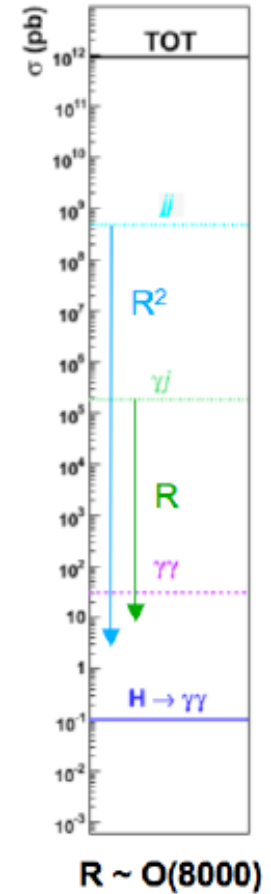


$O(\alpha_s \alpha)$ $O(\alpha_s \alpha)$ $O(\alpha_s^3 \alpha)$

Theoretical uncertainty: $\sim 30\%$ (dominated by NLO cross-section)

qqbar, qg $\sigma = 21 \text{ pb}$
gg $\sigma = 8 \text{ pb}$

γ -jet $\sigma = 1.8 \times 10^5 \text{ pb}$
jet-jet $\sigma = 4.8 \times 10^8 \text{ pb}$



γ -jet need rejection $R \sim O(10^4)$

jet-jet need rejection $R \sim O(10^7)$

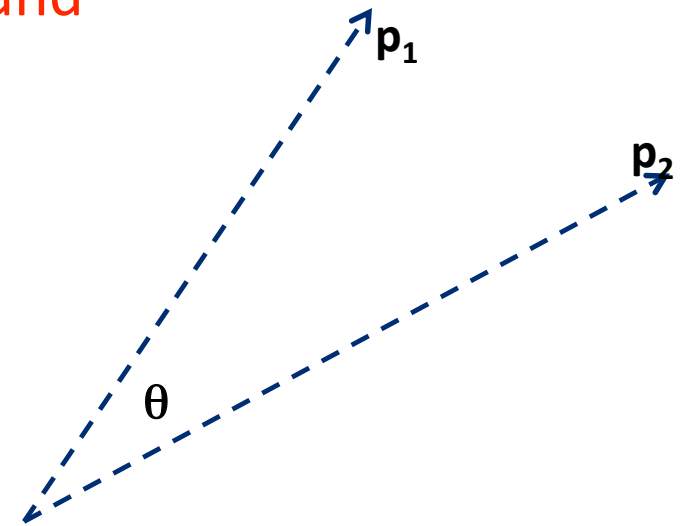
Main background is from leading π^0 's



A very accurate mass reconstruction is mandatory to detect a narrow peak on top of a smooth background

Mass reconstruction

$$m^2 = 2P_1P_2(1-\cos\vartheta) \cong P_1P_2\vartheta^2$$
$$\delta m/m = (1/\sqrt{2})(\delta P/P)\vartheta \oplus \delta\vartheta/\vartheta$$



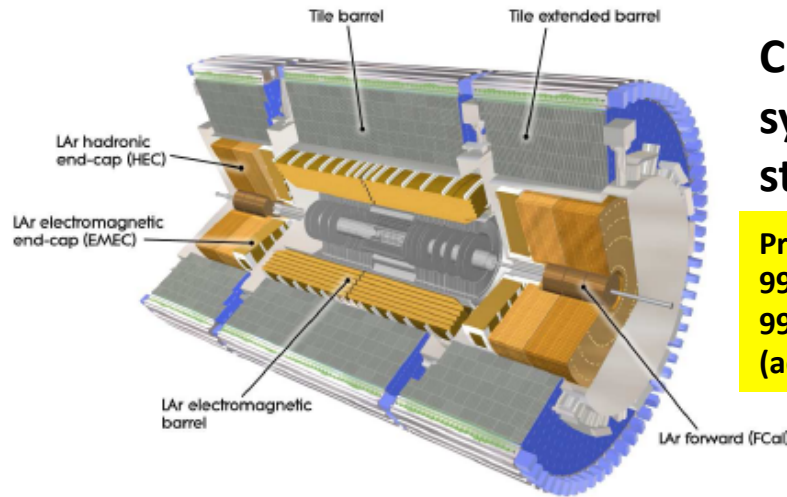
1. Very good γ energy measurement

2. Very good γ direction measurement:

- interaction vertex identification (vertex position accuracy is very good);
- very good photon impact point (with calorimeter) position measurement;

3. Strong jet rejection (as shown in previous slide)

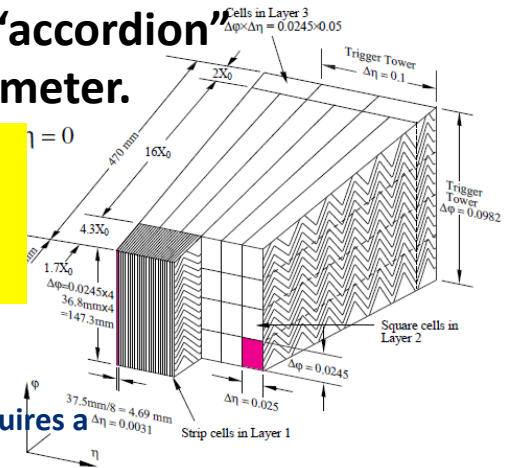
$$H \rightarrow \gamma\gamma$$



Slice view of the ATLAS calorimeter system.

Cut-away of the ATLAS Calorimeter system and sketch of the “accordion” structure of the EM Calorimeter.

Present status:
99.98 good Presampler channels
99.1 good channels in LAr Calorimeter
(additional 0.7% recovered recently)



lead Moliere radius: 1.24 cm → requires a granularity of about 0.01

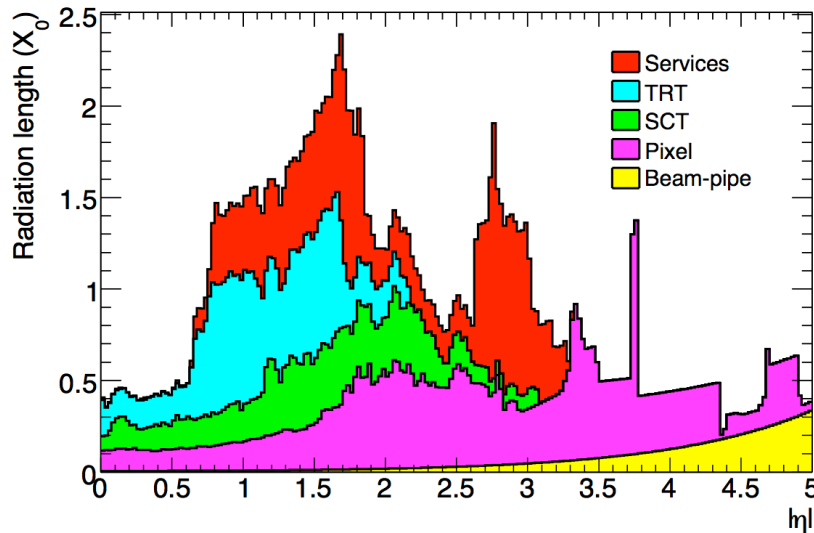
Layer	Granularity ($\Delta\eta \times \Delta\phi$)
Presampler	0.025 x 0.01
Front	0.003 x 0.1
Middle	0.025 x 0.025
Back	0.05 x 0.025

- ← Allows to account for the material behind the calorimeter;
- ← Allows to recognize and reject low-energy π^0 decays;
- ← Allows to account of the dead material between the presampler and the front layer;
- ← Measure the em shower at its maximum
- ← Measure the em shower at tail

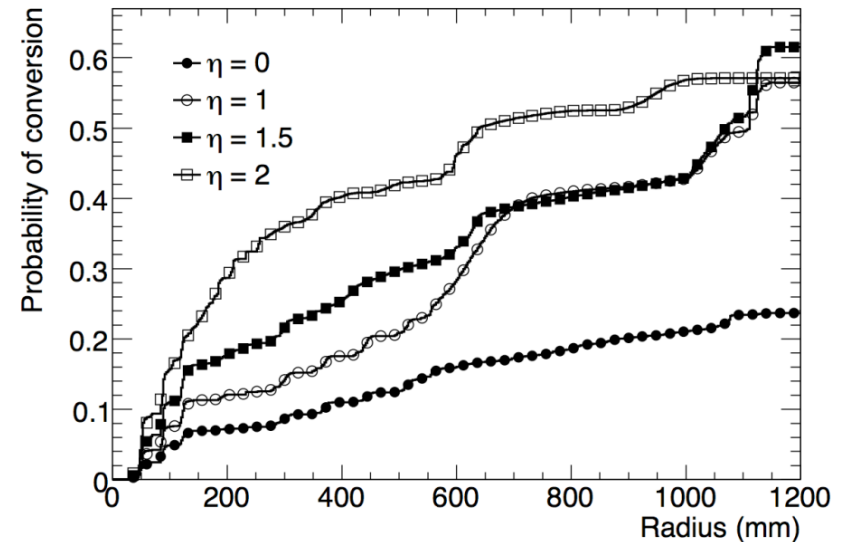
Energy resolution:

$$\frac{\sigma(E)}{E} = \frac{10\%}{\sqrt{E}} \oplus 0.7\%$$

$$H \rightarrow \gamma\gamma$$



The material in the ATLAS inner detector as a function of η .



Probability of a photon to convert as a function of radius at different values of η (ATLAS).

main consequence:

Interaction of photons with matter

- impact on the photon identification
- impact on the energy reconstruction: → energy scale; energy resolution
- photon conversion → photon identification

$$H \rightarrow \gamma\gamma$$

- The calibration of electron/photon clusters is done using also the Monte Carlo simulation (as demonstrated in Testbeam studies)
- Electrons energy will be finally calibrated using standard candles such as Z^0 and J/Ψ
- We don't have standard candles for photons: therefore we need to have a careful control of all material behind the calorimeter.

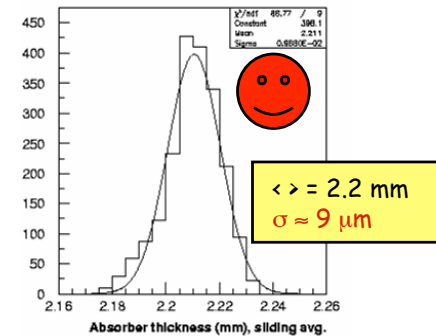
$$H \rightarrow \gamma\gamma$$

Contributions to energy resolution for a 60 GeV photon:

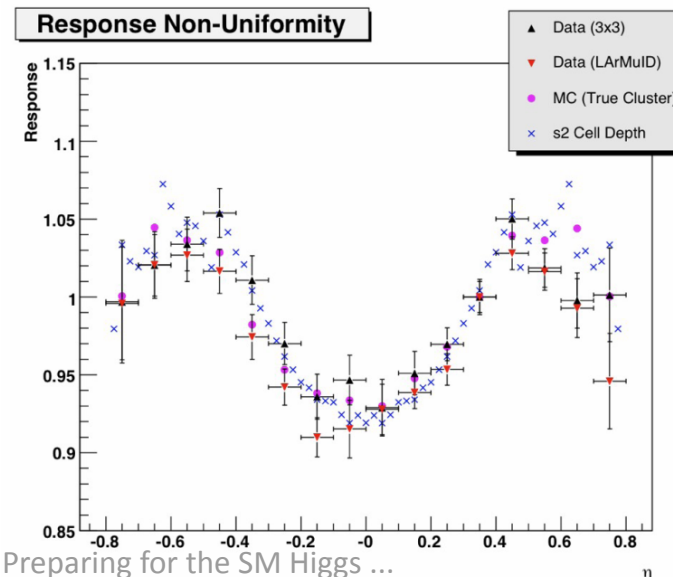
- stochastic term, 1.29 %;
- constant term, 0.7 %

1. **Geometry:** (e.g. deviation from Accordion modulation): $\sim 0.3\%$;
2. **Construction phase:** thickness of all 1536 absorber plates (1.5m long, 0.5m wide) within $\sim 10\mu\text{m}$ \rightarrow response uniformity $<\sim 0.3\%$;
3. **Pulse-Test:** calibration accuracy of each module $\sim 0.4\%$;
Overall “local” constant term: 0.5-0.6%.

Test-beam: 4 (out of 32) barrel modules and 3 (out of 16) endcap modules; Uniformity over units of size $\Delta\eta \times \Delta\phi = 0.2 \times 0.4: \sim 0.5\%$;



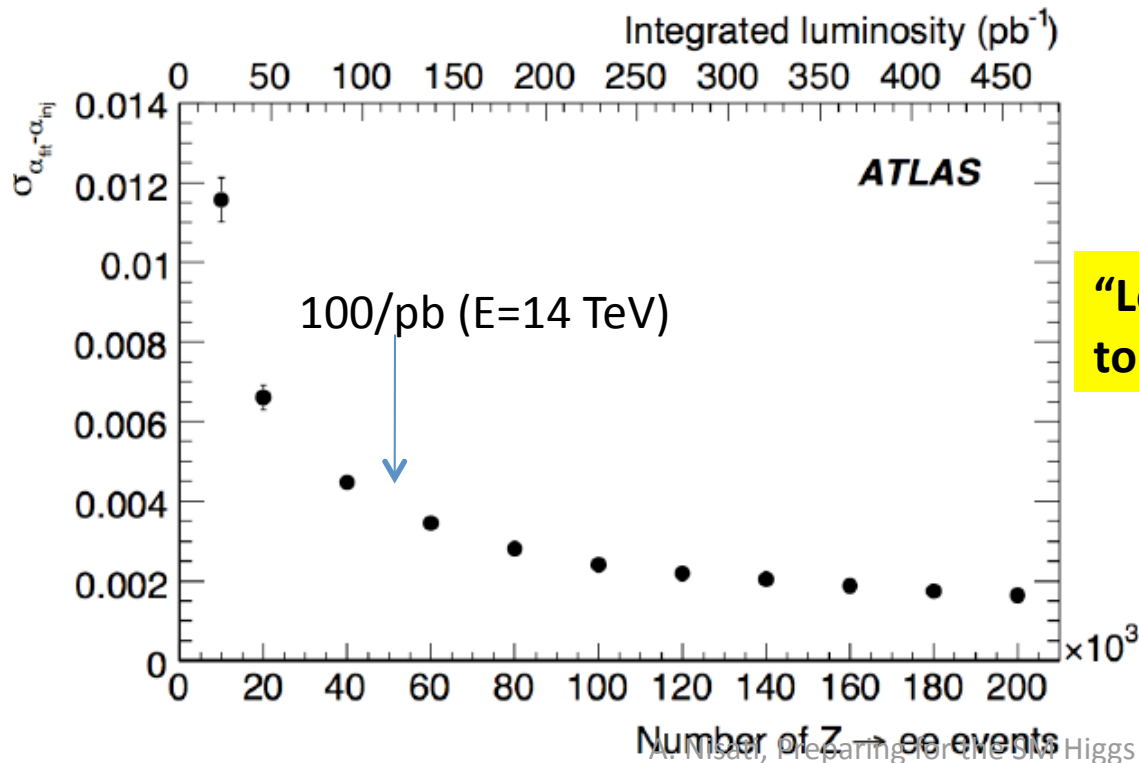
In-situ uniformity measurement



In-situ calorimeter uniformity was measured with cosmics in 2006/2007 for 9 modules (Inner Detector not available then). Agreement between MC and data better than 2%;



One more step: control and calibrate for “long-range” effects (Liquid Ar impurities and temperature, mechanical deformations, high voltage, ...) **intercalibration of the 384 regions** and calibration of the energy scale → analyse $Z \rightarrow e+e-$ decays.



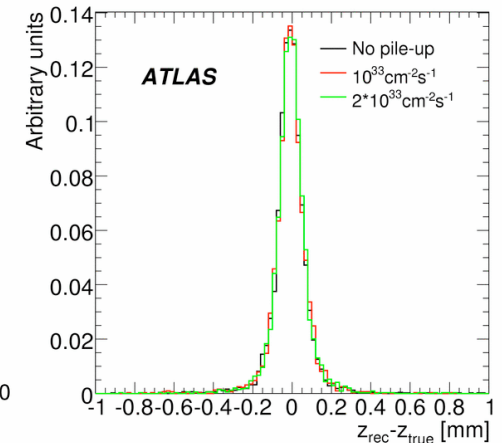
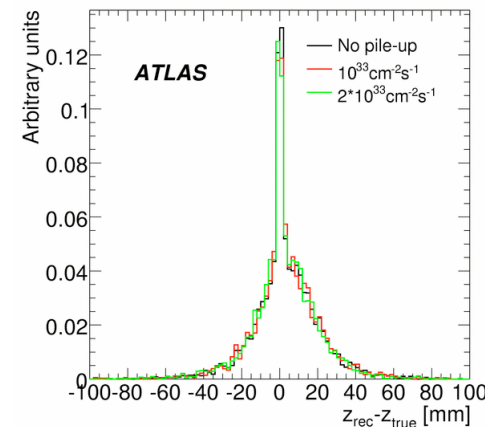
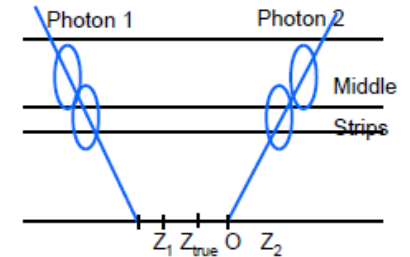
“Long-range” mis-calibrations limited to 0.4% with 100/pb of data



Photon direction measurement

- An accurate flight direction measurement of *unconverted* photons does require the use of:
 - the main interaction point;
 - the impact point of the photon with the calorimeter
 - in this way we obtain a RMS of 0.1 mm, to be compared with 17 mm obtained using the photon direction measurement from the calorimeter; Impact to the mass resolution: 1.4 GeV.
- Interaction vertex identification; two methods:
 - extrapolate the flight direction measured by the 1st and 2nd layer of the calorimeter down to the beam line and identify the closest vertex (ATLAS only);
 - use the tracks of the recoil system to identify the correct vertex (ATLAS and CMS)

- For *converted* photons we can use the conversion hit to measure the flight direction, and an accuracy of about 1 mm can be obtained:



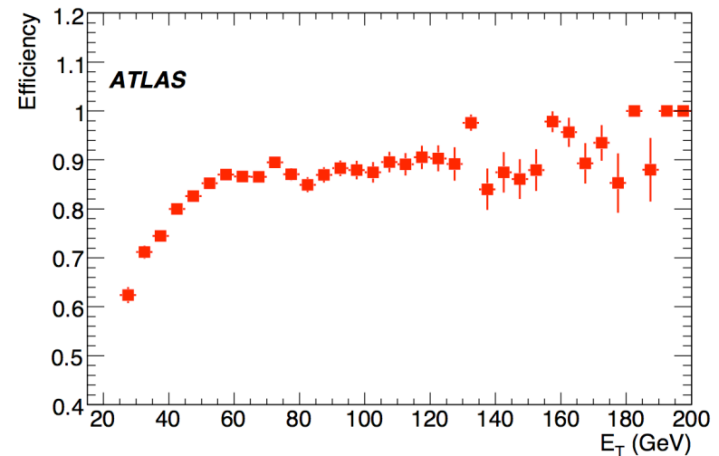
Difference between the reconstructed primary vertex position and the true position obtained from calorimetric pointing and conversion track information (when available) without/with the reconstructed primary vertex (left/right plot), for events without pile-up (black plots) and with pile-up evaluated for 10^{33} and $2 \cdot 10^{33} \text{ cm}^{-2}\text{s}^{-1}$ (red, green plots). The narrow peak on top of the broader one is due to events in which at least one photon has a reconstructed conversion vertex.

$$H \rightarrow \gamma\gamma$$

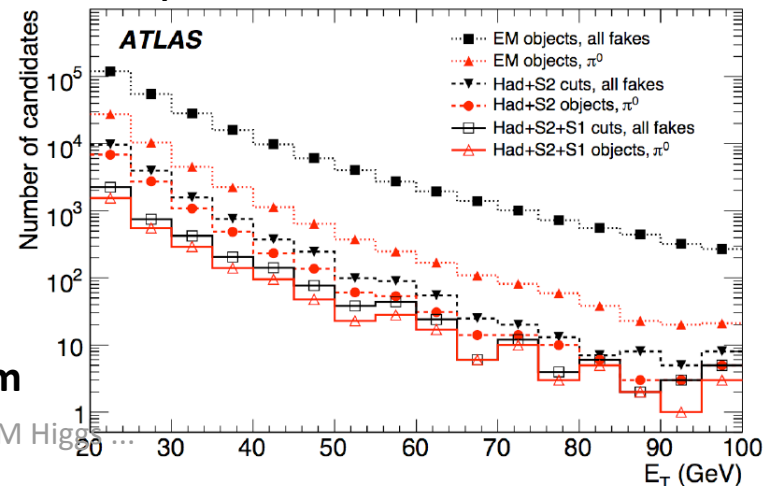
Photon Identification:

- Hadron leakage (small $E_T^{\text{had}}/E_T^{\text{em}}$)
 - EM Shower shape measured in the 1st and the 2nd LAr compartment
 - Track Isolation (small track activity around the EM cluster)
- efficiency close to 90% (for high- E_T photons) can be achieved;
 - a rejection of the order of 4000 is expected;
 - rejection is stronger for q-initiated jet (example: γ -jet production)

Right: ET distribution of fake-photon candidates in jets after different level of cuts. The contribution from “single- π^0 ” is also shown.

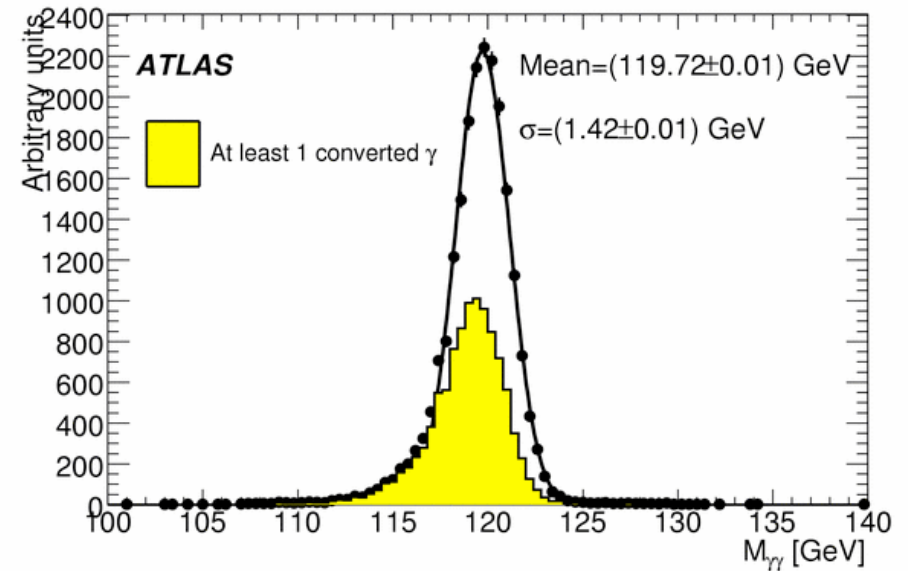


Top: Efficiency of the calorimeter cuts as a function of the transverse energy (bottom) of photons with $E_T > 25$ GeV from $H \rightarrow \gamma\gamma$, in the presence of event pile-up at $L=10^{33} \text{ cm}^{-2} \text{ s}^{-1}$;



$$H \rightarrow \gamma\gamma$$

- **Trigger:** at least 2 photons with $p_{T\gamma1} > 17$ GeV – not a big problem
- **Fiducial cut:** $0 < |\eta| < 1.37$ & $1.52 < |\eta| < 2.37$
- **Isolation cut:** $p_T < 4$ GeV/c, considering all tracks with $p_T > 1$ GeV/c in a $R=0.3$ cone around the electromagnetic cluster.
- **Momentum cut:** $p_{T\gamma1} > 25$ GeV;
 $p_{T\gamma2} > 40$ GeV

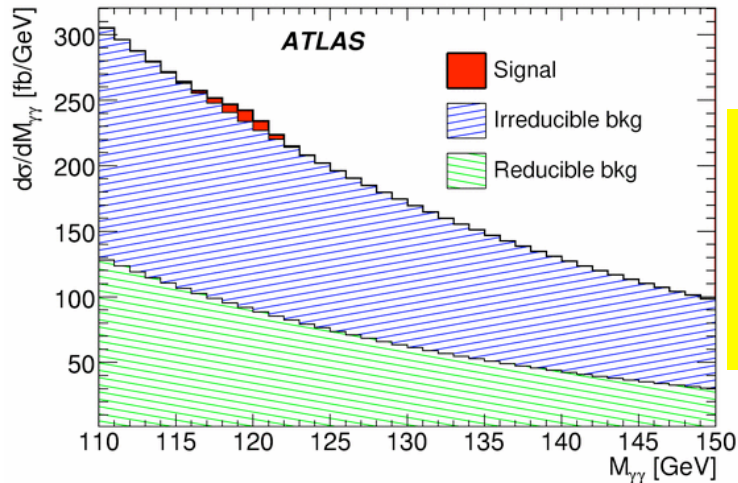


Selection efficiency (inclusive analysis):

- $\epsilon = 36\%$ (without pileup)
- $\epsilon = 32\%$ (with pileup)

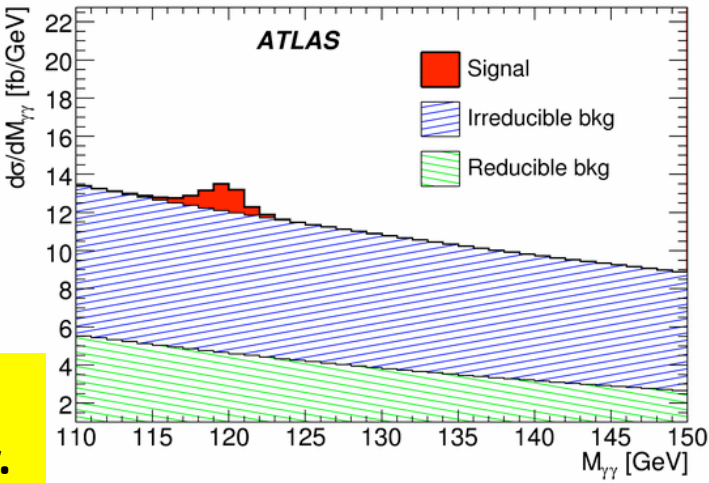
(converted photon calibration not optimal in this plot: there is room for improvements)

$$H \rightarrow \gamma\gamma$$



$m_H = 120 \text{ GeV};$
 $L=10/\text{fb}$

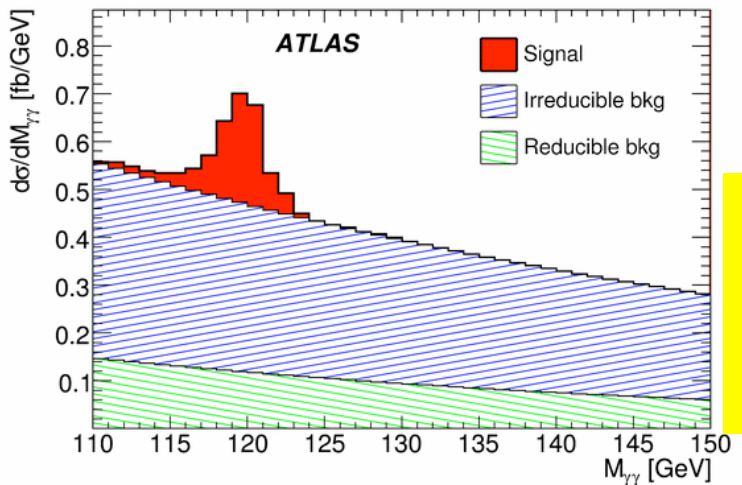
$S = 254 \text{ ev.}$
 $B = 9470 \text{ ev.}$
 $S/B \sim 2.7 \%$
 $S/\sqrt{B} \sim 2.6$



$S = 40 \text{ ev.}$
 $B = 490 \text{ ev.}$
 $S/B \sim 8.2 \%$
 $S/\sqrt{B} \sim 1.8$

Top-Left: Diphoton invariant mass spectrum after the application of cuts of the **inclusive** analysis.

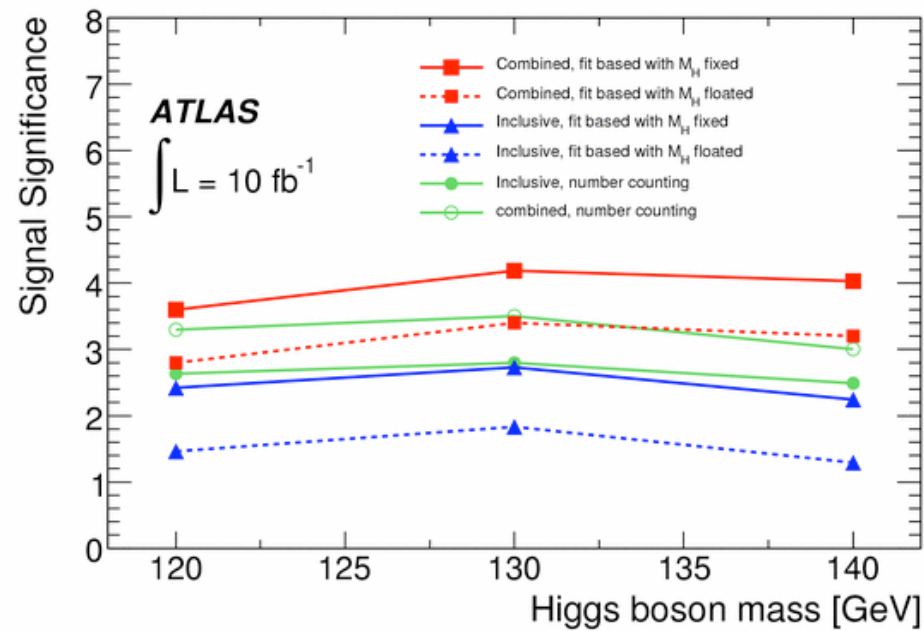
Top-Right: Diphoton invariant mass obtained with the Higgs boson **plus one jet** analysis



$S = 9.7 \text{ ev.}$
 $B = 19.5 \text{ ev.}$
 $S/B \sim 50 \%$
 $S/\sqrt{B} \sim 2.2$

Bottom-Left: Diphoton invariant mass spectrum obtained with the Higgs boson **plus two jet** analysis

$$H \rightarrow \gamma\gamma$$

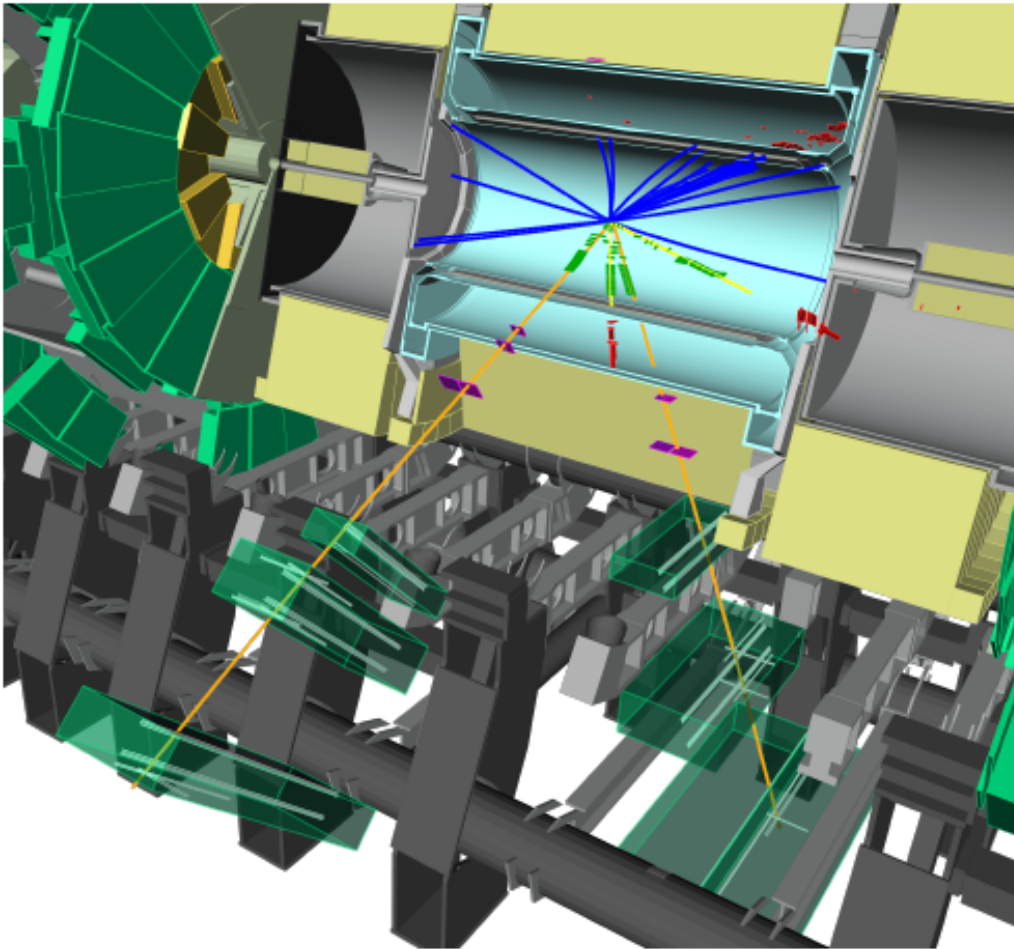


Expected signal significance for a Higgs boson using the $H \rightarrow \gamma\gamma$ decay for 10 fb^{-1} of integrated luminosity as a function of the mass.

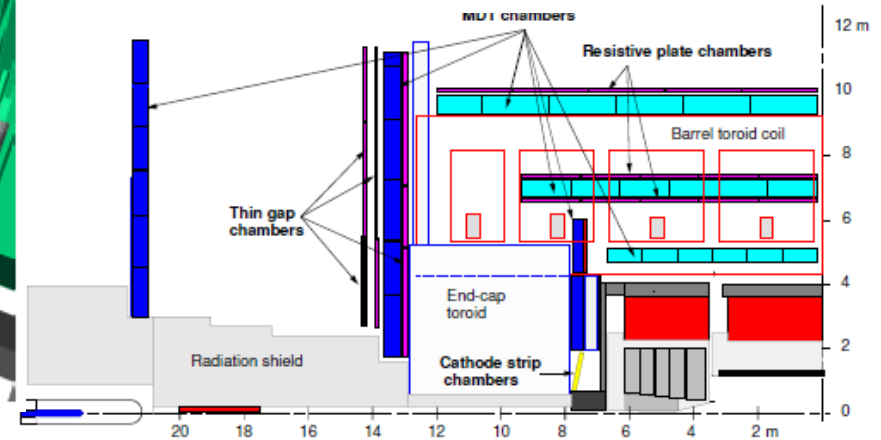
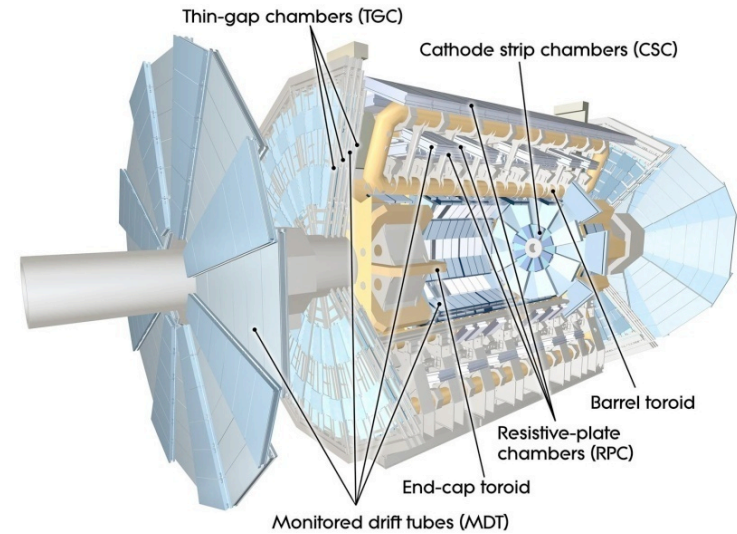
$$H \rightarrow ZZ^* \rightarrow 4l$$

- The so-called “**gold-plated**” channel;
 - Very important in the mass range $m_H > 130$ GeV; with the exception of a small region around $2M_W$;
- ... but it could easily become a “**brass-plated**” channel, mainly with the initial data...!
- **The issues:**
 - single lepton offline (and trigger) reconstruction efficiency ϵ_l : if ϵ_l single lepton reconstruction efficiency, the Higgs reconstruction efficiency ϵ_H goes as $\epsilon_H \approx \epsilon_l^4$
 - The single lepton energy resolution immediately follows.

$$H \rightarrow ZZ^* \rightarrow 4l$$

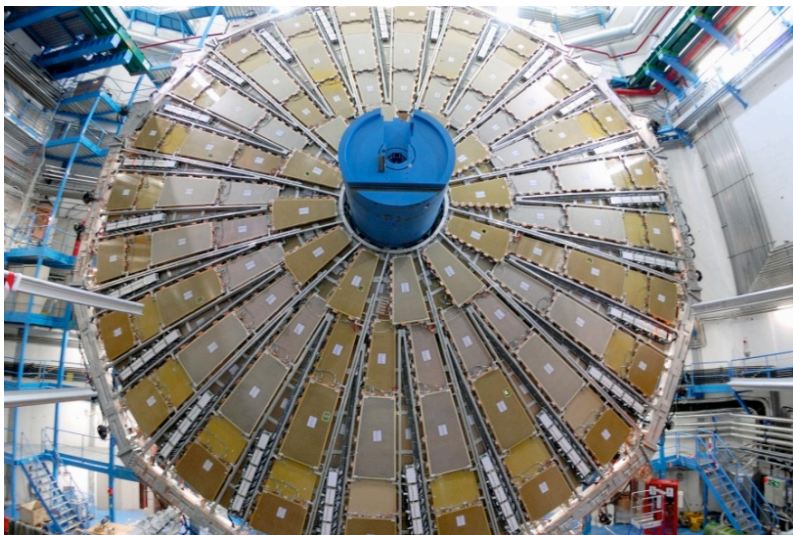
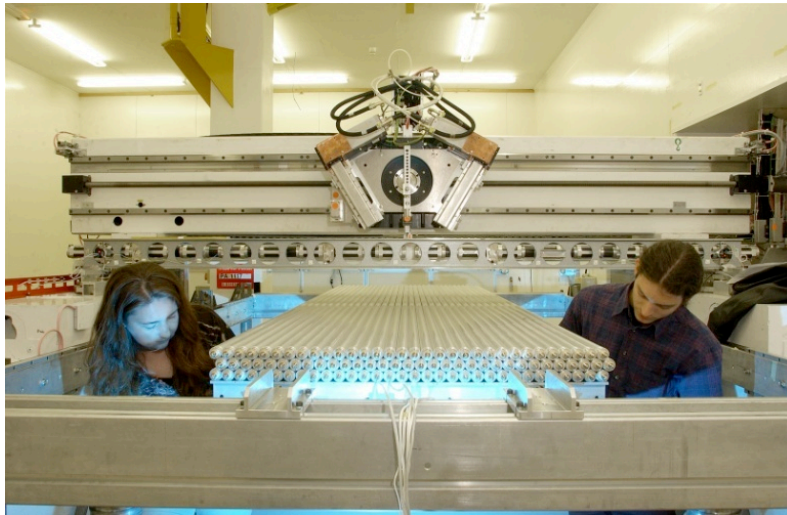


Display of a high- p_T $H \rightarrow ZZ \rightarrow ee\mu\mu$ decay ($m_H = 130$ GeV), after full simulation and reconstruction in the ATLAS detector. The four leptons and the recoiling jet with $E_T = 135$ GeV are clearly visible.



Top: artist's view of the Muon Spectrometer;
Bottom: Scheme of the Muon Spectrometer layout

$$H \rightarrow ZZ^* \rightarrow 4l$$



The challenges of the ATLAS Muon System:

1. Very high muon detection efficiency
2. Very high momentum reconstruction accuracy:
 - Single hit position accuracy: $30 \mu\text{m}$
 - Chamber (relative) alignment $30 \mu\text{m}$
3. Very robust and fast Muon Trigger: time resolution better than 25 ns

• Four technologies in ATLAS

• MDTs and CSCs

• RPCs and TGCs

• In this page some MDT and TGC pictures

$$H \rightarrow ZZ^* \rightarrow 4l$$



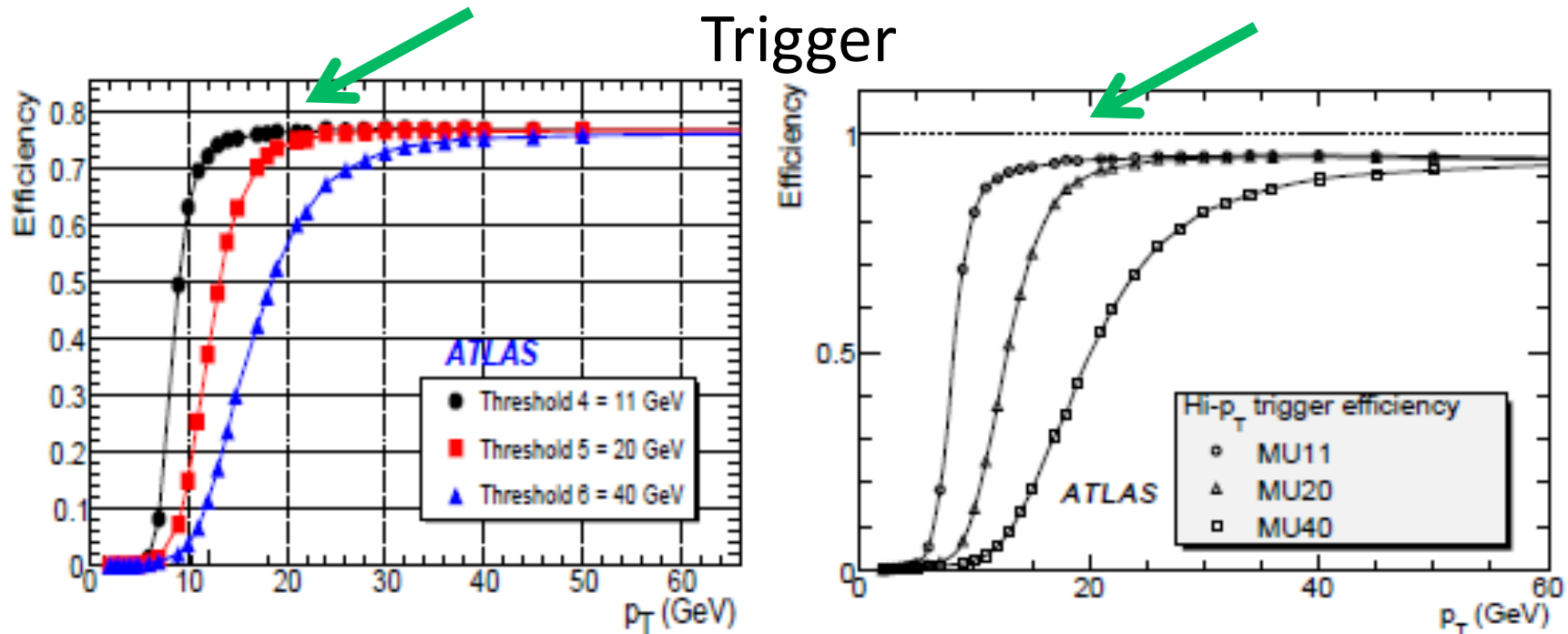
$$H \rightarrow ZZ^* \rightarrow 4l$$

- Where the problems will/could be?
 - The muon trigger and tracking chambers hw conditions:
 - High-Volt., Low-Volt., gas, Read/Out
 - Dead/hot channels
 - Muon chamber alignment
 - The Inner Detector hw conditions
 - High-Volt., Low-Volt., gas, Read/Out
 - Dead/hot channels
 - ID planes relative alignment
 - Muon System – ID relative alignment

$$H \rightarrow ZZ^* \rightarrow 4l$$

- Muon chambers operation in ATLAS
 - Tracking chambers
 - MDTs, 1088 chambers, with 339k channels; >99% operational; dead/noisy channels: 0.1/0.2%;
 - CSCs, 32 chambers, 31k channels; 99% operational;
 - Trigger chambers (RPCs, TGCs):
 - RPCs, 544 chambers, 359k channels; 9.5% (->98.5%) operational;
 - TGCs, 3588 chambers, 318k channels, almost 100% operational;
- Alignment (mainly with Optical System)
 - Endcap: 50 ÷ 100 μm ;
 - Barrel: 100 ÷ 200 μm (up to 1 mm in Small Sectors);

$$H \rightarrow ZZ^* \rightarrow 4l$$

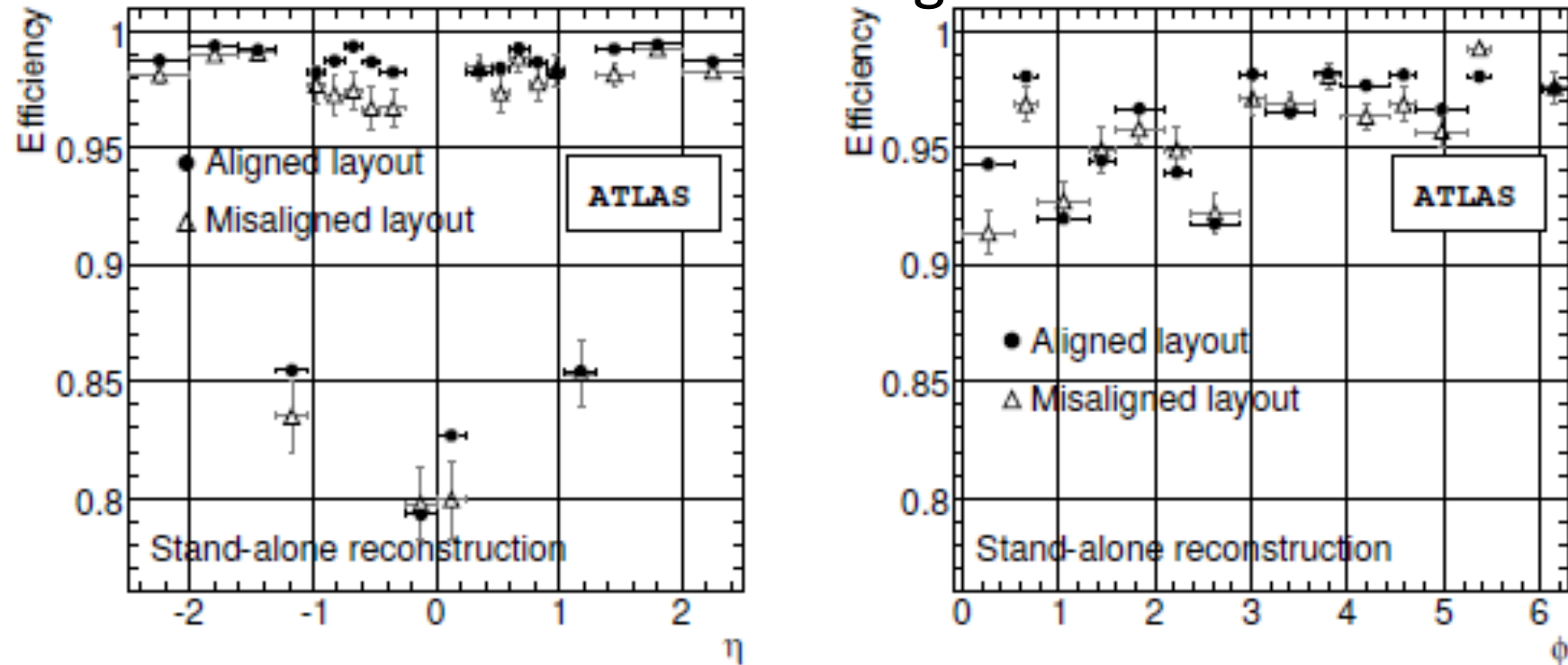


Ultimate Level-1 single muon trigger efficiency as a function of the p_T trigger threshold, the muon true p_T , for the barrel (left) and the endcap (right) systems.

The acceptance plateau height is OK (we trigger at most on two high- p_T leptons); but we must carefully monitor it stays (very!) close at the ultimate level

$$H \rightarrow ZZ^* \rightarrow 4l$$

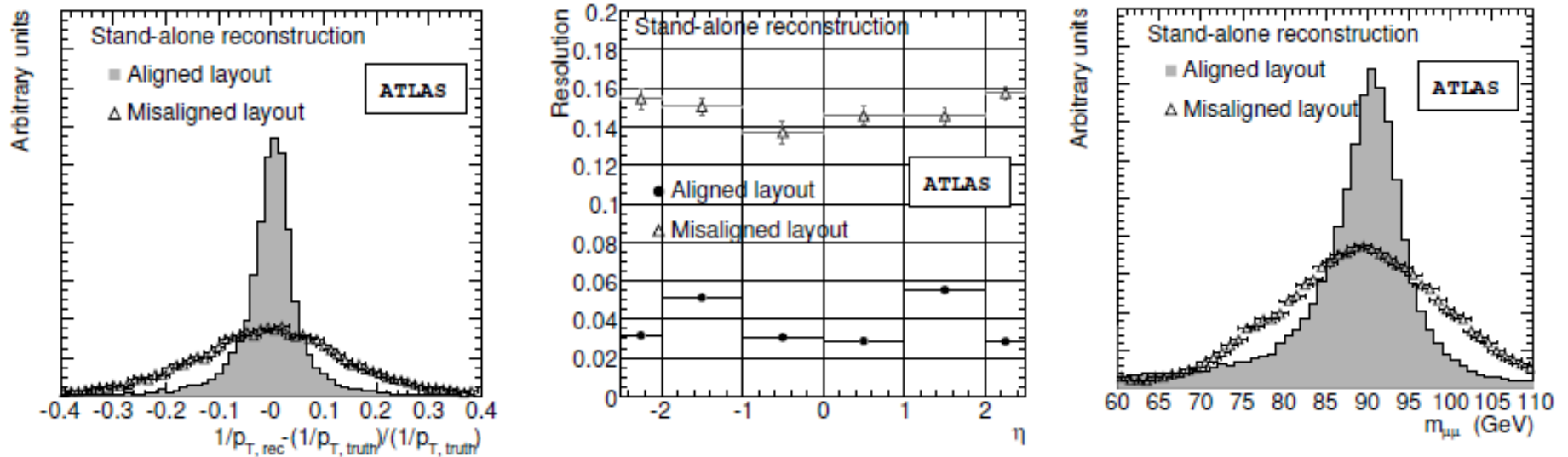
Tracking



Impact of misaligned muon chambers to the reconstruction efficiency of 50 GeV p_T isolated muons, as a function of η (left) and ϕ (right).

The chambers were randomly shifted from the nominal positions with Gaussian distribution centred at 0 and a standard deviation of 1 mm and rotated randomly with Gaussian distribution centred at 0 and a standard deviation of 1 mrad. Deformations of the chambers which are monitored by an optical system mounted on the chambers were not considered in these studies.

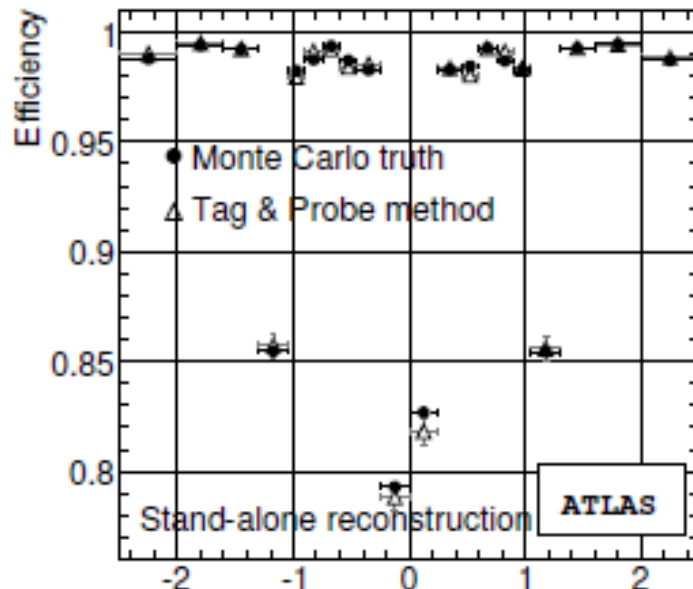
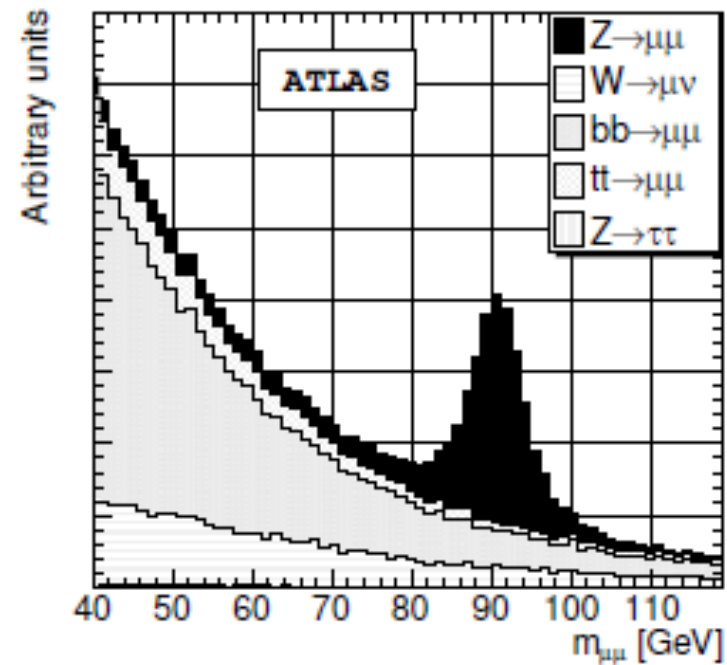
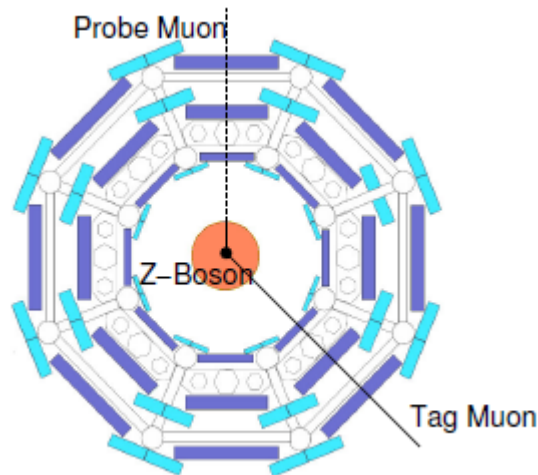
$$H \rightarrow ZZ^* \rightarrow 4l$$



Left, Center: Impact of misaligned muon chambers to the reconstructed muon transverse momentum of 50 GeV p_T isolated muons. In the reconstruction geometry, the chambers were randomly shifted from the nominal positions with Gaussian distribution centered at 0 and a standard deviation of 1 mm, and rotated randomly with Gaussian distribution centered at 0 and a standard deviation of 1 mrad. Deformations of the chambers which are monitored by an optical system mounted on the chambers were not considered in these studies.

Right: reconstruction of the Z^0 in the aligned/misaligned cases.

$$H \rightarrow ZZ^* \rightarrow 4\ell$$



Top-Left: measuring the trigger & reconstruction efficiency from data: the Tag & Probe method.

Top-Right: the $m_{\mu\mu}$ invariant mass distribution (before selection cuts).

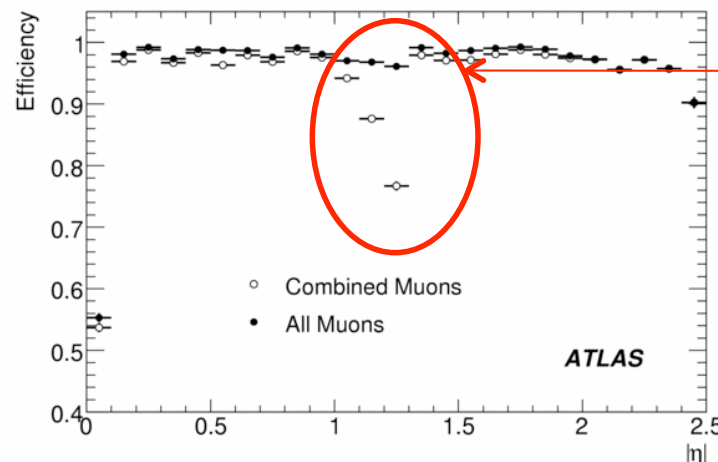
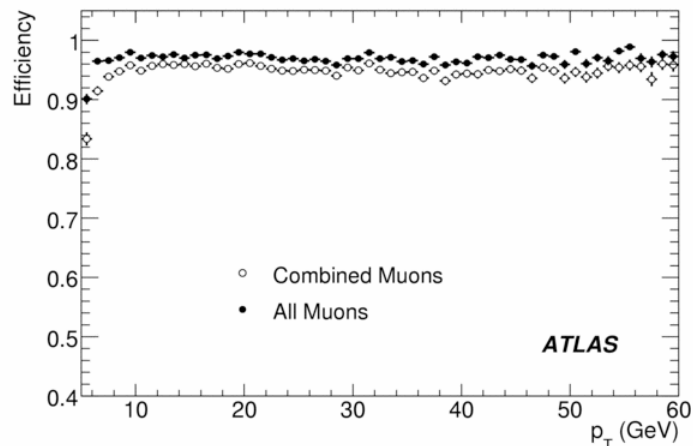
Bottom-Left: Reconstruction efficiencies “measured” with the Tag&Probe compared with the “true” efficiencies (MC).

$$H \rightarrow ZZ^* \rightarrow 4\mu$$

Muon reconstruction efficiency

Muons with $p_T > 10$ GeV, $|\eta| < 2.5$, associated with W decays in $t\bar{t}$ events:

	no pileup		pileup	
	eff.	fakesx1000	eff.	fakesx1000
• Muon System Standalone:	0.951	4.4	0.996	8.2
• Inner Detector Standalone:	0.996		0.995	
• Combined Muon Rec.:	0.943	9.6	0.941	11.2



No “BEE” chambers in simulation;
Now are installed !
➔ Superior reconstruction efficiency

Muon reconstruction efficiency as a function of p_T (left) and $|\eta|$ (right). Empty (filled) markers show the efficiency of the combined (combined+extrapolated from the ID) algorithm. Reconstructed muons of a Higgs boson sample of 130 GeV mass decaying into four muons are used.

$$H \rightarrow ZZ^* \rightarrow 4l$$

- ... and for electron final states?
 - See the discussion made for the photon calibration

Electron Identification:

“Loose”

- Hadron leakage (small $E_T^{\text{had}}/E_t^{\text{em}}$);
- EM Shower shape measured in the 2nd LAr compartment;

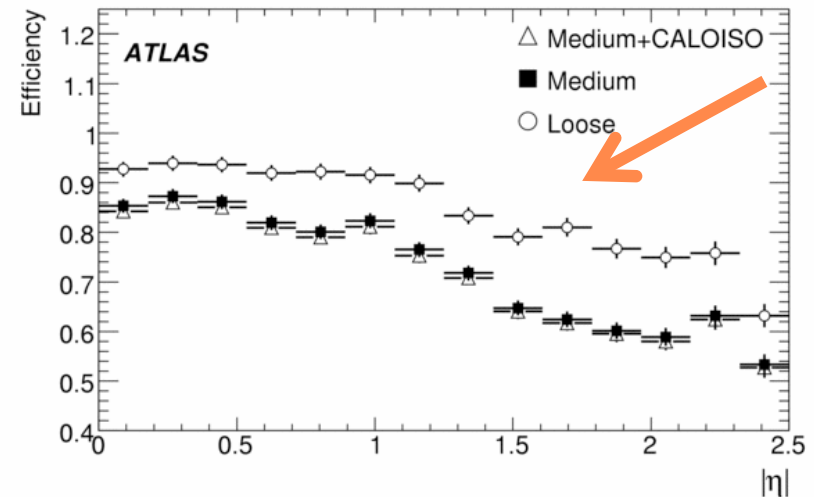
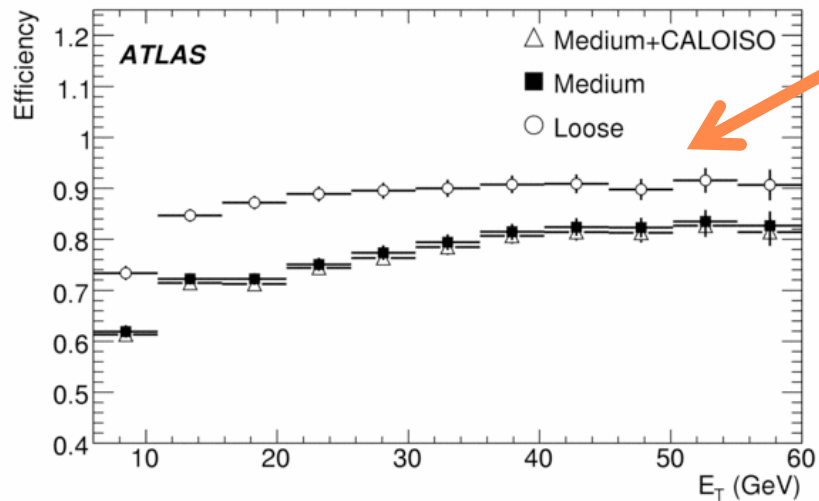
• “Medium”

- Loose cuts and:
- EM Shower shape measured in the 1st LAr compartment;
- Loose associated track quality

• “Tight”

- Medium cuts and:
- Isolation (ratio of ET in a cone $DR < 0.2$);
- Tight associated track quality, tight cluster-track position, ratio E/p;

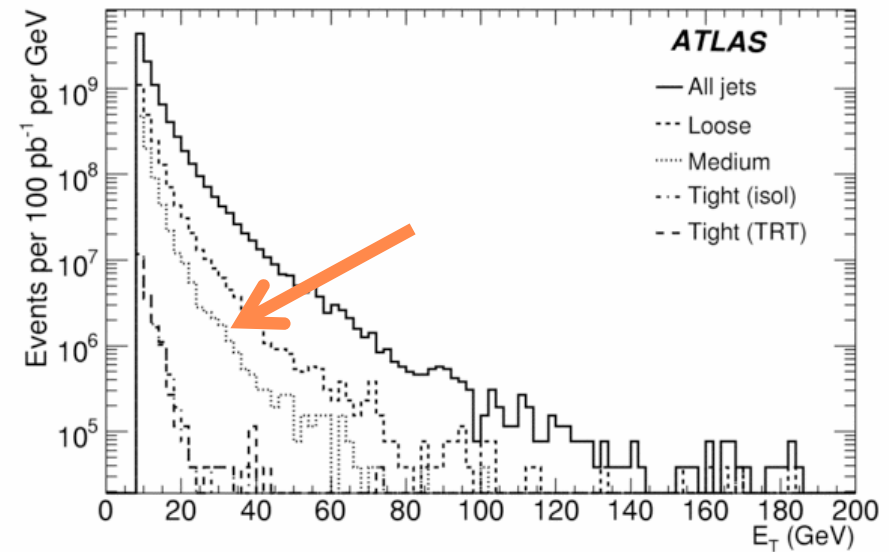
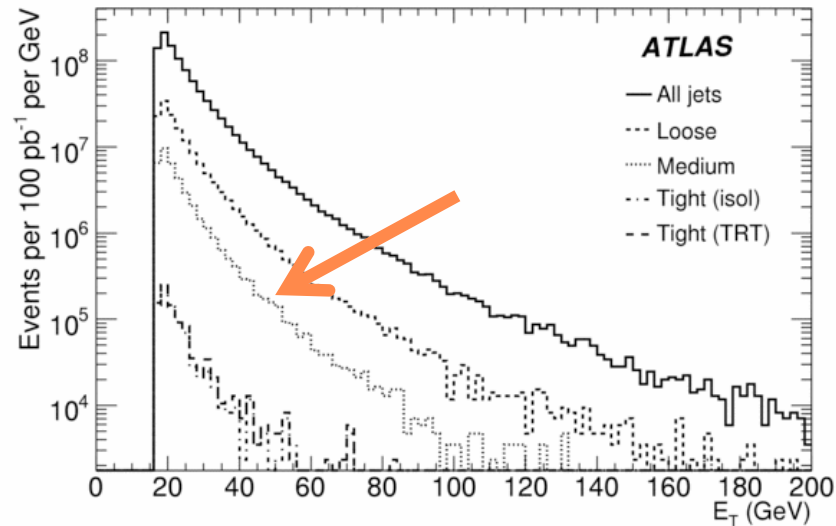
$$H \rightarrow ZZ^* \rightarrow 4e$$



Electron reconstruction efficiency as a function of E_T (left) and η (right). Reconstructed electrons of a Higgs boson sample of 130 GeV mass decaying into four electrons are used.

The electron reconstruction efficiency will have to be monitored with care.

$$H \rightarrow ZZ^* \rightarrow 4l$$



Differential cross-sections as a function of E_T before identification cuts, and after loose/medium/tight cuts, for an integrated luminosity of 100/pb and for the simulated filtered di-jet sample (left; $E_T > 17$ GeV) and for inclusive jets ($E_T > 8$ GeV)

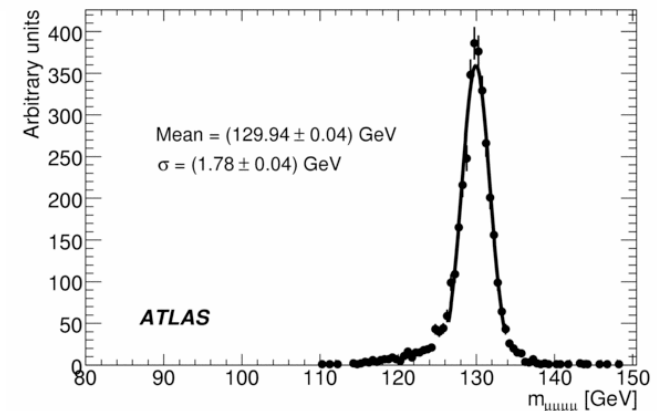
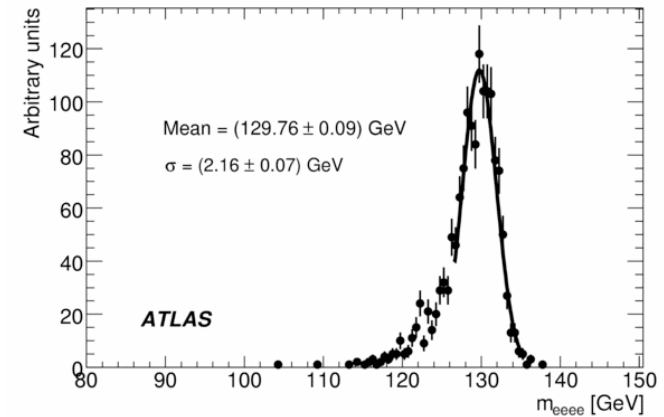
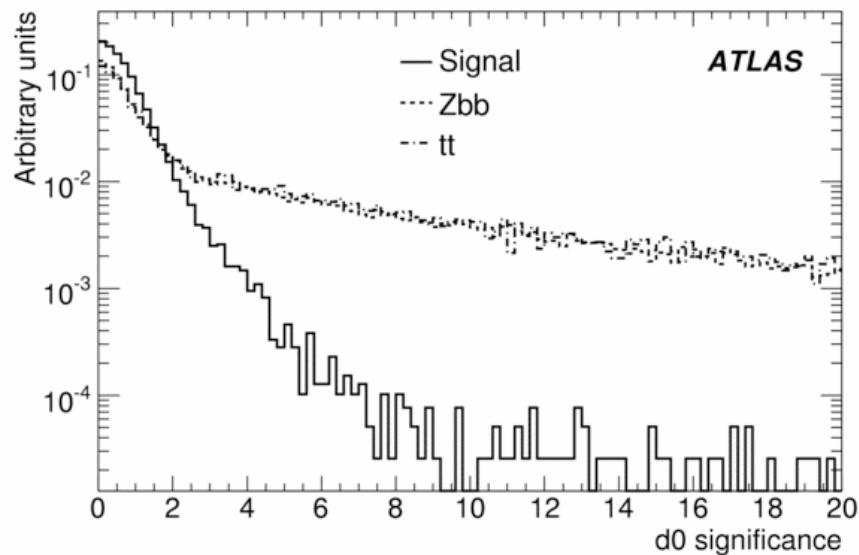
The electron quality needs to be “good” to make sure fake electrons produced by jets are rejected below an acceptable level.

$$H \rightarrow ZZ^* \rightarrow 4l$$

- Main backgrounds: diboson production (ZZ,WZ,...), ttbar, Zbbbar, but also Z+jets has to be monitored very carefully...
- This channel is powerful also because it allows an “easy” background measurement from data (side bands, invariant mass fits, ...)
 - However it could suffer from low event statistics, in particular with early data analyses.
- Analysis:
 - Two same flavor opposite charge leptons with $p_T > 20$ GeV, other two same flavor opposite charge leptons $p_T > 7$ GeV; all in $|\eta| < 2.5$;
 - Electrons must be “medium” quality;
 - Muons are “combined”, i.e. reconstructed in both ID and MS;
 - Reconstruction of (at least) a Z;
 - Mass window around the Higgs peak;

$$H \rightarrow ZZ^* \rightarrow 4l$$

- The kinematic selection will not be sufficient to suppress the $t\bar{t}$, $Zb(\bar{b})$ and Z +jets background: the heavy-flavour lepton production (genuine or fake) is not tolerable \rightarrow measure the association of selected leptons to the primary vertex, as well as their isolation.

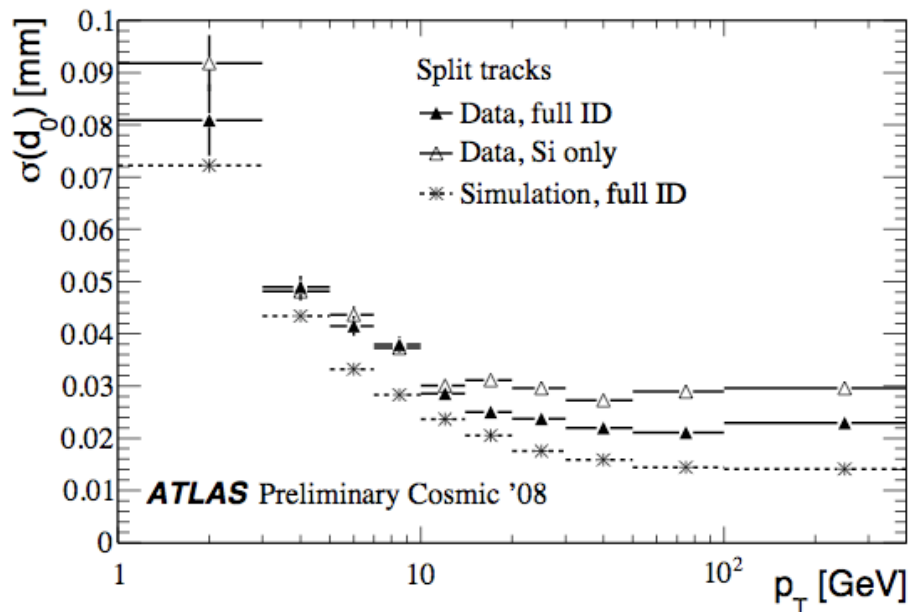
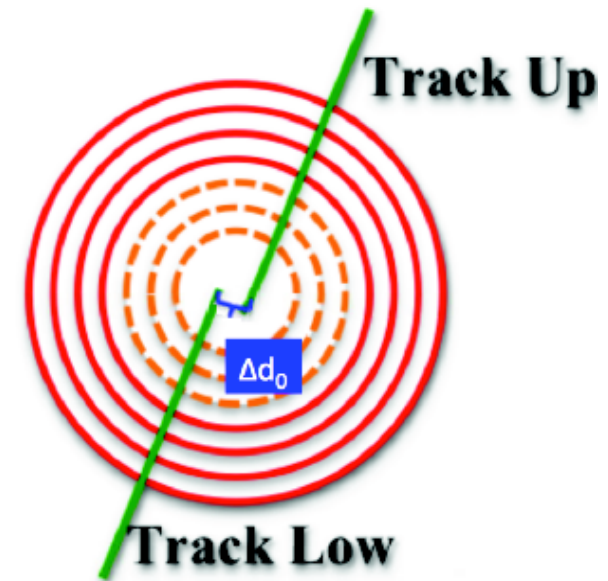


Reconstructed $H(130 \text{ GeV}) \rightarrow 4e$ (top) $H \rightarrow 4\mu$ (bottom) mass after application of the Z-mass constraint fit.

$$H \rightarrow ZZ^* \rightarrow 4l$$

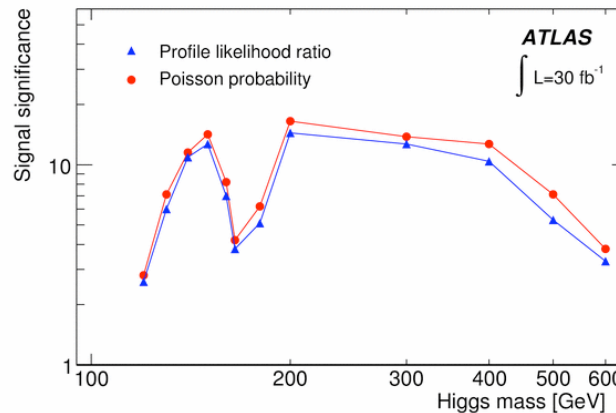
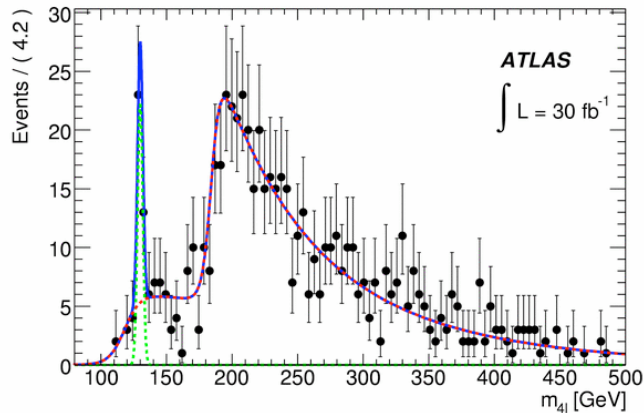
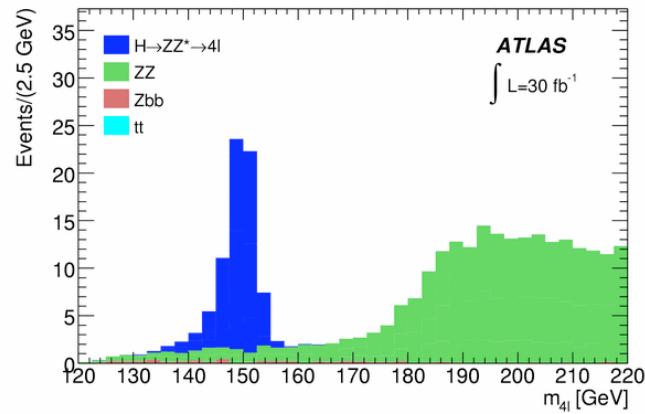
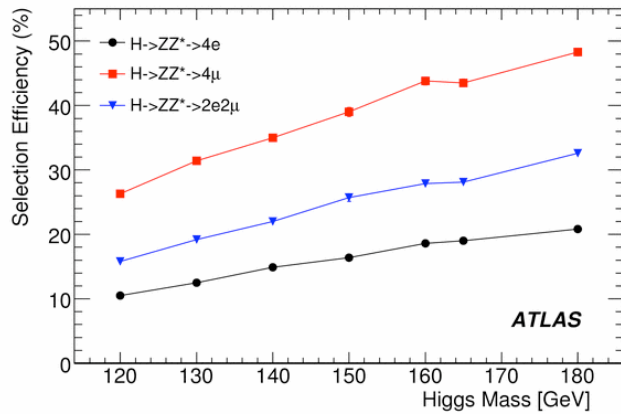
Alignment of the ID will be crucial to not only measure with high precision the track transverse momentum and the Primary Vertex, but also to evaluate the track association to that vertex.

Furthermore, the calo isolation is also crucial to reject leptons associated to jets.



Plot: Cosmic tracks crossing the entire ID leave hits in both the upper and lower halves of the ID. These tracks can be split near the interaction point and fit separately, resulting in two collision-like tracks that can then be compared. The plots shows the difference in the z_0 track parameter between the two split tracks.

$H \rightarrow ZZ^* \rightarrow 4l$



Left: Selection efficiency as a function of the Higgs boson mass, for each of the three decay channels, for the case of only one on-shell Z.

Right: Reconstructed 4-lepton mass for signal and background processes, in the case of a 150 GeV Higgs boson, normalized to a luminosity of 30 fb^{-1} .

Left: A pseudo-experiment corresponding to 30 fb^{-1} of data for a Higgs boson mass of 130 GeV. The functions fitting the signal and the background are shown.

Right: Significance obtained from the profile likelihood ratio, as a function of the Higgs boson mass. The result is compared with the one not including systematic errors on signal and the significance has been calculated using Poisson statistics.

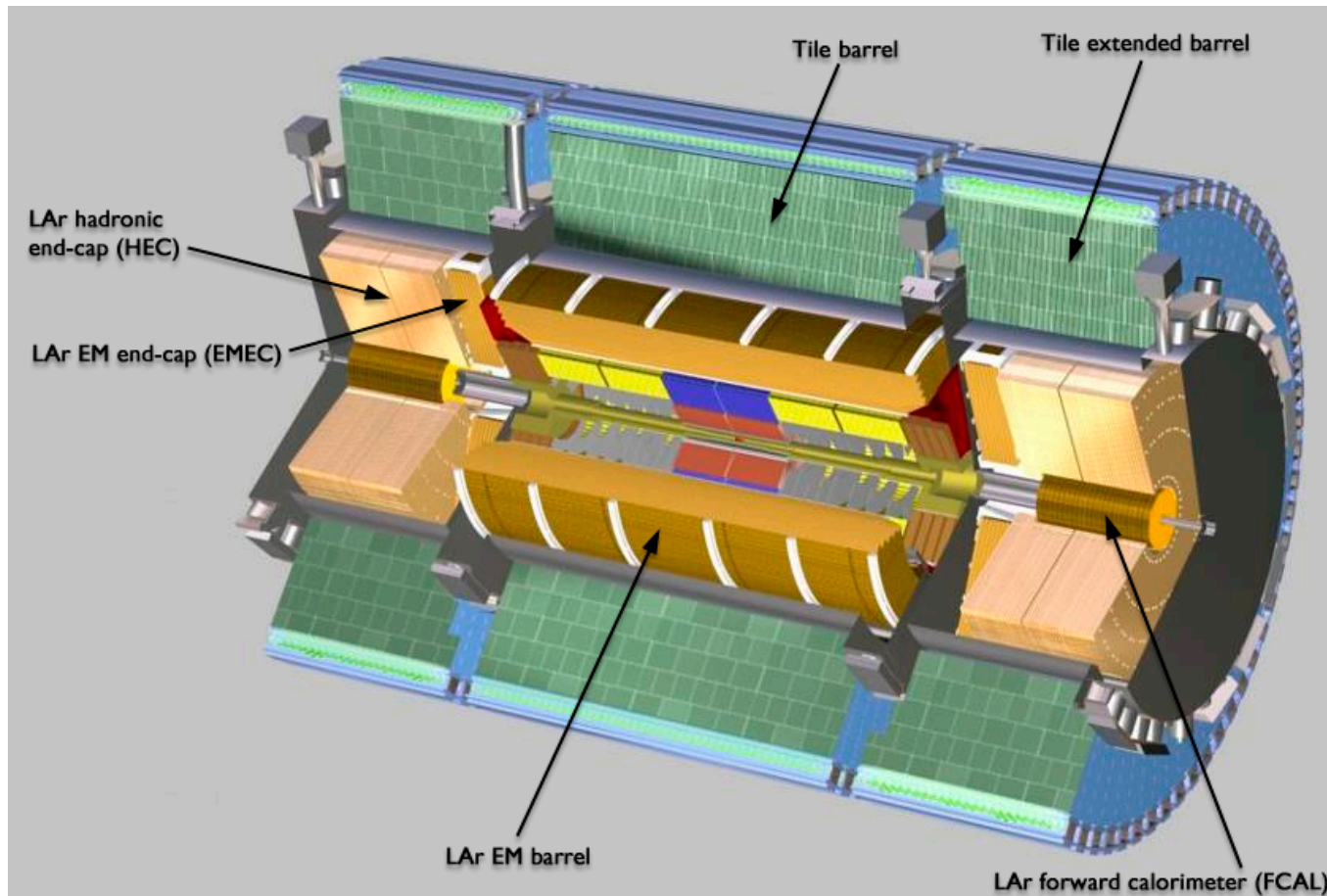
Event yield

	L=10/fb	120 GeV	130 GeV	150 GeV
Signal		2.8	8.2	19.4
Backg.		14.9	19.7	17.2

$$H \rightarrow WW^{(*)} \rightarrow 2l/2\nu$$

- The experimental signature is 2 leptons (electrons or muons) + transverse missing energy (E_T^{miss}) (+ jets if VBF processes are explored).
- Particularly interesting for $2M_W < M_H < 2M_Z$ (but its sensitivity extends also to lower masses) where all other decay modes are suppressed.
- No mass peak \rightarrow use transverse mass; counting experiment.
- High background, needs to be well understood: WW, Wt, ttbar, $Z \rightarrow 2l$, ..., and measured from data.
- Reconstruction:
 - Two processes: 0 jets (gg-fusion) or 2-forward jets (VBF).
 - Trigger : single or double lepton selection
 - ATLAS: 1 μ 20i or 1e25i;
 - Offline: select events with exactly two isolated (tracking and calorimeter) opposite sign primary leptons and E_T^{miss} .

$$H \rightarrow WW^{(*)} \rightarrow 2l/2\nu$$



The ATLAS Calorimeter(s)

A. Nisati, Preparing for the SM Higgs ...

$$H \rightarrow WW^{(*)} \rightarrow 2l/2\nu$$

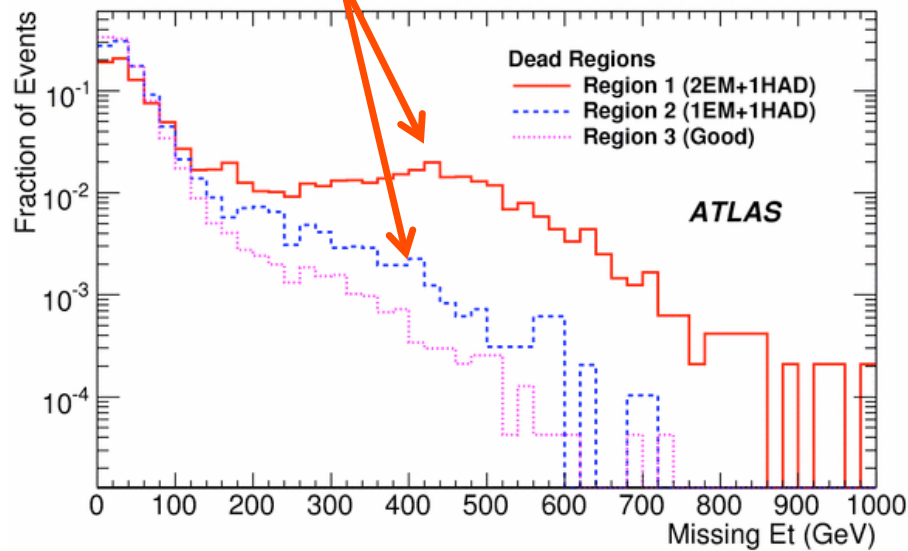
- This channel strongly depends also on the quality of the reconstruction of the transverse missing Energy E_T^{miss} ;
 - $E_T^{\text{miss}}(x,y) = -[\sum_{i=\text{calo_cells}} E_T^{\text{Calo}}(x_i,y_i) + \sum_{j=\text{muons}} E_T^{\text{MS}}(x_j,y_j)]$;
 - $E_T^{\text{Calo}}(x_i,y_i)$ is the $x(y)$ component of the transverse energy measured by Calorimeter cells (after noise suppression);
 - $E_T^{\text{MS}}(x_j,y_j)$ is the $x(y)$ component of the muon transverse momentum measured by standalone Muon System (MS);
- The two main problems with E_t^{miss} :
 - The “energy scale” associated to E_t^{miss} (linearity) and the its resolution;
 - Importance of calibration; global calibration (using energy density); or “Refined” calibration (looking to the nature of the object hitting the calo cells)
 - The “fake” E_t^{miss} ;

$$H \rightarrow WW^{(*)} \rightarrow 2l/2\nu$$

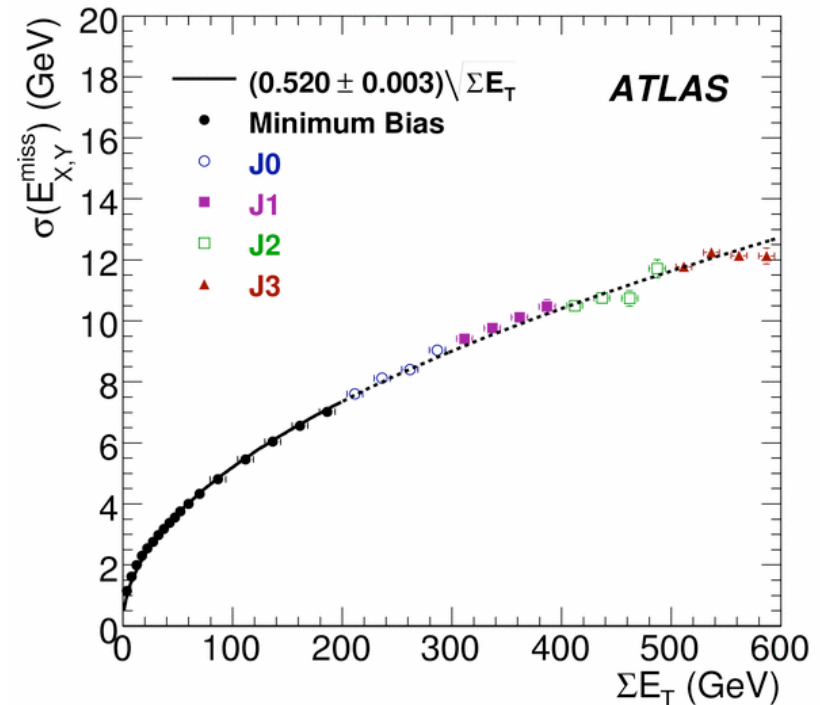
- The fake E_t^{miss} sources:
 - From muons;
 - Unreconstructed muons \rightarrow produce E_t^{miss} in the muon direction;
 - Fake muons \rightarrow produce E_t^{miss} in the direction opposite to the muon;
 - Badly measured muons \rightarrow produce E_t^{miss} in the same/opposite direction of the muon;
 - From calorimeter:
 - Non-instrumented regions, cracks, ...;
 - Jet energies badly reconstructed;
 - From instrumental effects:
 - In real data there will be sources of E_t^{miss} sources which are not modeled in Monte Carlo simulations: examples: mis-modeling of material distribution, dead/hot cells not masked, hw failures (High Voltage, Low Voltage, ReadOut,...)

$$H \rightarrow WW^{(*)} \rightarrow 2l/2\nu$$

Instrumental MET!



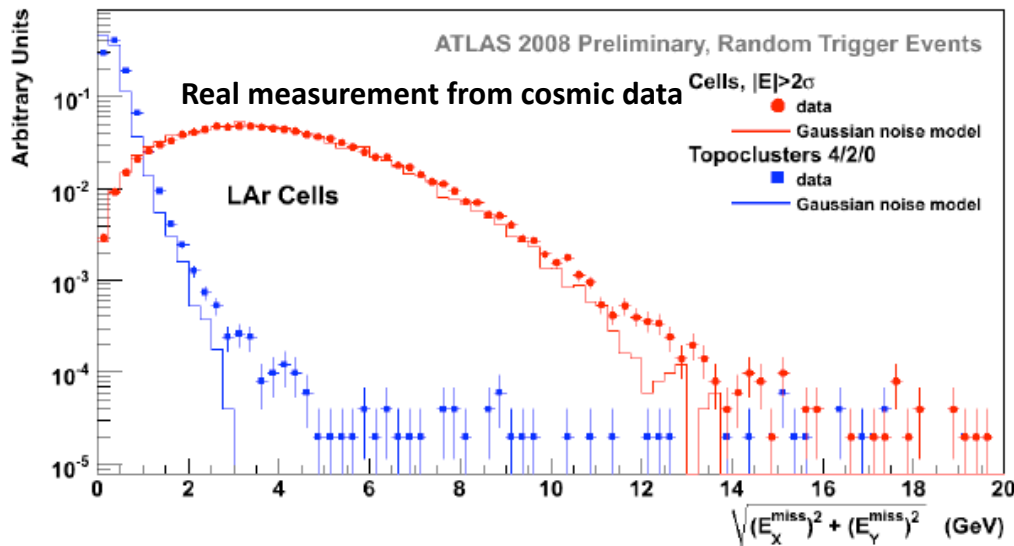
In this plot, we compare the E_t^{miss} distribution produced by QCD MC events reconstructed with the nominal ATLAS detector (Region 3), killing one EM Calorimeter RO crate and one HAD Calorimeter RO crate (Region 1), and killing two EM crates and one HAD crate (Region 2).



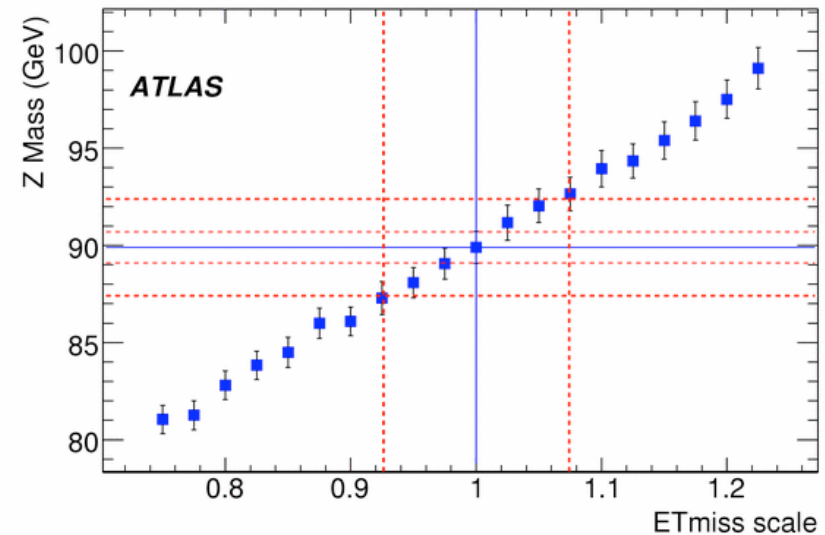
One of the first MET measurement we'll do!

The $E_t^{\text{miss}}(x,y)$ resolution as a function of ΣE_T in minimum bias and dijets events. An integrated luminosity of the order of $10^{-5}/\text{pb}$ is used.

$$H \rightarrow WW^{(*)} \rightarrow 2l/2\nu$$



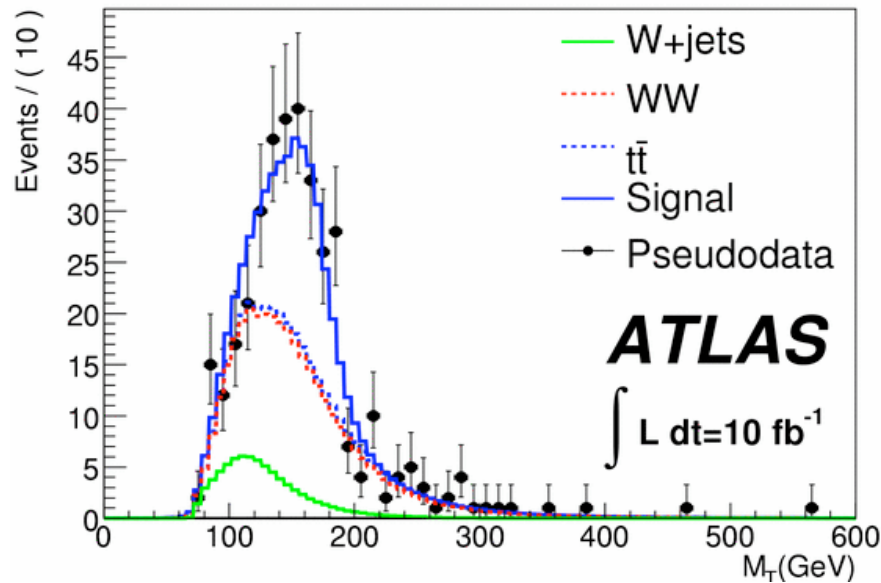
Cosmic data: Inclusive distributions of E_T^{miss} measured in events taken with random trigger. Different methods to define cell clusters are used. A comparison with MC expectations based on a Gaussian model of the noise is also shown.
 → We have a very good starting point for the understanding of the MET in our detector!



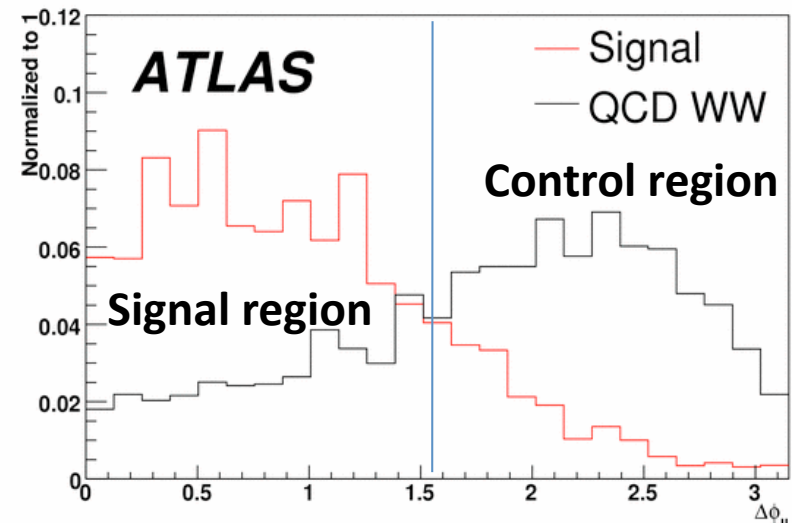
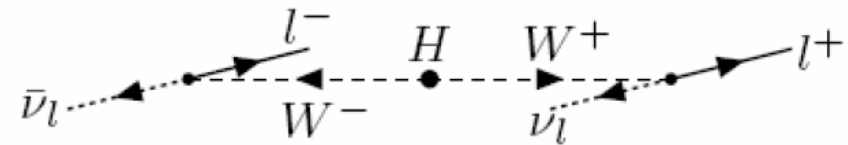
Reconstructed invariant mass of the pair of τ leptons for $Z \rightarrow \tau\tau$ decays as a function of the E_T^{miss} scale. The horizontal lines correspond to $\pm 1\sigma$ and to $\pm 3\sigma$ w.r.t. the Z peak position. The analysis is based on an integrated luminosity of 100 pb^{-1} of data.

We get a statistical accuracy of about 3%; including systematic effects we reach 8%. Similar results are obtained using $W \rightarrow l\nu$ events, with much less data.

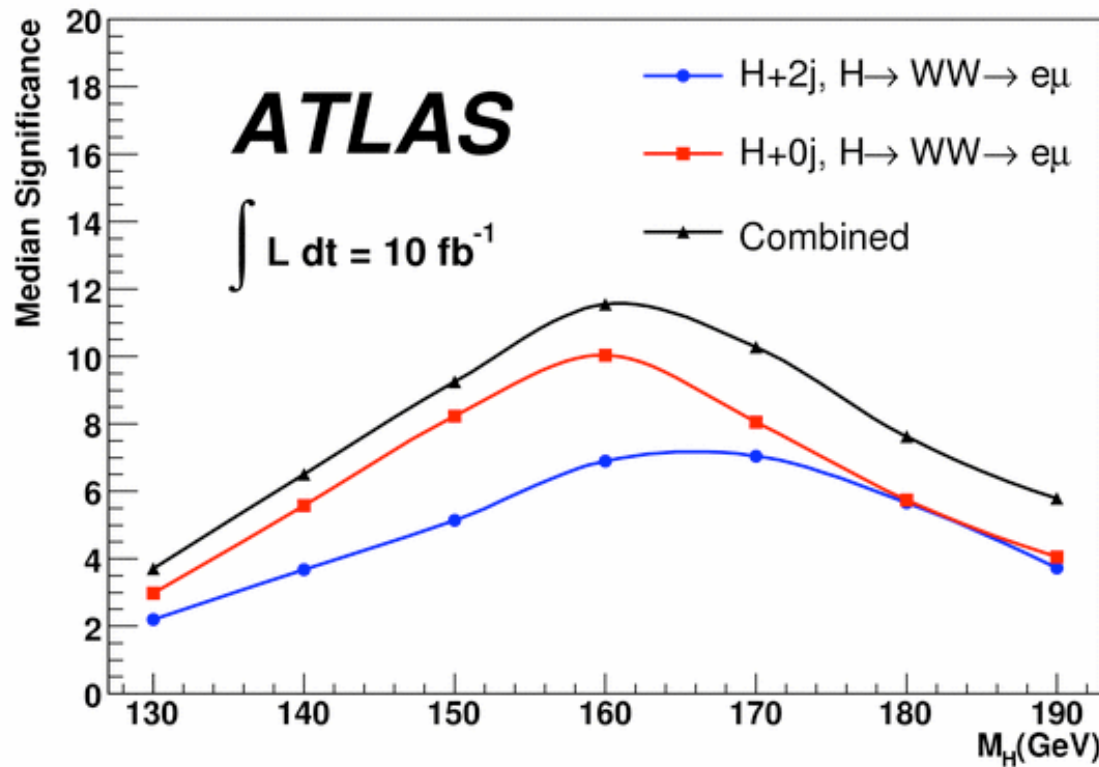
$H \rightarrow WW^{(*)} \rightarrow 2l 2\nu$



The challenge: we need precise knowledge of the backgrounds: fit the transverse mass and the transverse momentum of the candidates in two bins of the dilepton opening angle $\Delta\phi$ in the transverse plane; account for the ratio of the background in the two regions \rightarrow extract the signal and background mixture in the signal region.



$$H \rightarrow WW^{(*)} \rightarrow 2l/2\nu$$



$L = 1/\text{fb}$	$m_H = 170 \text{ GeV}$
Signal	50.6
Back.	126

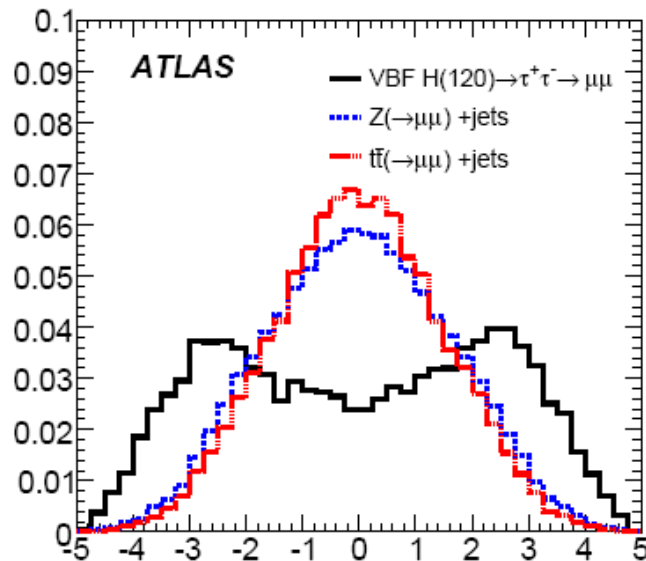
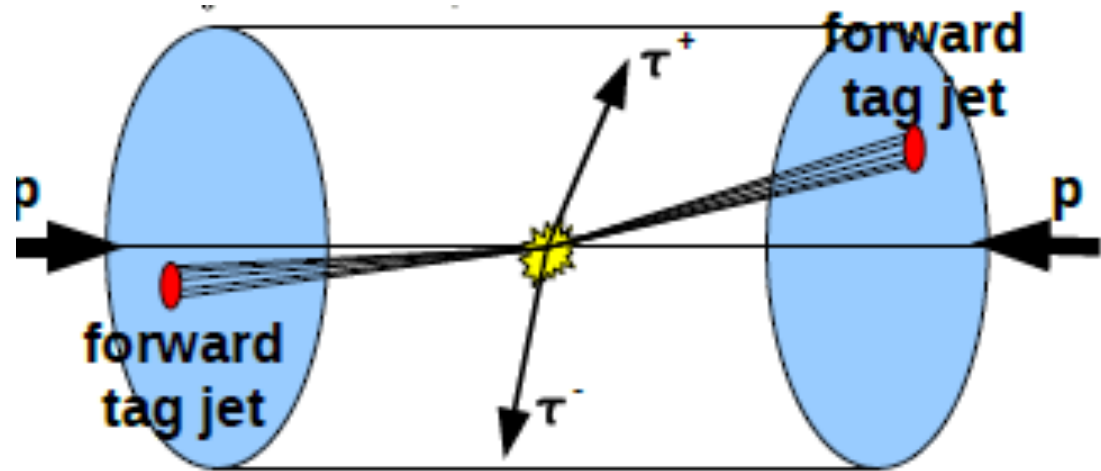
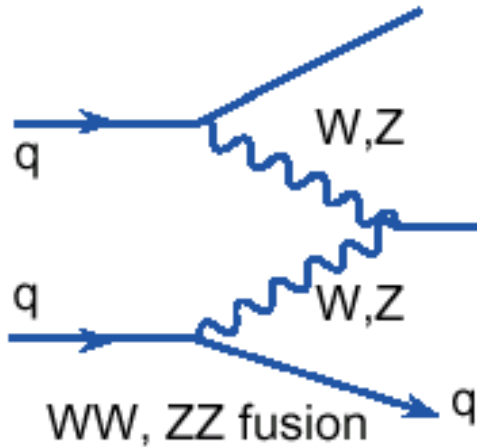
Number of events in 1/fb of data, for the 0-jet channel, $e\mu$ final state.

The expected significance at $L=10 \text{ fb}^{-1}$. The results expected from the gluon-gluon process, as well as the one from the VBF process, are shown

VBF $H \rightarrow \tau\tau$

- The SM Higgs decay to $\tau\tau$, for $m_H < 140$ GeV, is the channel with the largest branching ratio, after the dominant $b\bar{b}$ final state: about 7% at $m_H = 120$ GeV: it also offers the opportunity to search for the Higgs through di-fermion final states, and to contribute to the measurement of Higgs couplings.
- The VBF signature has an attractive S/B ratio;
- Three main sub-channels here:
 1. Both τ decay to leptons: $H \rightarrow \tau_l \tau_l$
 2. One τ decays to leptons, the other one hadronically: $H \rightarrow \tau_l \tau_h$
 3. Both τ 's decay hadronically: $H \rightarrow \tau_h \tau_h$The first 2 channels have been considered so far by ATLAS and CMS.

VBF $H \rightarrow \tau\tau$



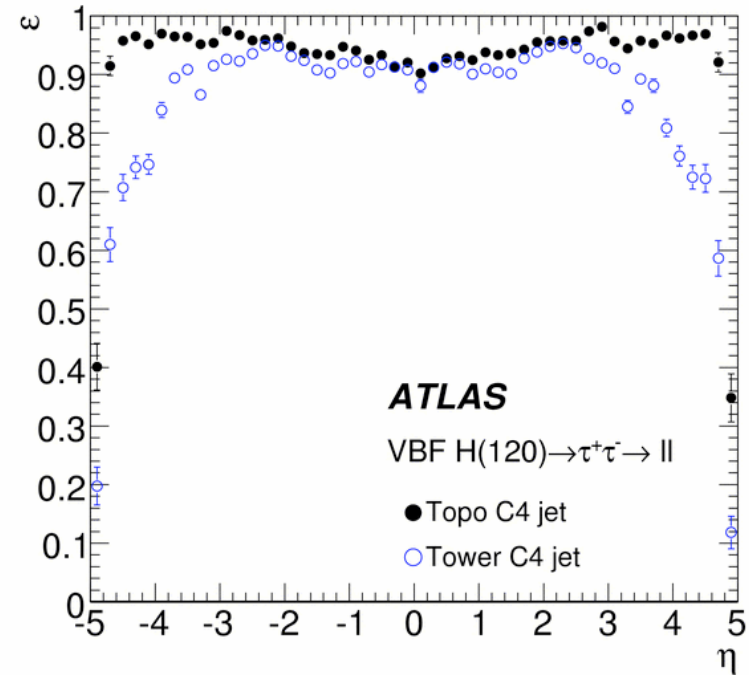
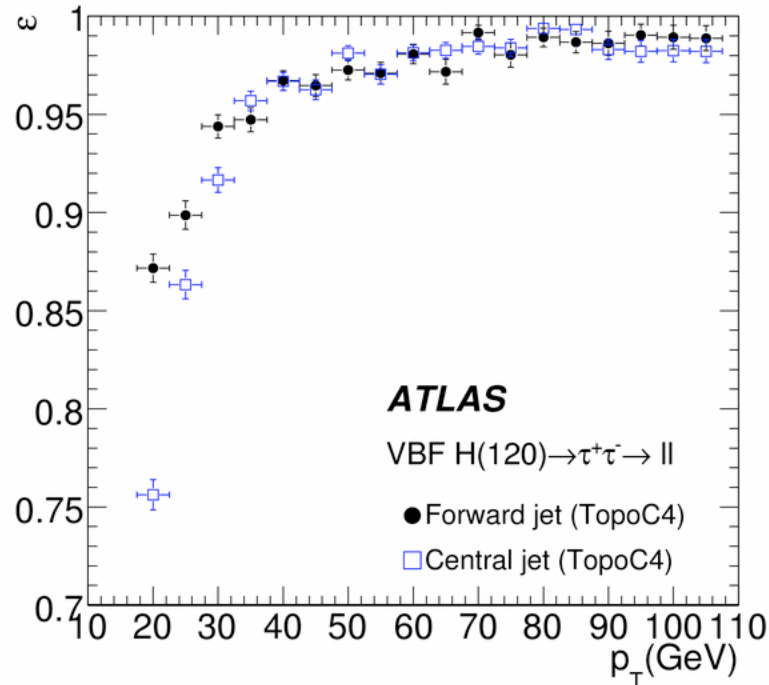
Two distinct signatures:

1. Two forward “tag” jets (large η separation with high- p_T) with large M_{jj}
2. No **jet** activity in the central region (no color flow between the two tag jets): jet veto.

VBF $H \rightarrow \tau\tau$

- Experimentally:
 - $H \rightarrow \tau_l \tau_l$; clean, see discussion made for electrons and muons, plus the missing transverse energy. BR = 12.4%;
 - $H \rightarrow \tau_l \tau_h$ involves **hadronic τ reconstruction** and missing transverse energy; BR = 45.6%;
 - $H \rightarrow \tau_h \tau_h$ involves **hadronic τ reconstruction** for both taus and missing transverse energy; BR = 42.0%;
 - Jet reconstruction;
- **The challenge:**
 - **Trigger on τ_h (in particular for purely hadronic final states);**
 - **Efficient τ_h identification with high separation from fake- τ originating from QCD jets.**
 - **Good tau energy resolution (in conjunction with very good $E_{T\text{miss}}$ energy resolution)**
 - **Jet reconstruction down to low energies and large rapidity.**

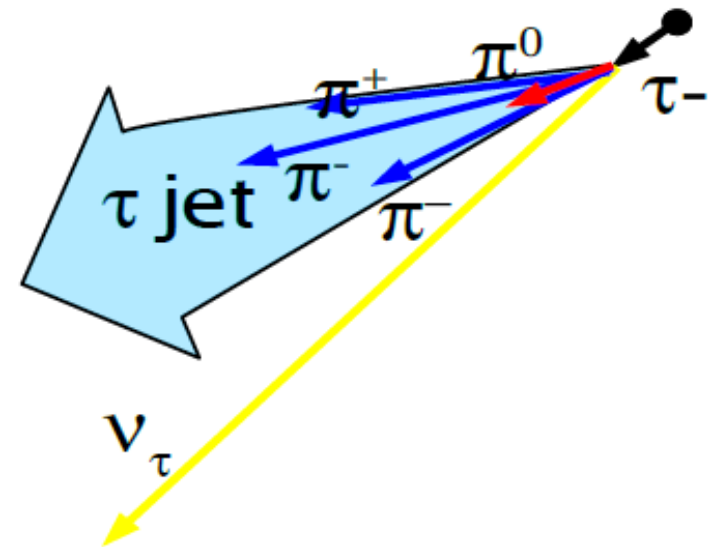
VBF H \rightarrow $\tau\tau$



Jet reconstruction efficiency for the Cone jet algorithm with $R = 0.4$ as a function of the generator-level jet p_T for the jets based on TopoClusters (a) and η for Tower- and TopoCluster-based jets (b).

VBF $H \rightarrow \tau\tau$

- The tau appears as a narrow jet of particles with aperture m_τ/E_τ ;
- Composition: mostly neutral and charged pions (1 or 3);
- \rightarrow look for narrow isolated cluster of calorimeter cells (both electromagnetic and hadronic), associated to a pencil jet of a small number of charged tracks pointing to the cluster barycentre.
- Two algorithms are developed in ATLAS (the so-called **cluster-based** and **track-based**), used together.



VBF $H \rightarrow \tau\tau$

Reconstruction

- 1) seed: **jets, with $ET > 10$ GeV**
- 2) all cells with $\Delta R < 0.4$ around the barycentre are H1-style calibrated for energy estimation
- 3) tracks within $\Delta R < 0.3$ and $p_T > 1$ GeV from the cluster centre are assigned to Candidate
- 4) Direction from leading associated track

Parameters used to identify tau objects:

- **REM** – the radius of the EM cluster
- **Isolation fraction** – the transverse energy deposited in isolation region ($0.1 < DR < 0.2$) divided by the energy in the cone $DR < 0.4$;
- **Electromagnetic and hadronic energies of cluster**
- **strip-width** – width of the cluster in the η -strip layer of EM calorimeter;
- **Nstrip-cells** – number of strip cells over energy threshold;
- **Ntrack** – track multiplicity of tau candidate
- ...

VBF $H \rightarrow \tau\tau$

→ The tau reconstruction and identification is a complex task!

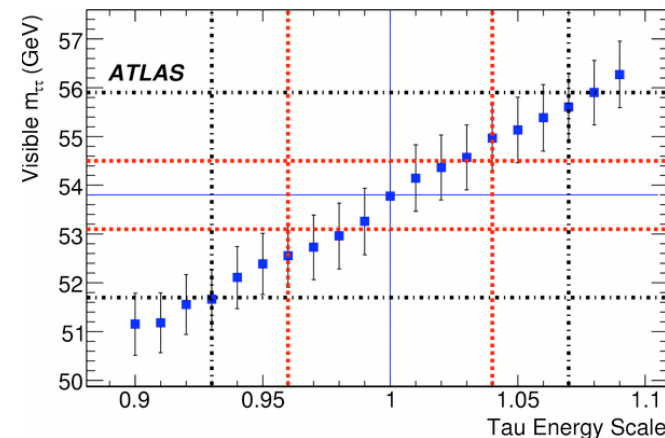
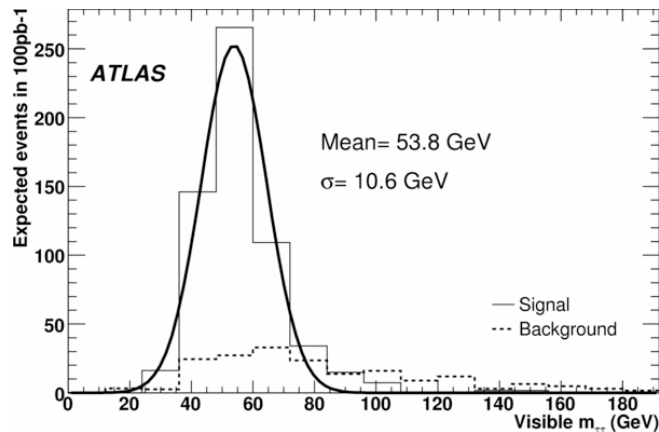
The understanding of this lepton in ATLAS with the first data will be crucial for search physics .

The reconstruction of $Z \rightarrow \tau\tau$ process, and the measurement of its production cross section will be mandatory to “commission” the tau reconstruction and identification in ATLAS.

The $W \rightarrow \tau\nu$ appears very attractive as its production cross-section times BR is ten times large, BUT it is more difficult from the trigger point of view, and for the analysis.

VBF $H \rightarrow \tau\tau$

- Analysis optimized for the first 200/pb; select opposite sign (OS) $l\tau_h$ events;
- Trigger on high-pT electrons/muons to collect a sample of $Z \rightarrow \tau\tau \rightarrow l\nu\nu\tau_h\nu$ events with very low background which then can be used to determine the τ_h energy scale, and then the E_T^{miss} scale from the complete Z reconstruction (including neutrinos)



Left: The reconstructed visible mass of the ($l\tau_h$) pair for $Z \rightarrow \tau\tau$ decays (solid line) and QCD, $W \rightarrow l\nu$, $Z \rightarrow ll$ backgrounds (dashed line). Right: The reconstructed visible mass of the ($l\tau_h$) pair from $Z \rightarrow \tau\tau$ decays as a function of the τ_h energy scale (right). The dashed lines correspond to $\pm 1\sigma$ and $\pm 3\sigma$ with respect to the reconstructed peak position. The results were obtained with the calorimeter-based algorithm.

- Analysis of the same-sign (SS) events will monitor the mis-tag efficiency;

VBF $H \rightarrow \tau\tau$

VBF $H \rightarrow \tau\tau$

- **Trigger:** electron/muon trigger for leptonic/semi-leptonic channels; tau + E_T^{miss} trigger for the fully hadronic chan

Analysis

- Besides the VBF and E_T^{miss} cuts, thresholds for e/ μ / τ identification are optimized for identification efficiency and fake rejection.
- Low MT(l - E_T^{miss}) to reduce the W+jet background.
- jet veto (uncertainty on the robustness of the jet veto with respect to radiation in the underlying event and to the presence of pile-up: so far VBF channels studied at low luminosity only).
- The H mass can be reconstructed using the collinear approximation ($\Delta m \approx 8$ -10 GeV)

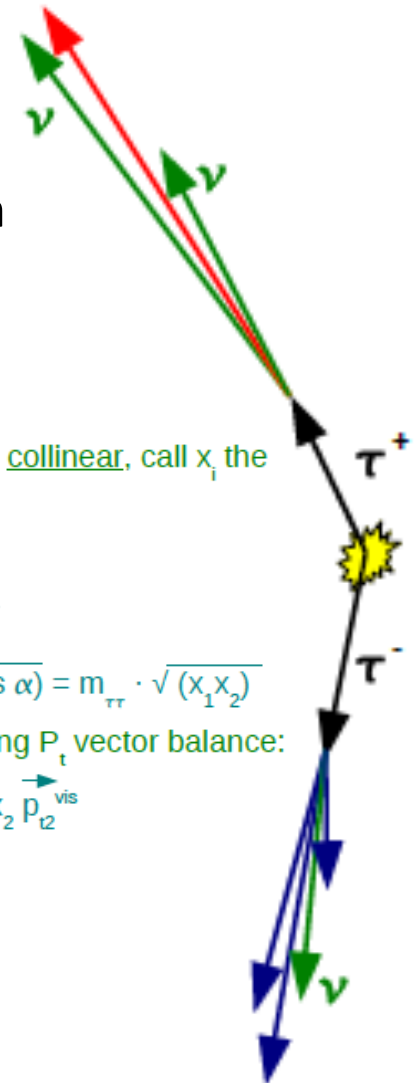
- Assume all τ decay products are collinear, call x_i the visible momentum fraction of τ_i :

- $m_{\tau\tau} = \sqrt{2 p_1 p_2 (1 - \cos \alpha)}$

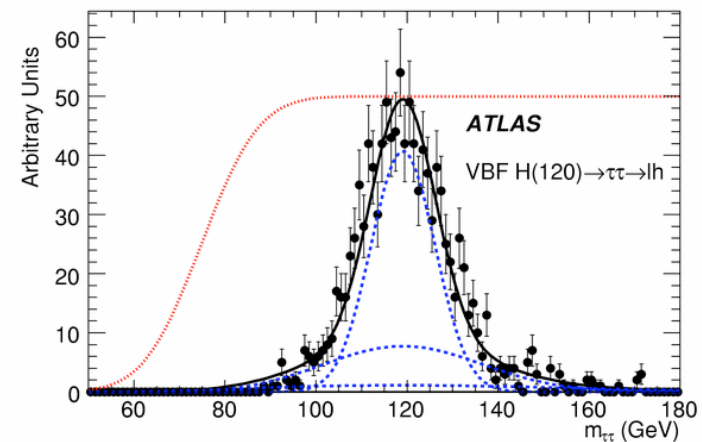
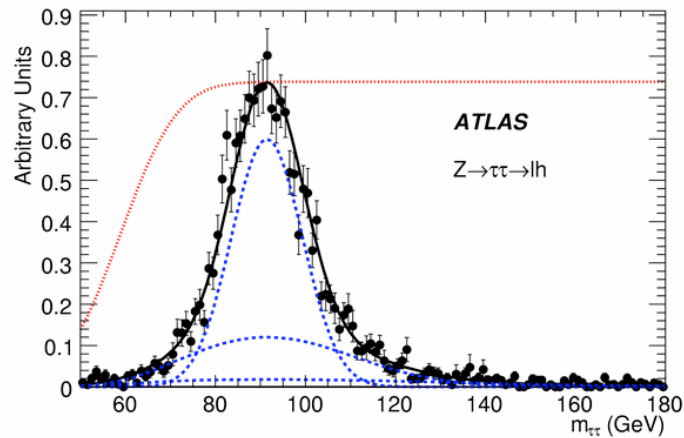
- $m_{\tau\tau}^{\text{vis}} = \sqrt{2 p_1^{\text{vis}} p_2^{\text{vis}} (1 - \cos \alpha)}$
 $= \sqrt{2 (x_1 p_1) (x_2 p_2) (1 - \cos \alpha)} = m_{\tau\tau} \cdot \sqrt{(x_1 x_2)}$

- solve for x_1, x_2 by imposing missing P_t vector balance:

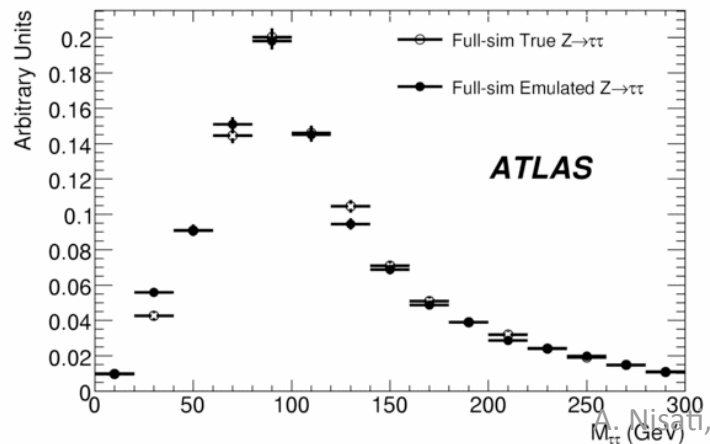
- $\vec{P}_t^{\text{miss}} = (1-x_1)/x_1 \vec{p}_{t1}^{\text{vis}} + (1-x_2)/x_2 \vec{p}_{t2}^{\text{vis}}$



VBF H \rightarrow $\tau\tau$



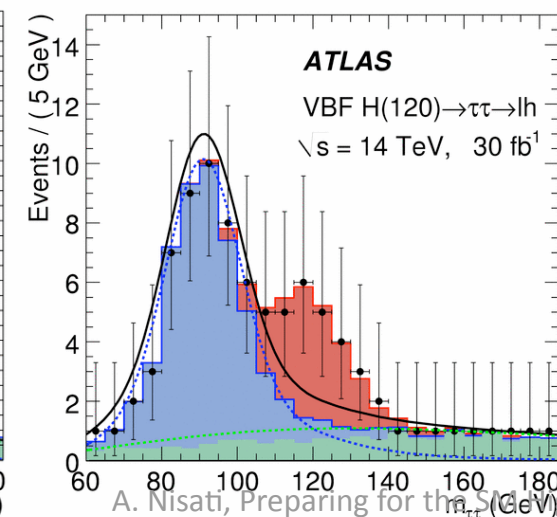
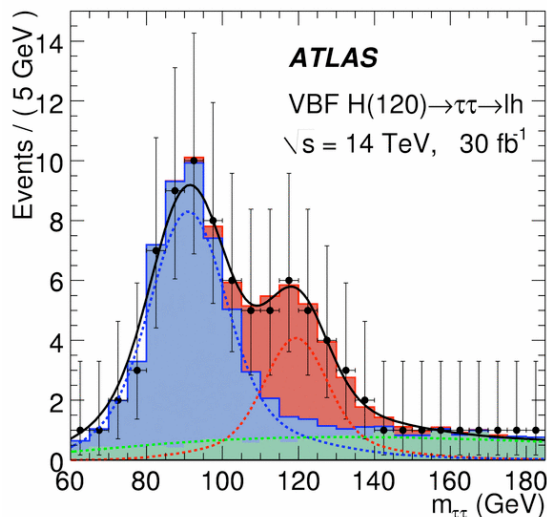
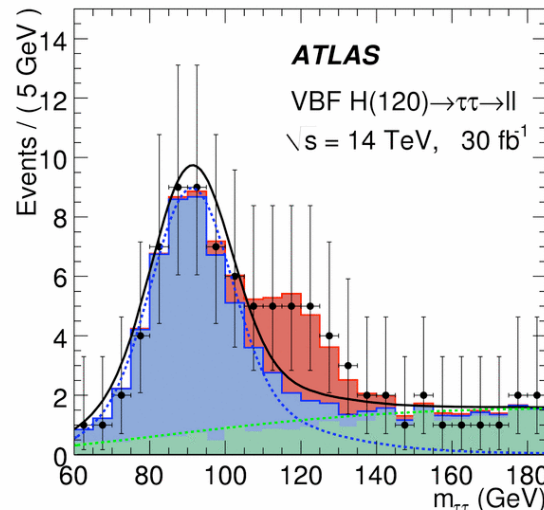
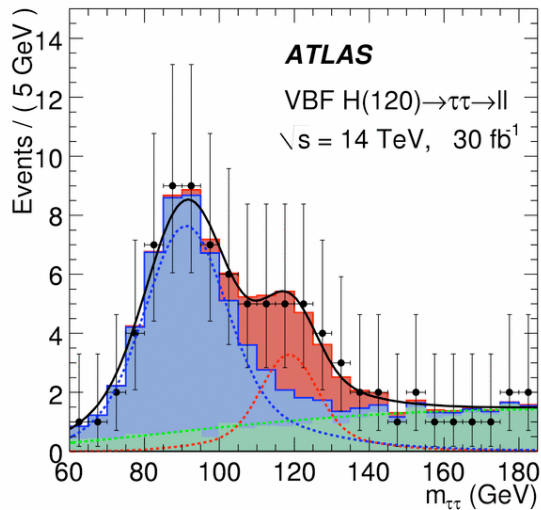
Figures (a) and (b) show the result of a fit to a pure Monte Carlo samples of $Z \rightarrow \tau\tau$ and signal ($m_H = 120$ GeV) in the lh -channel, respectively. The dashed lines represent the three components of the model and the dotted curve represents the $\text{erf}()$ efficiency envelope. These samples do not include pileup.



Measurement of the $Z \rightarrow \tau\tau$ + jets background shape, after event selection, directly from real data:

- Select a clean sample of $Z \rightarrow \mu\mu$ events, replace the muons with taus (removing the average energy deposit in the calorimeter), and simulate the tau decays.
- Apply the analysis cuts.
- Normalize to the measured tau-tau invariant mass measured distribution.

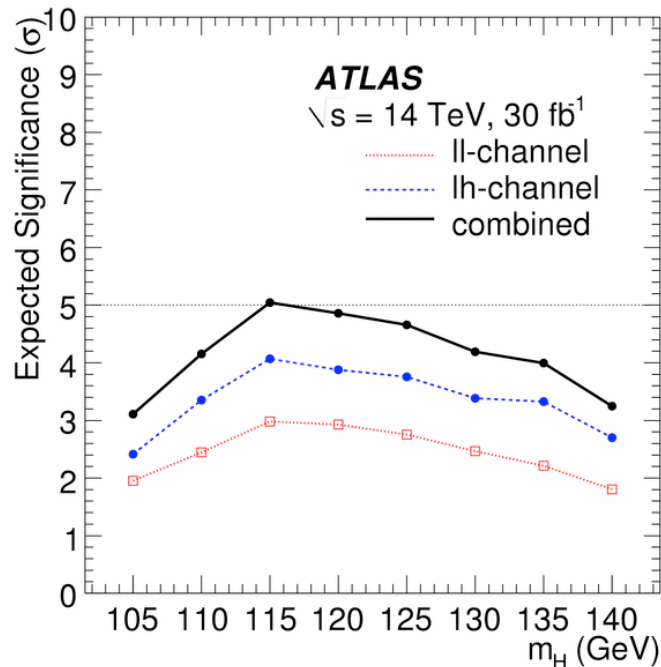
VBF H \rightarrow $\tau\tau$



Example of a fully data driven analysis: simultaneous fits to signal and control samples.

Fits to a data sample with the signal-plus-background (a,c) and background only (b,d) models for the ll- and lh-channels at $m_H = 120$ GeV with 30 fb^{-1} of data. Not shown are the control samples that were fit simultaneously to constrain the background shape. The fits are performed to the signal and background expectation (histograms), while the overlaid data with error bars are only indicative of a possible data set. These samples do not include pileup.

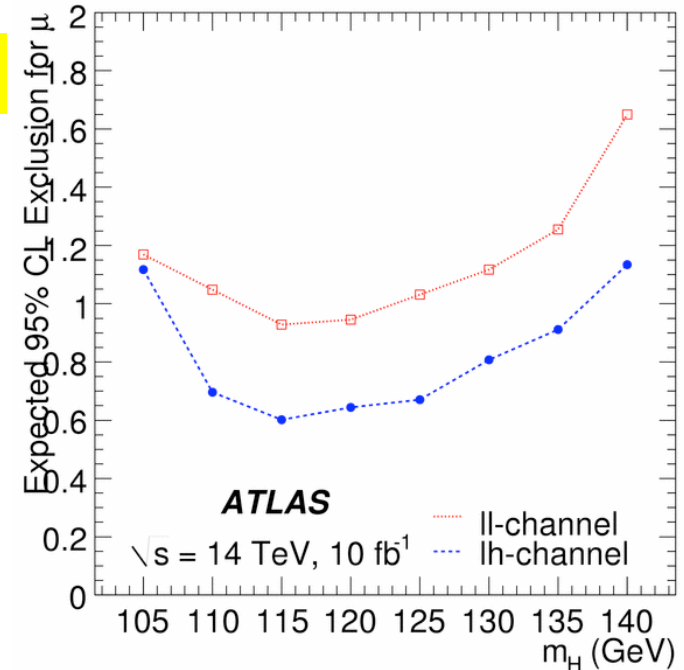
VBF $H \rightarrow \tau\tau$



$m_H = 120 \text{ GeV}; L=30/\text{fb}$

Event yield

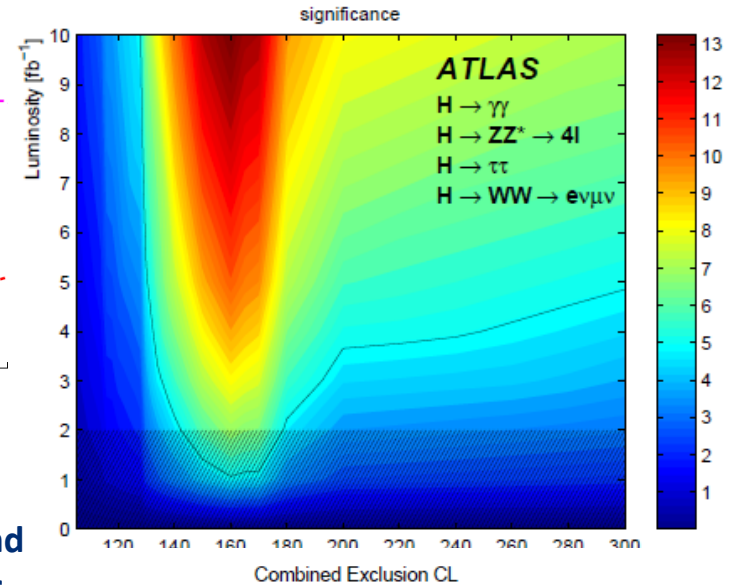
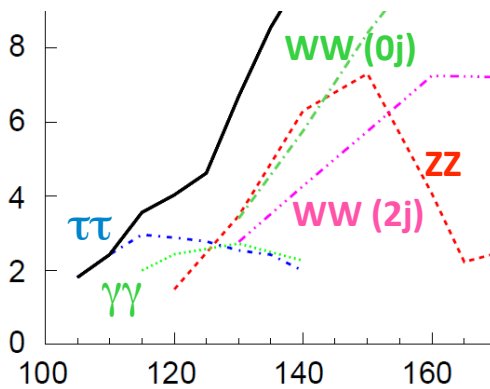
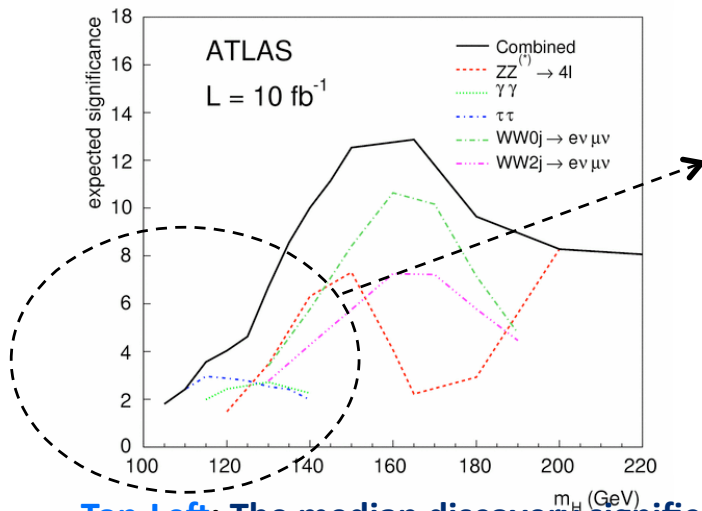
	signal	back.	S/B
ll	13.5	13.3	1/1
lh	18.3	6.3	3/1
hh	10.2	37	1/4



Expected signal significance for several masses based on fitting the $m_{\tau\tau}$ spectrum. Background uncertainties are incorporated by utilizing the profile likelihood ratio. These results do not include the impact of pileup.

Expected 95% exclusion of the signal rate in units of the Standard Model expectation, μ , as a function of the Higgs boson mass for the ll and lh-channels with 10 fb^{-1} of data. The exclusion takes into account t uncertainties on the signal efficiency.

SM Higgs Statistical Combination



Top-Left: The median discovery significance for the various channels and the combination with an integrated luminosity of 10 fb⁻¹ for the lower mass range.

Top-Right: Significance contours for different Standard Model Higgs masses and integrated luminosities. The thick curve represents the 5σ discovery contour. The median significance is shown with a colour according to the legend. The hatched area below 2 fb⁻¹ indicates the region where the approximations used in the combination are not accurate, although they are expected to be conservative.

Bottom: The expected luminosity required to exclude a Higgs boson with a mass m_H at a confidence level given by the corresponding colour. The hatched area below 2 fb⁻¹ indicates the region where the approximations used in the combination are not accurate, although they are expected to be conservative.

Conclusion

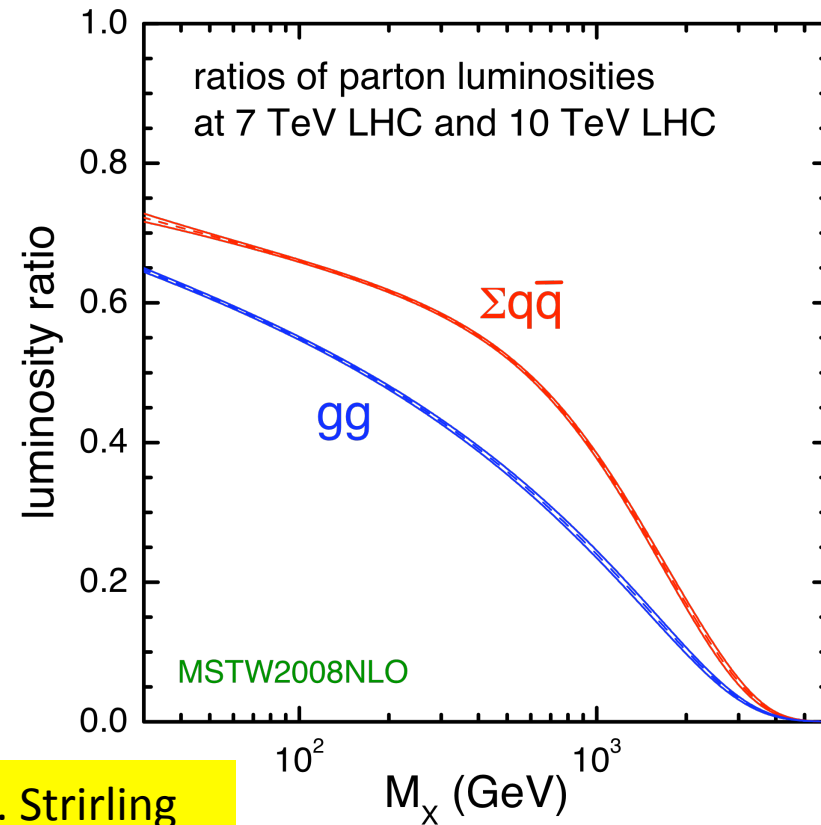
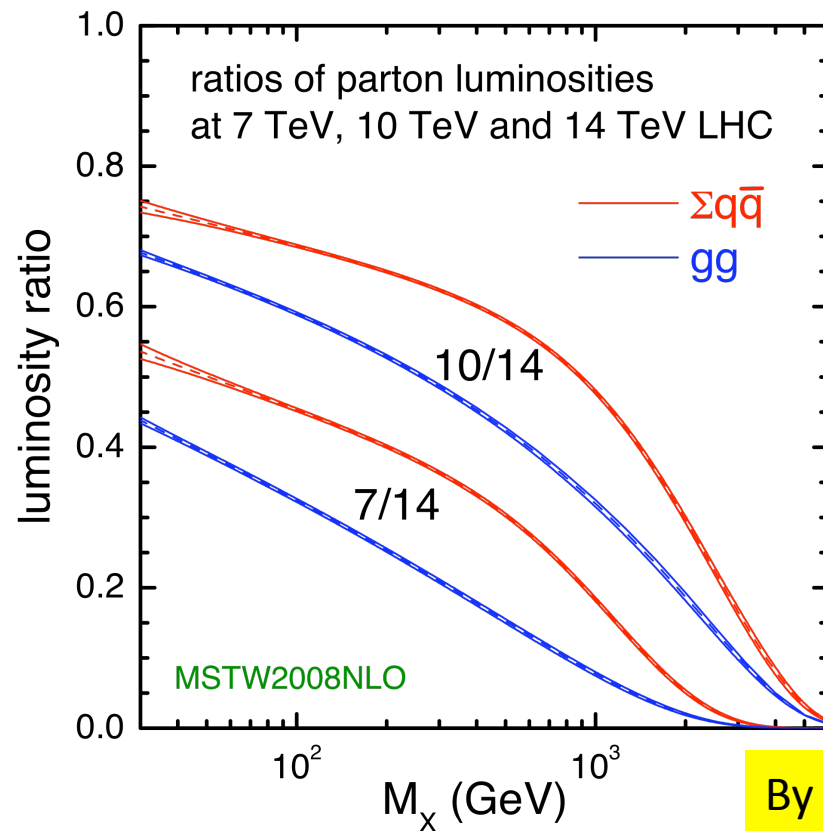
- The search for the Standard Model Higgs Boson at the LHC in the mass region between the LEP limit and $2M_Z$ will require the study of several final states, in particular for values of m_H close to 110 GeV: assuming $\sqrt{s}=14$ TeV, with a luminosity of 2fb^{-1} , the expected (median) sensitivity is at the 5σ level or greater for discovery of a Higgs boson in the mass range between 143 and 179 GeV;
- These final states do require a good level of understanding of the detector physics performance, of the reconstruction of photons, leptons, jets and MET;
- The measurement of SM backgrounds directly from data will be crucial to reveal new particle production processes;
- A very long season of MC studies, measurements performed in test-beam and cosmics stand experiments, as well as recent measurements performed with the ATLAS and CMS detectors with cosmic rays, allowed an initial and good understanding of our experimental apparatuses:
The calibration of the detector and the understanding of the initial data will take some time ... but have already some knowledge of our detector!
- **The real challenge...?? →**



...this is the challenge!!

BACKUP

LHC running at 7 – 10 – 14 TeV



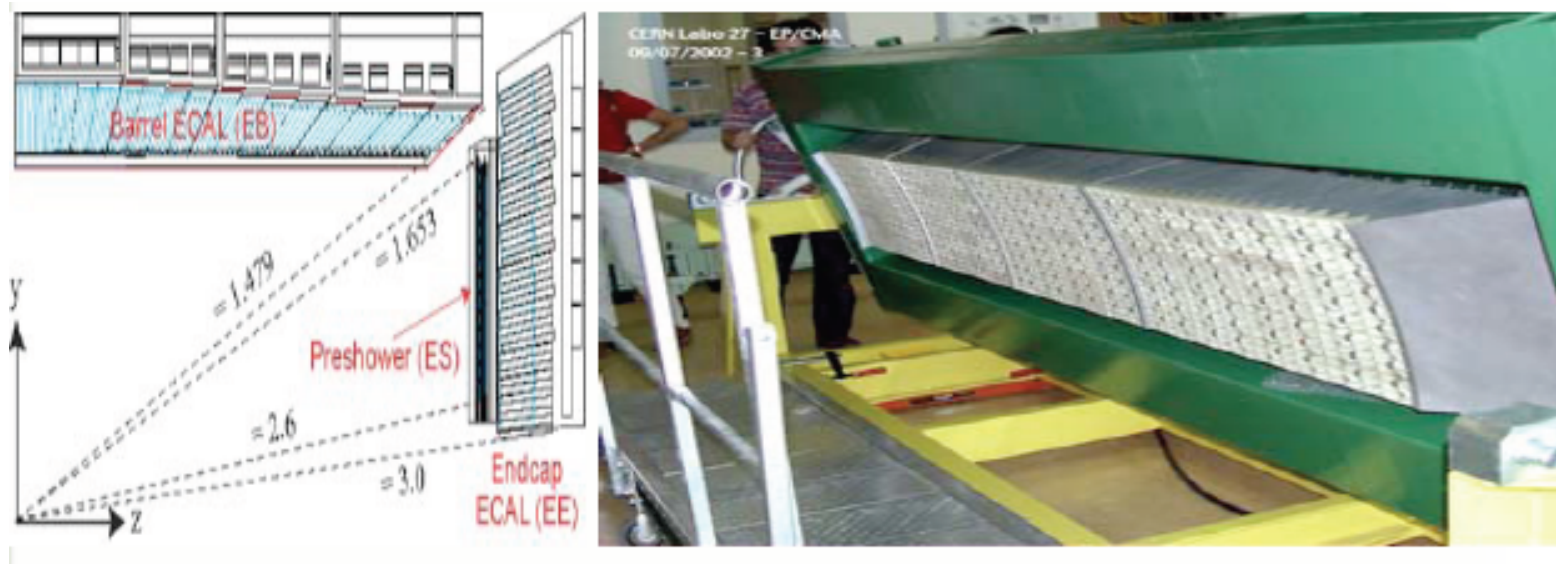
By J. Stirling

Examples of cross section suppression in going from 14 TeV to 7 TeV:

- $W, Z \sim 45\%$
- $H (120 \text{ GeV}) \sim 30\%$
- $Z' (1 \text{ TeV}) \sim 18\%$

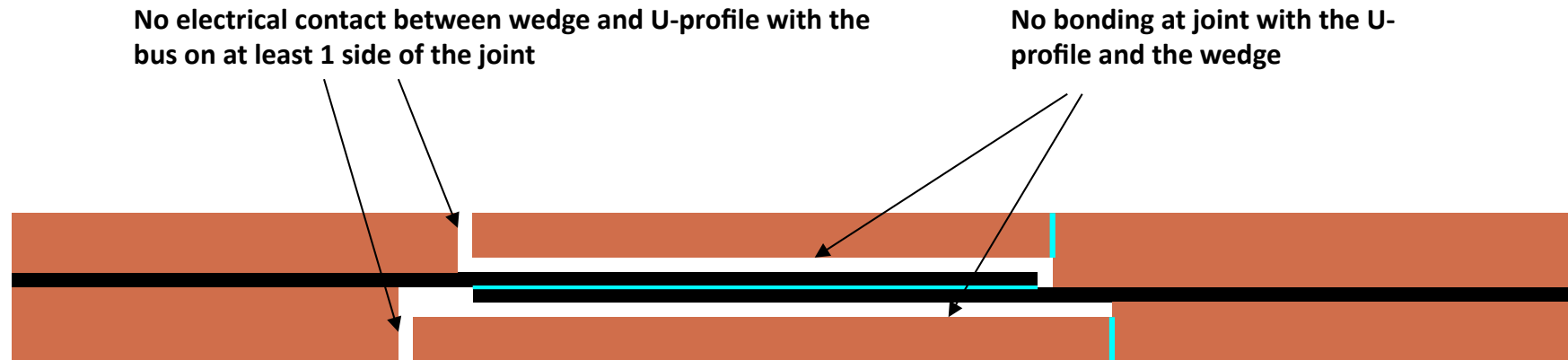
$$H \rightarrow \gamma\gamma$$

Different technology used by CMS, based on scintillating crystals.



Transverse section through the CMS ECAL, showing geometrical configuration and photograph of a CMS ECAL supermodule . The CMS ECAL is composed of $\sim 80,000$ lead tungstate (PbWO_4) scintillating crystals with a granularity of $\Delta\eta \times \Delta\phi = 0.0175 \times 0.0175$ in the barrel region.

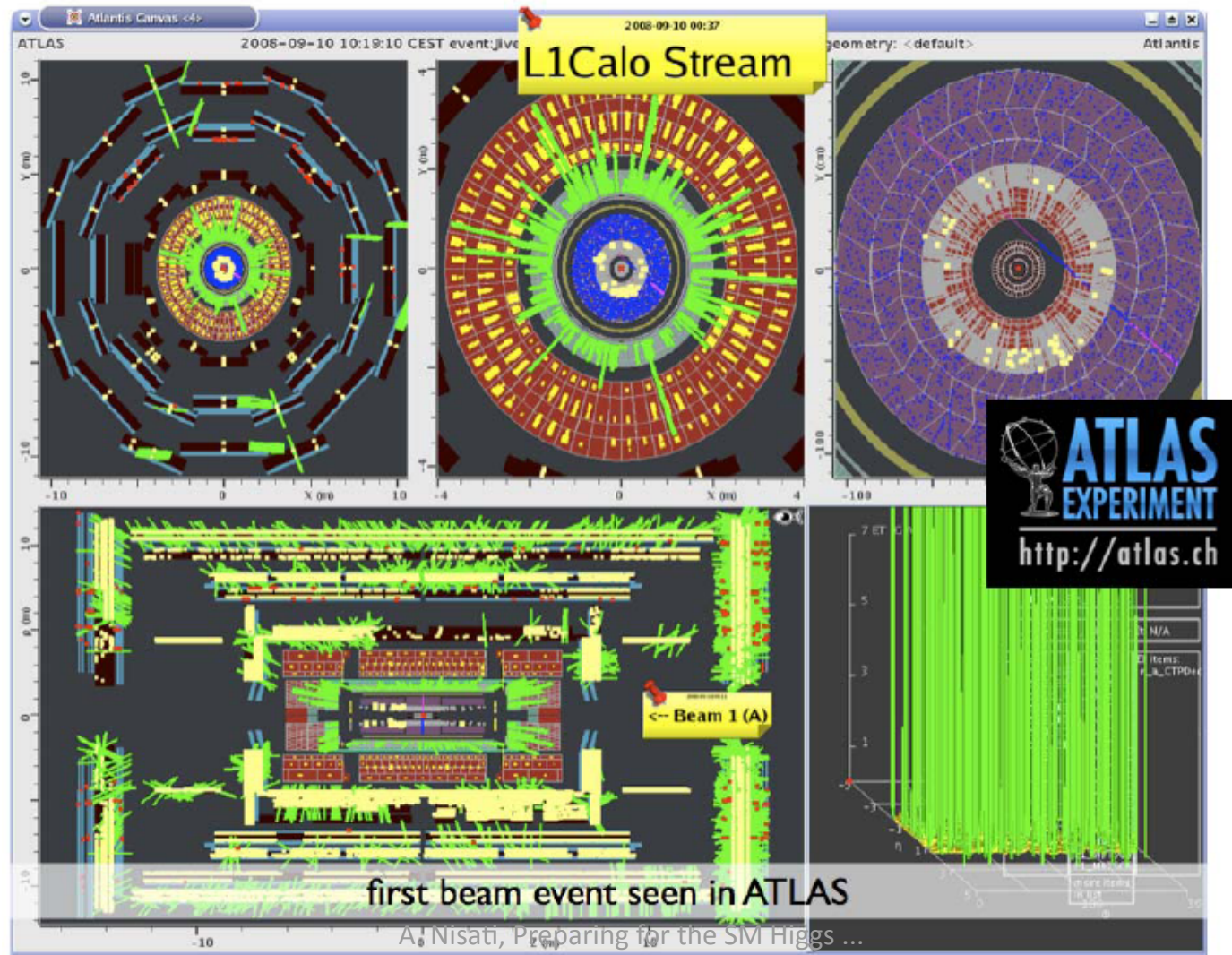
A resistive joint of about 220 nΩ with bad electrical and thermal contacts with the stabilizer



- ⇒ Loss of clamping pressure on the joint, and between joint and stabilizer
- ⇒ Degradation of transverse contact between superconducting cable and stabilizer
- ⇒ Interruption of longitudinal electrical continuity in stabilizer

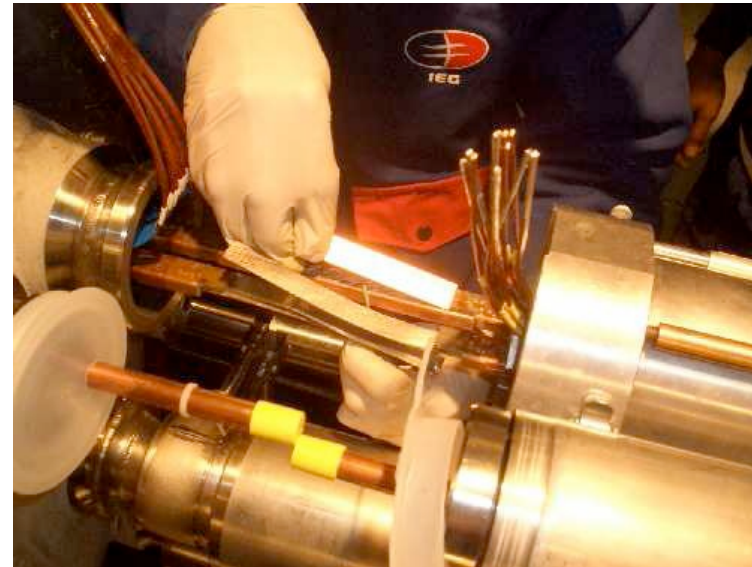
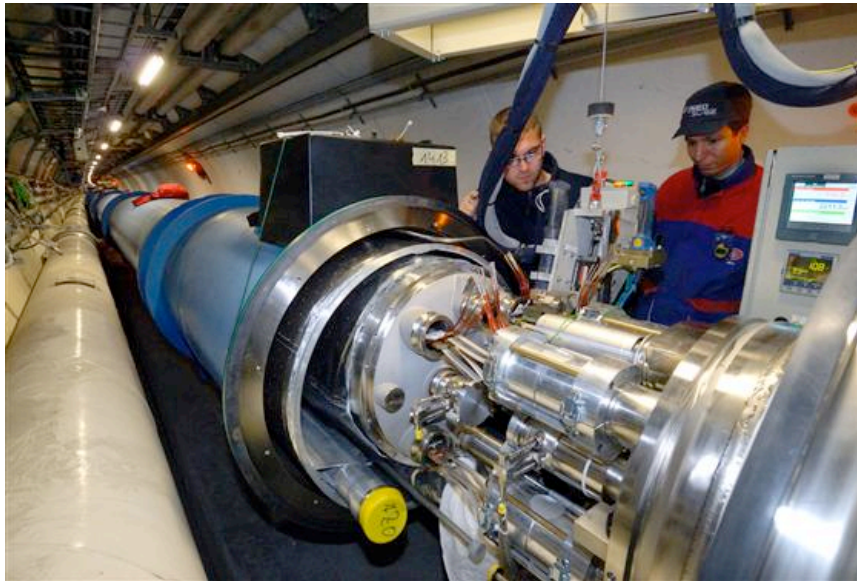
The Large Hadron Collider

September 10, 2008: beam splashes from this machine



The Large Hadron Collider

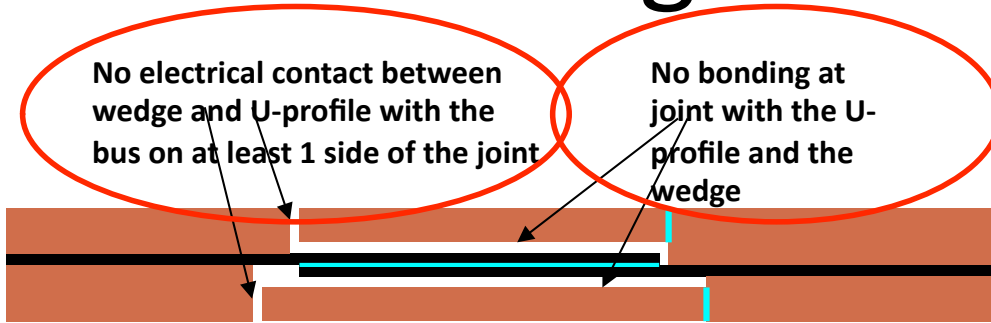
- 19 September 2008: the LHC accident; what happened?



A. Nisati, Preparing for the ...

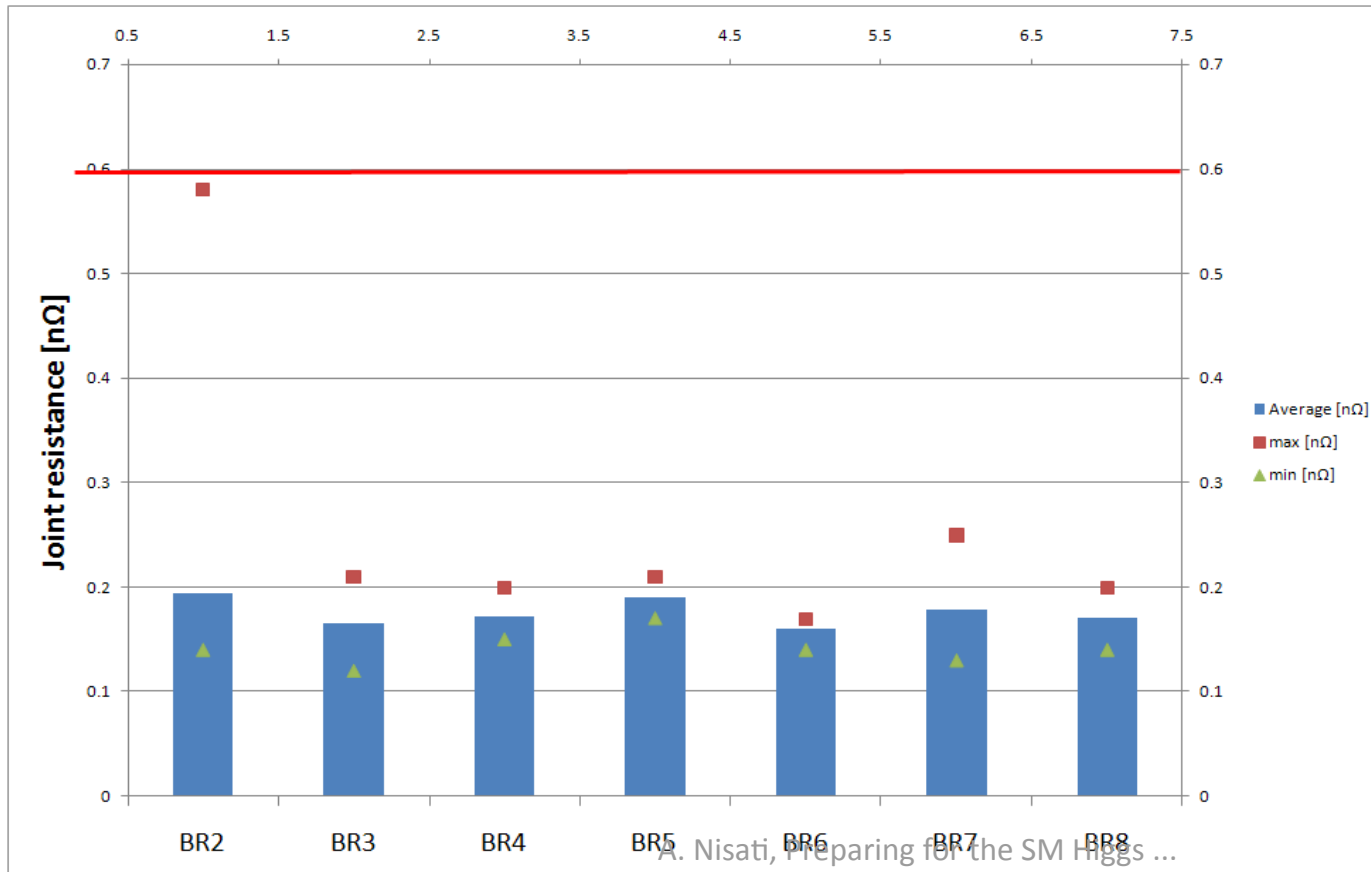
Main dipole electrical connections are ensured by 12 kA bus bars.

The Large Hadron Collider



The electrical cold joint

➔ About 220 nΩ resistance



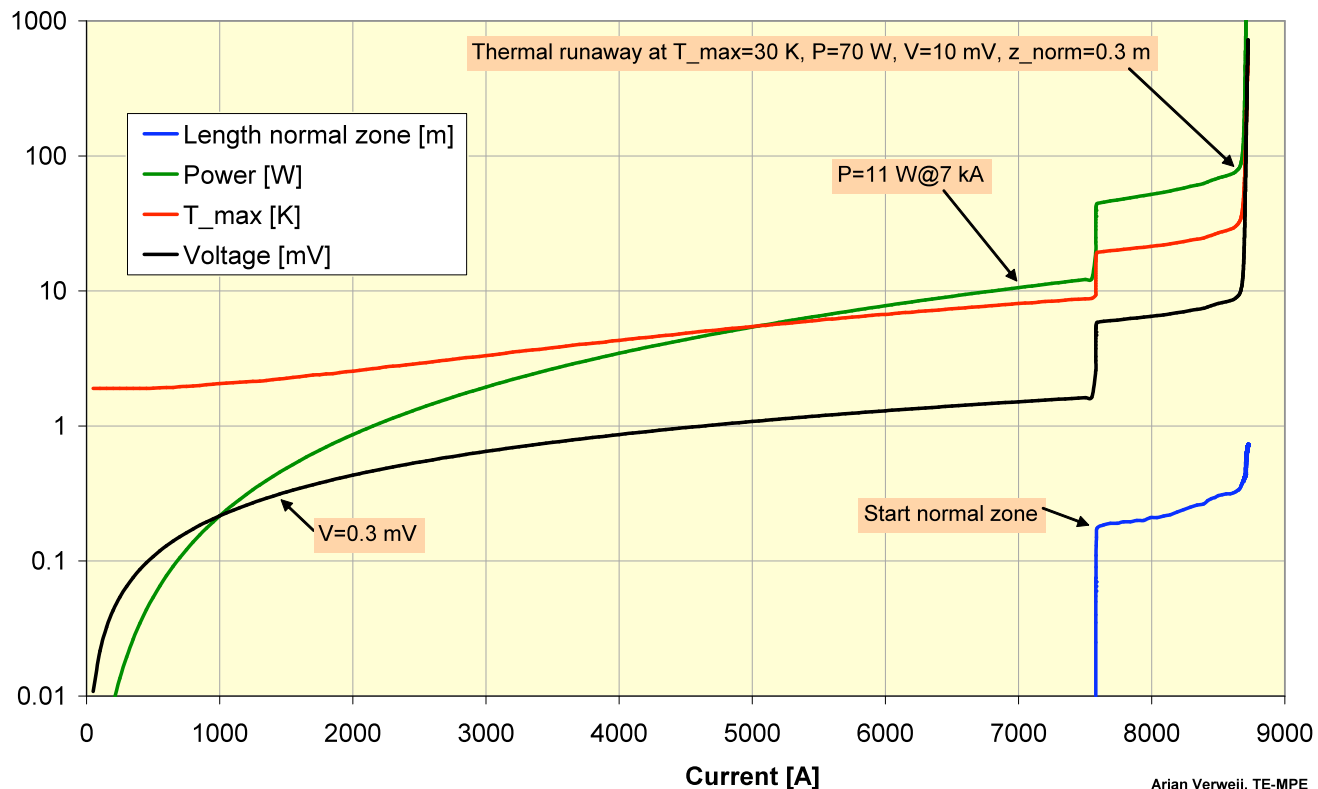
Main dipole electrical connections are ensured by 12 kA bus bars.

Typical electrical resistance (at low T): 0.2 nΩ ;

One joint in sector 34 had an anomalous resistance of 220 nΩ
➔ ...

The Large Hadron Collider

- 19 September 2008: the LHC accident; what happened?



Current : 7 kA;
Power = $I^2 \times R = 11 \text{ W} !$

- **QUENCH!** The electrical resistance increases drastically

- The local temperature goes to very high temperatures; the joint melts;

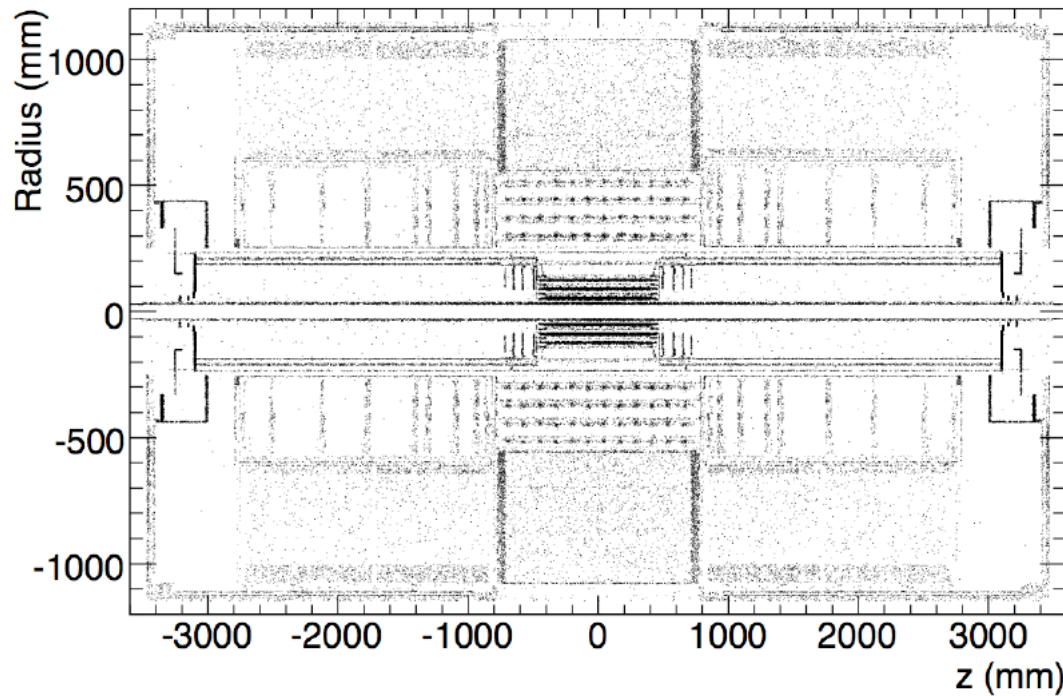
- the electrical circuit breaks in that point

- all the energy stored in the dipole, about 2 GJ, is "discharged"

- → electrical arc

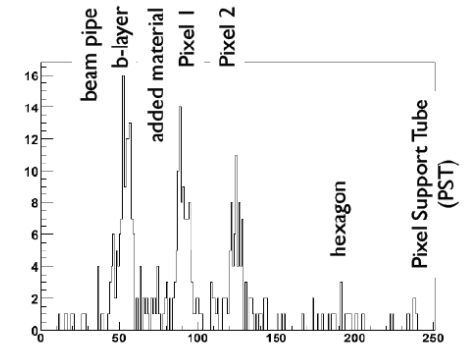
- → holes in the cryostat... the rest is widely known.

$$H \rightarrow \gamma\gamma$$



$$|\eta| < 1.0$$

Layer	Nc	$x/X0(\%)$	$\delta x/x$
beam pipe	11	0.45	-
b-layer	127	5.3 ± 1.6	31%
extra material	16	0.7 ± 0.2	35%
Pixel 1	103	4.3 ± 1.3	31%
Pixel 2	76	3.1 ± 1.0	31%
PST	7	0.29 ± 0.2	66%

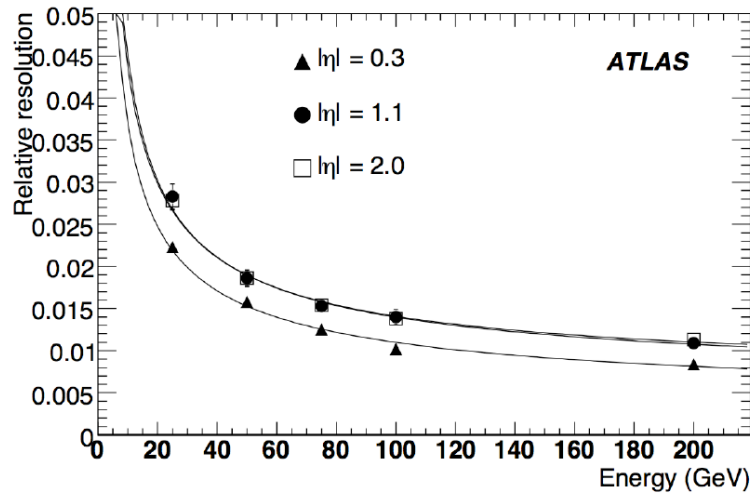


350k events:
 With 10 times more statistics : 10 %
 With 100 times more statistics: 3 %
 With 500 times more statistics: 1 %

Location of the ATLAS Inner Detector material as obtained from the **true position** of the fully simulated photon conversions in minimum bias events. The majority of the conversions are recoverable.

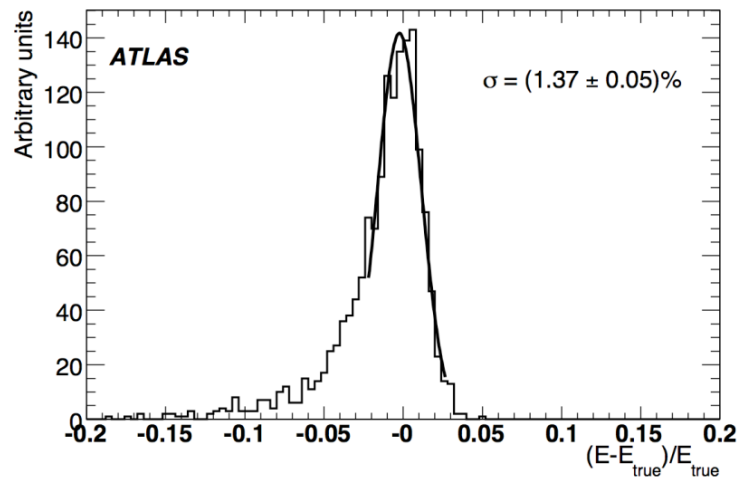
Location of the ATLAS Inner Detector material as obtained from the **reconstructed** position of the fully simulated photon conversions in minimum bias events

$$H \rightarrow \gamma\gamma$$

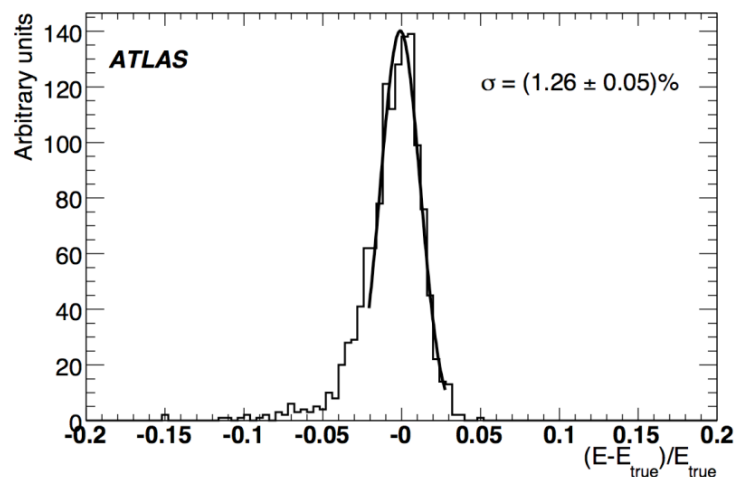


Photon relative resolution as a function of energy and eta.

The presence of material causes non-Gaussian tails in the energy reconstruction. The effect is particularly visible if converted photons are considered.



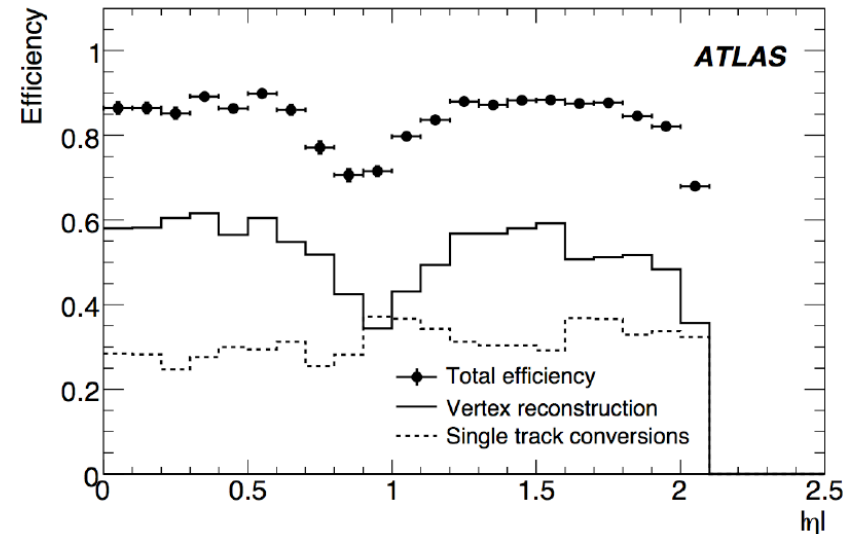
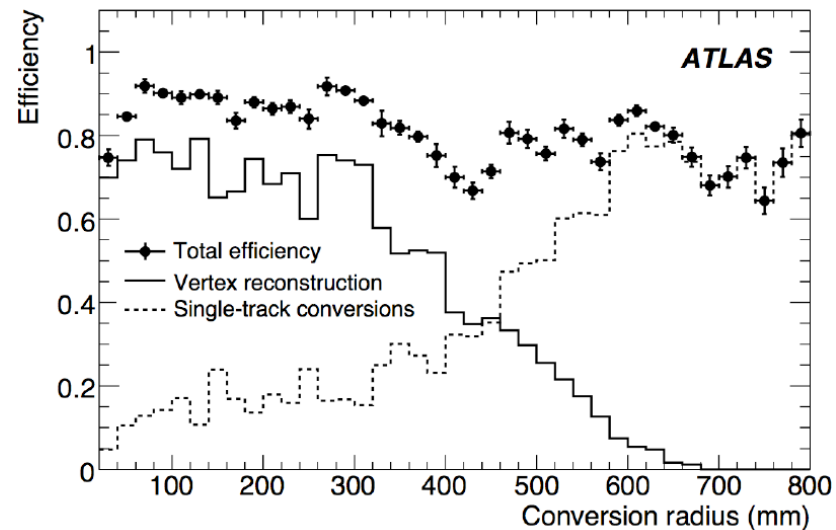
All photons: difference between measured and true energy normalised to true energy ($\eta=1.075$)



Unconverted photons: difference between measured and true energy normalised to true energy ($\eta=1.075$)

$$H \rightarrow \gamma\gamma$$

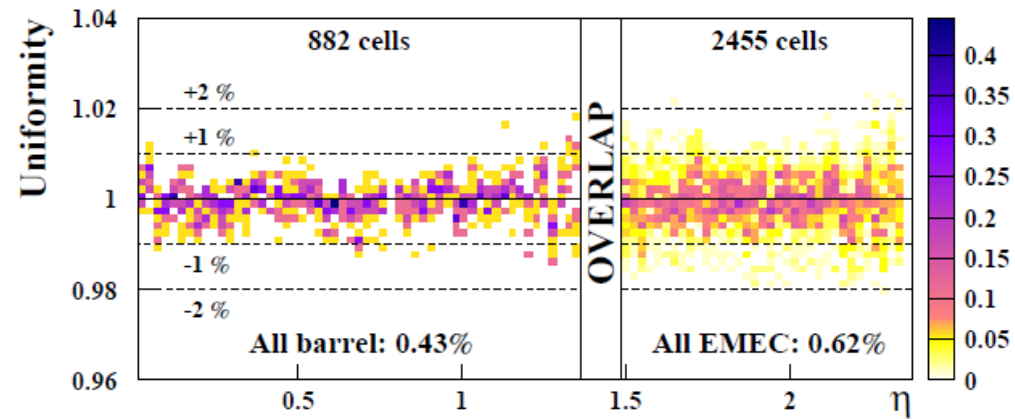
- About 60% of the photons from $H \rightarrow \gamma\gamma$ decays have a conversion in the material in front of the calorimeter. The reconstruction of conversions is important for improving both the efficiency and the accuracy of these decays.



Reconstruction efficiencies for conversions from 20 GeV pT photons as a function of conversion radius (left) and pseudorapidity (right). The points with error bars show the total reconstruction efficiency, the solid histograms show the conversion vertex reconstruction efficiency, and the dashed histograms show the single-track conversion reconstruction efficiency.

$$H \rightarrow \gamma\gamma$$

Test-beam data ; 245 GeV electrons

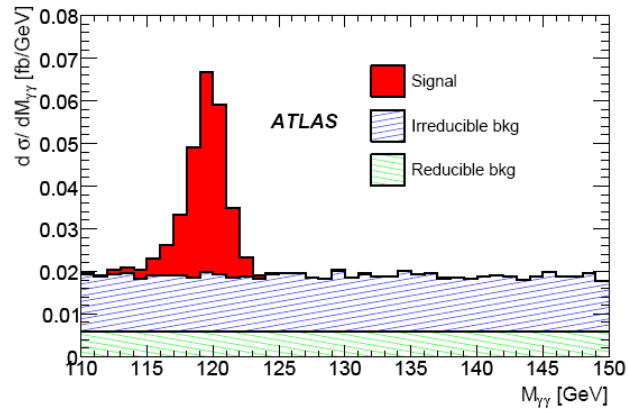


Distribution of the average energies measured in all cells of all tested modules as a function of the cell η , normalised to the mean energy measured in the modules. In the barrel, this mean energy was 245 GeV, while it was 120 GeV in the endcap.

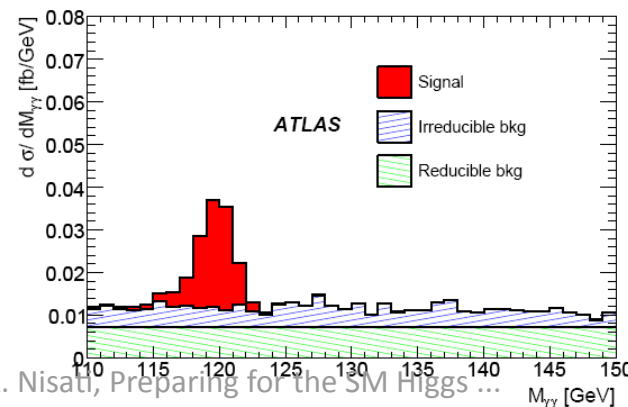
$$H \rightarrow \gamma\gamma$$

Associated production

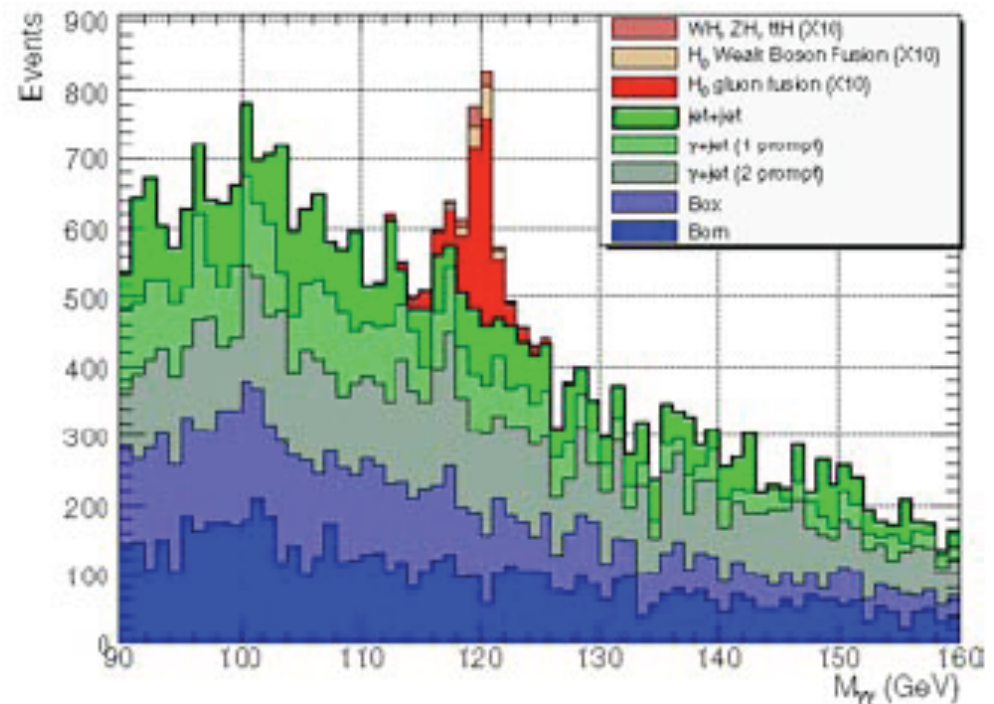
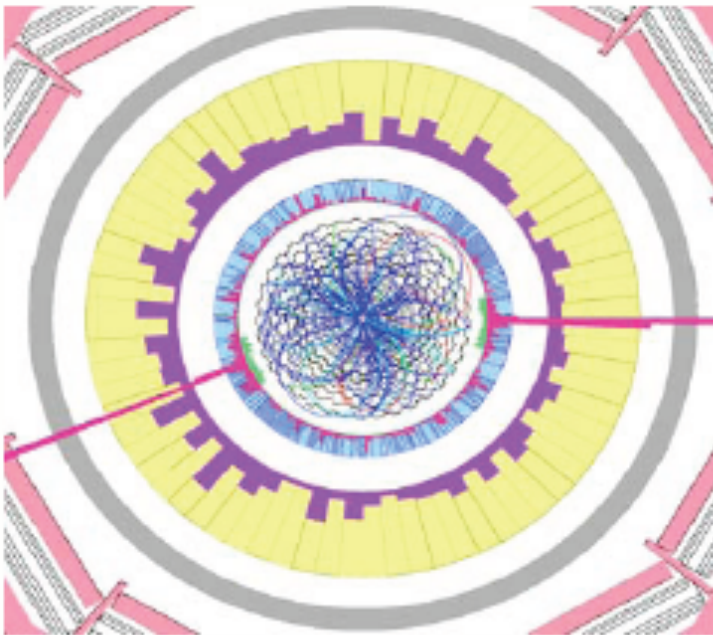
$H + E_T^{\text{miss}} + 1l$
 $S/B \sim 2$
 ttH WH



$H + E_T^{\text{miss}}$
 $S/B \sim 2$
 ZH WH



$$H \rightarrow \gamma\gamma$$



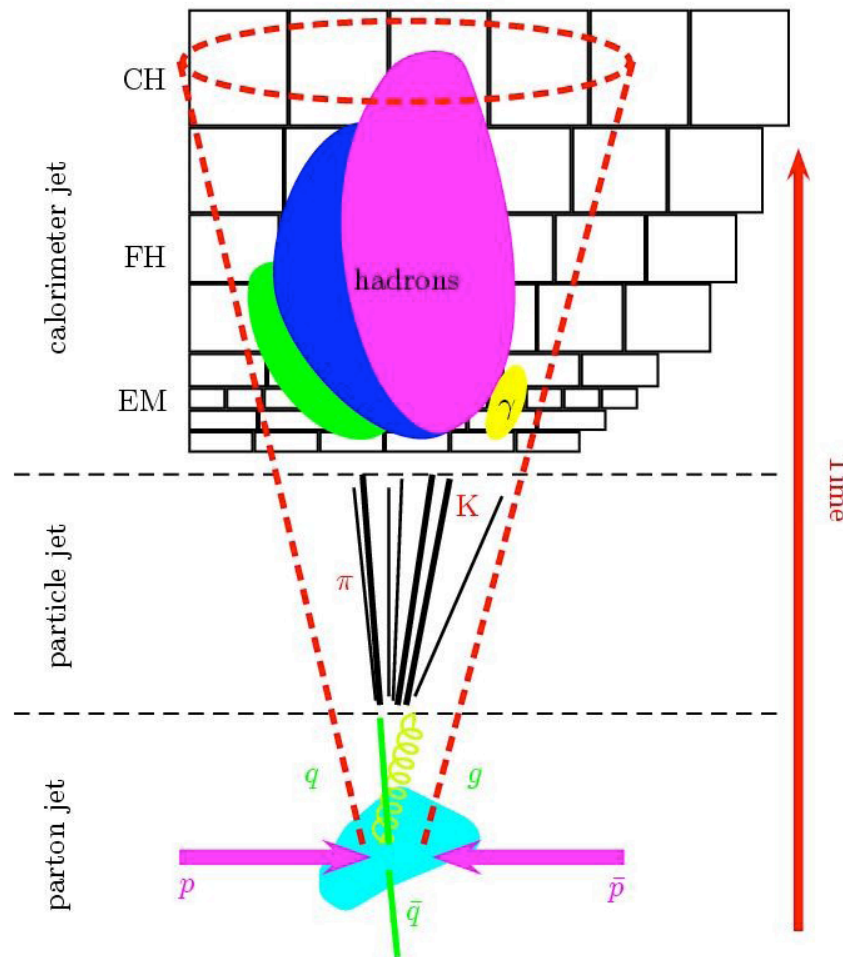
Left: Example of a $pp \rightarrow H + X$ event in the CMS detector with Higgs particle decay $H \rightarrow \gamma\gamma$. The two ECAL energy deposits are clearly visible.

Right: The $\gamma\gamma$ mass distribution for each source for barrel events with kinematic neural net. Events are normalised to an integrated luminosity of 7.7 fb^{-1} and the **Higgs signal** ($M_H=120 \text{ GeV}/c^2$) **is scaled by a factor 10**.

VBF $H \rightarrow \tau\tau$

- Jets: A **jet** is a narrow cone of neutral and charged particles (mostly hadrons) produced by the hadronization of a quark or gluon.
- The reconstruction of a jet is a complex task: in most cases the reconstruction of the initial parton momentum represents the ultimate goal of the jet energy measurement.
- Several steps to reach the energy reconstruction of a jet:

VBF $H \rightarrow \tau\tau$



The measurement starts from the signals recorded in the calorimeter cells which have been calibrated at the **electromagnetic scale** (set in test beam experiments; reproduces correctly electron beam energies);

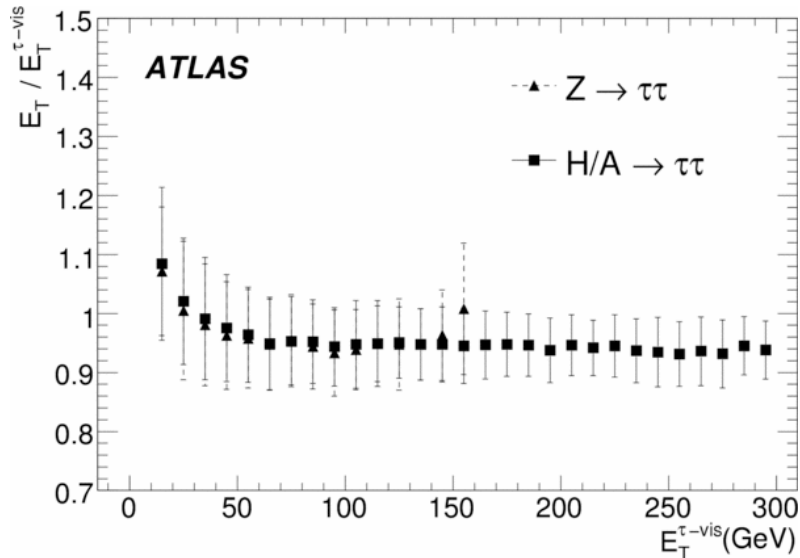
Reconstruct jets as clusters of calorimeter cells (example: cone algorithm, kt algorithm); the raw energy of jet is defined by the sum of the individual cell energy belonging to that jet.

Jet calibration procedure: first corrections are made for detector effects (non-compensation, noise, losses in dead materials and cracks, leakage, etc...); after this procedure the jet is calibrated at the **hadronic scale**. Then corrections to account such as ISR/FSR, underlying event (and pileup) can be applied, but they are process-related: we reach the **parton scale** calibration.

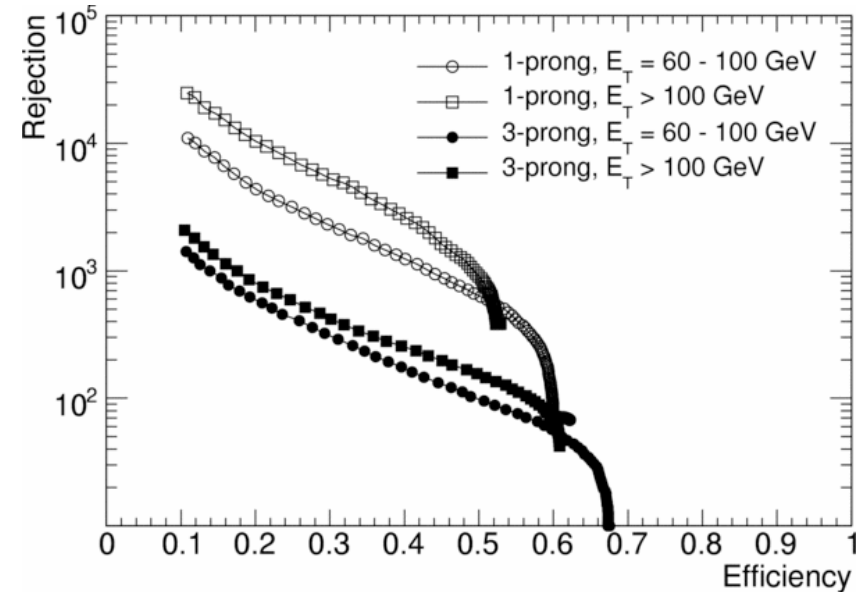
The validation of the whole procedure has to be performed in-situ using suitable processes.

Simulation procedures are also very important.

VBF H \rightarrow $\tau\tau$



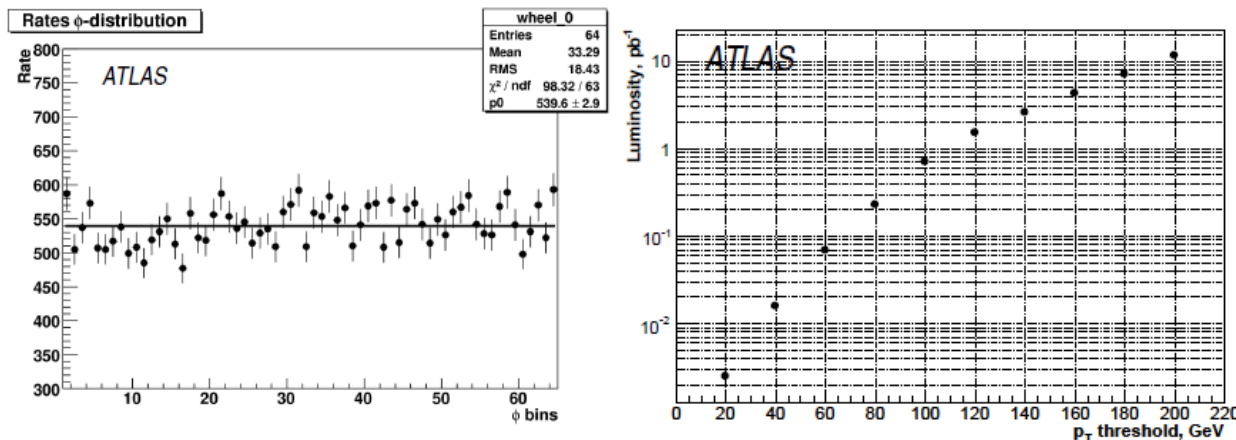
The ratio of the reconstructed E_T and the true ($E_T^{\tau\text{-vis}}$) transverse energy of the hadronic τ decay products is shown as a function of the visible true transverse energy $E_T^{\tau\text{-vis}}$ (left), calculated in $|\eta| < 2.5$ and $|\eta|$ (right) for taus from $Z \rightarrow \tau\tau$ (triangles) and $A \rightarrow \tau\tau$ with $m_A = 800$ GeV (squares) decays. The ordinate value is the mean and the error bars correspond to the sigma of the Gaussian fit performed in the range $0.8 < E_T / E_T^{\tau\text{-vis}}$. The results are obtained after applying the loose likelihood selection, see below.



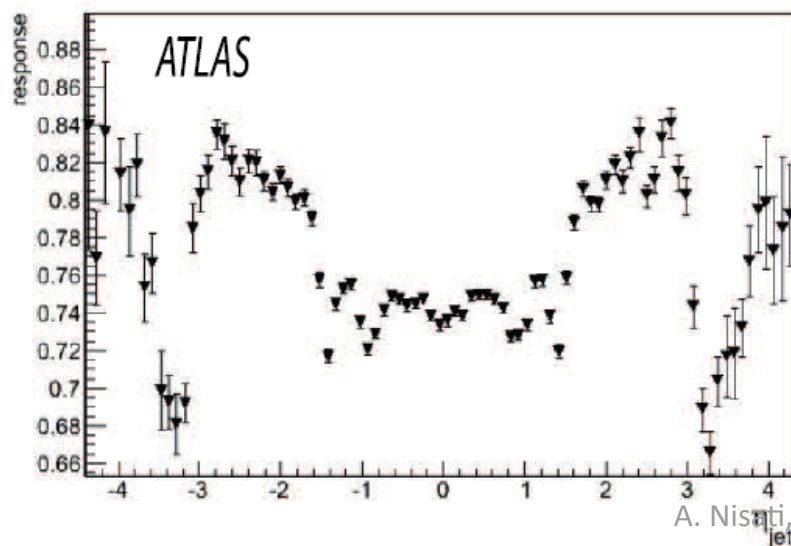
Expected performance for the calorimeter-based algorithm with the likelihood selection. The rejection rates against jets from Monte-Carlo particles as a function of the efficiency for hadronic τ decays for various ranges of the visible transverse energy are shown. For signal events $Z \rightarrow \tau\tau$ and bbH , $H \rightarrow \tau\tau$ with $m_H = 800$ GeV were used, for the background QCD dijet samples were

VBF $H \rightarrow \tau\tau$

- Minimum bias events. di-jet events. Z/γ +jet(s) events



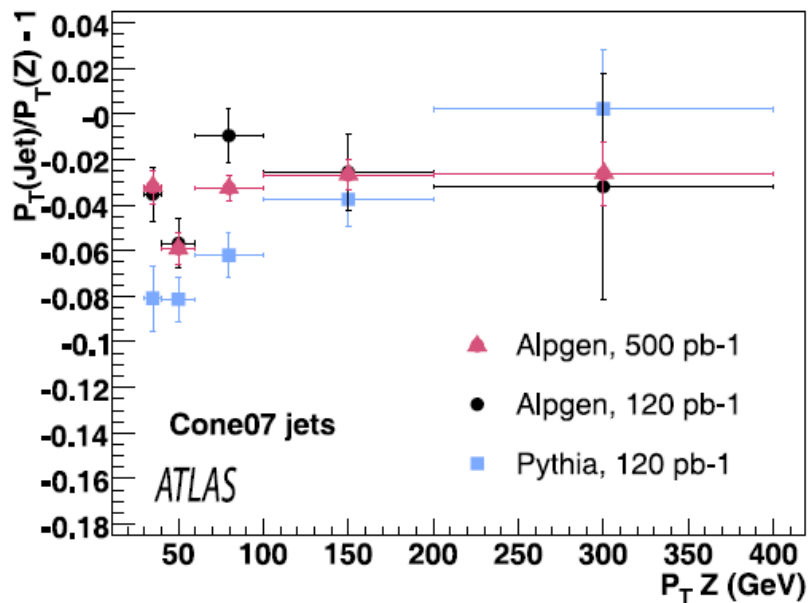
Intercalibration in ϕ : using the “ ϕ -symmetry”. Left: the jet rate as a function of ϕ . Right: Integrated luminosity required to collect 1000 events with jets above a certain threshold in each of the 64 ϕ sectors in the region $|\eta| < 0.1$.



Intercalibration in η : the jet response $p_T^{\text{rec}}/p_T^{\text{truth}}$ at the EM scale versus the jet pseudorapidity η . Correct this response using the “tag & probe” method and checking with simulation.

VBF $H \rightarrow \tau\tau$

- The jet energy scale: important to measure with no bias the energy of reconstructed jets.
- Several methods explored: γ -jet(s) processes, Z-jet(s) processes, Missing-ET projection method,...



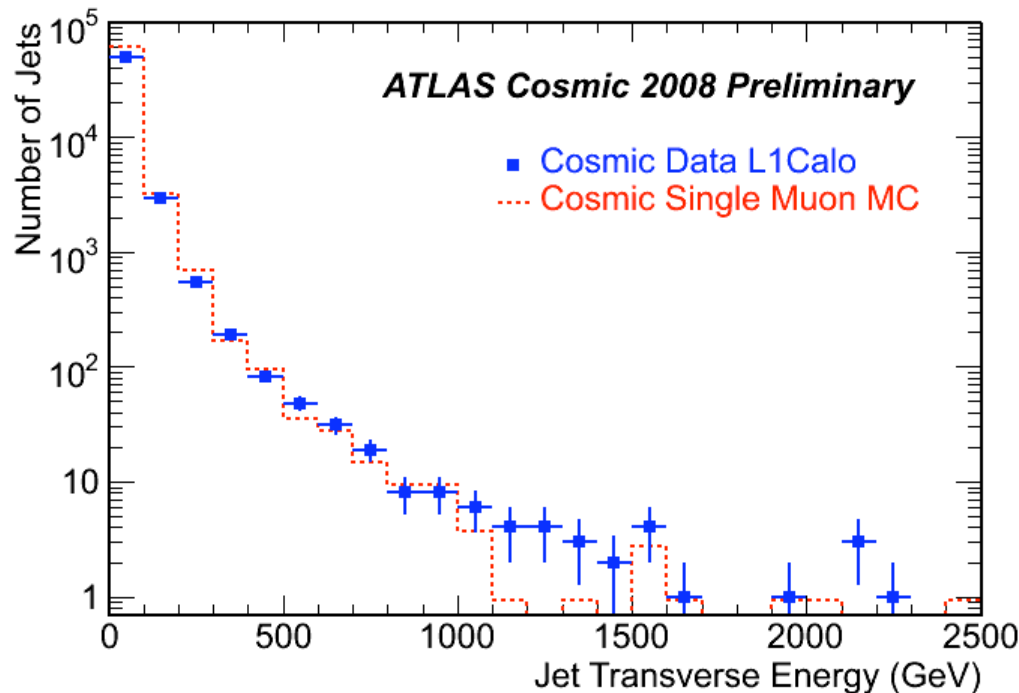
- In leading order of perturbation theory the final state of γ/Z +jet events can be considered as a two-body system in which $p_T^{\text{jet}} = p_T^{\gamma,Z}$.
- Measure $B_1 = p_T^{\text{jet}} / p_T^{\gamma,Z} - 1$

Plot: the p_T balance for an integrated luminosity of 120/pb and 500/pb in events generated with ALPGEN and PYTHIA in bins of p_T , for cone jets with $R=0.7$.

The balance is affected by various physics effects which systematically limit the precision of the in-situ validation procedure. These effects can be as large as 5–10% at 20 GeV and tend to decrease to the percent level at about 100 GeV.

VBF $H \rightarrow \tau\tau$

A lot of work done to start understanding the calorimeter and the jet reconstruction:

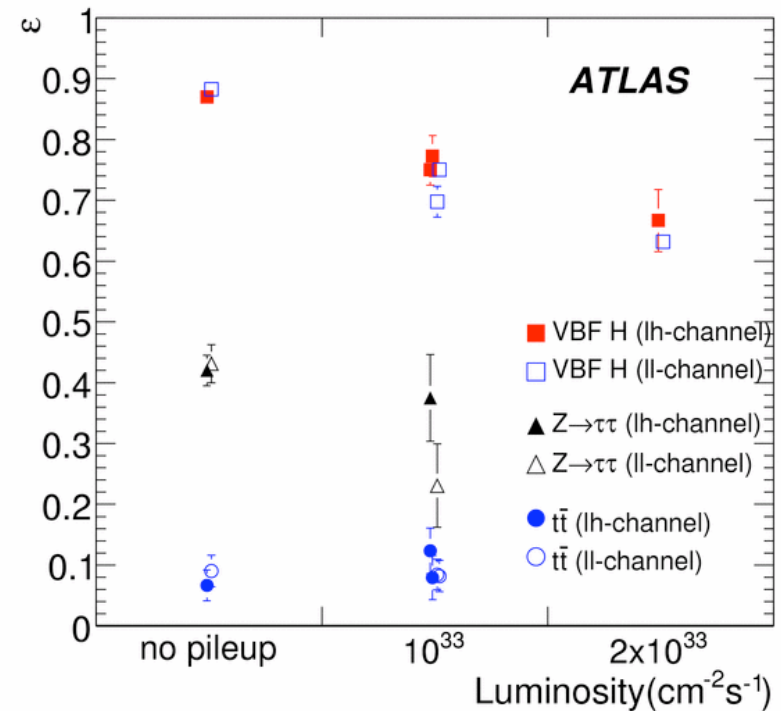


- Distribution of jet transverse energy from the cosmic L1Calo stream (run 90272 in Sep. 2008) and cosmic Monte Carlo. The same normalization factor as for the figure above is applied. The ATLAS Cone Jet algorithm with a cone size 0.4 is used. Calorimeter clusters reconstructed with the topological clustering algorithm are the inputs for the jet reconstruction. Only jets with $ET > 20$ GeV are shown. The jet energy is at the electromagnetic scale. The shape of the distribution is well described by the simulation. At high ET , more events are found in the data than in the MC. This might be explained by the limited MC statistics and by air shower events not included in the simulation.

VBF H \rightarrow $\tau\tau$

Influence of pile-up

- In average about 2.3 pp inelastic collision per each bunch crossing \rightarrow 2.3 “minimum bias” events in addition to the triggered event.
- Additional activity in the central rapidity region \rightarrow impact to the central jet veto;
- Degradation of the measurement of E_t^{miss} \rightarrow impact to the tau mass resolution;
- Degradation of the hadronic tau lepton identification;



Central jet veto performance in the presence of varying levels of pileup for signal and background samples.

VBF $H \rightarrow \tau\tau$

- Monitoring **detector response** stability: with $\sim 1-8 \times 10^6$ triggers to reach 1% stability
- **Cell-to-cell calibration**
 - Using phi-symmetry of MB triggers, inter-calibrate cells with equal dimensions/positions (2x64 cells)
- **Jet calibration**; based on weights estimated from Monte Carlo studies; ingredients:
 - **Jet fragmentation** modelling: electromagnetic jet energy fraction, energy and multiplicity of charged hadrons, etc..
 - **Hadronic shower models**, benchmarked in comparison with test beam data;
 - Description of dead material in **simulation** (fraction of “lost energy” in dead material from \sim few% to 15 %)

VBF H \rightarrow $\tau\tau$

- Systematic uncertainties

Source	Relative uncertainty	Effect on signal efficiency
luminosity	$\pm 3\%$	$\pm 3\%$
muon energy scale	$\pm 1\%$	$\pm 1\%$
muon energy resolution	$\sigma(p_T) \oplus 0.011 p_T \oplus 1.7 \cdot 10^{-4} p_T^2$	$\pm 0.5\%$
muon ID efficiency	$\pm 1\%$	$\pm 2\%$
electron energy scale	$\pm 0.5\%$	$\pm 0.4\%$
electron energy resolution	$\sigma(E_T) \oplus 7.3 \cdot 10^{-3} E_T$	$\pm 0.3\%$
electron ID efficiency	$\pm 0.2\%$	$\pm 0.4\%$
tau energy scale	$\pm 5\%$	$\pm 4.9\%$
tau energy resolution	$\sigma(E) \oplus 0.45 \sqrt{E}$	$\pm 1.5\%$
tau ID efficiency	$\pm 5\%$	$\pm 5\%$
jet energy scale [†]	$\pm 7\%$ ($ \eta \leq 3.2$) $\pm 15\%$ ($ \eta \geq 3.2$) $\pm 5\%$ (on E_T^{miss})	$+16\% / -20\%$
jet energy resolution	$\sigma(E) \oplus 0.45 \sqrt{E}$ ($ \eta \leq 3.2$) $\sigma(E) \oplus 0.67 \sqrt{E}$ ($ \eta \geq 3.2$)	$\pm 1\%$
b-tagging efficiency	$\pm 5\%$	$\pm 5\%$
forward tagging efficiency	$\pm 2\%$	$\pm 2\%$
central jet reconstruction efficiency	$\pm 2\%$	$\pm 2\%$
total summed in quadrature		$\pm 20\%$



Needs a careful control of the jet and MET energy scale

SM Higgs Statistical Combination

- Build a likelihood function $L(\mu, \theta)$ from a model; $\mu = 0 \rightarrow$ no signal ; $\mu = 1 \rightarrow$ SM signal;
- θ : array of “nuisance” parameters needed in the model (background rate, efficiency, shapes' params, ...);
- $L(\mu, \theta)$ may describe one or more decay channels;
- Maximize $L(\mu, \theta)$ to fit data at best, either by varying μ, θ altogether ($\rightarrow \mu^{\wedge}, \theta^{\wedge}$), or by varying only θ at fixed μ ($\rightarrow \theta^{\wedge\wedge}$); then build
 $\lambda(\mu) = L(\mu, \theta^{\wedge\wedge}) / L(\mu^{\wedge}, \theta^{\wedge}); q_{\mu} = -2 \ln \lambda(\mu);$
- q_{μ} distributed as a $\chi^2(1 \text{ df})$, easy to compute the p-value, the probability of q_{μ} to be larger than the observed q_{μ}^{obs} value.

SM Higgs Statistical Combination

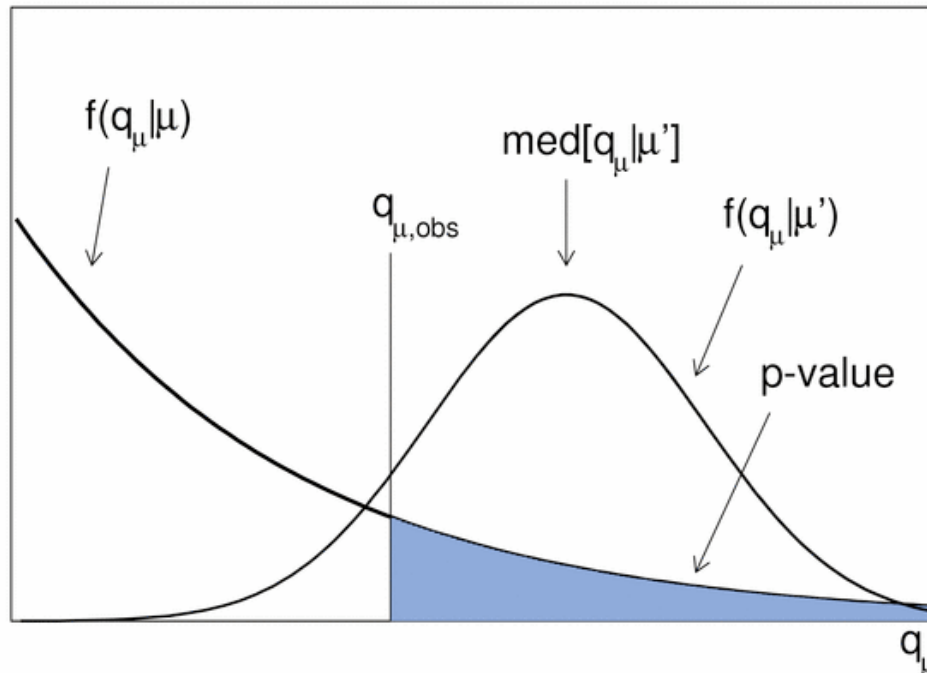


Illustration of the determination of the p -value of a hypothesized value of μ .

The left-hand curve indicates the pdf of q_μ for data generated with the same value of μ as was used to define the statistic q_μ ; this is used to determine the p -value of μ , shown as the shaded region. The right-hand curve indicates the pdf of q_μ for data generated with a different value of the strength parameter, μ' .

Discovery: Assume no signal ($\mu = 0$) and evaluate q_0 from data; if p -value $< 2.87 \times 10^{-7}$ claim for a discovery at 5σ significance!

Exclusion: Assume signal ($\mu = 1$) and evaluate q_1 from data; if p -value < 0.05 exclude signal at 95% confidence level.